KERNFORSCHUNGSANLAGE JÜLICH GmbH

Institut für Plasmaphysik
Association EURATOM - KFA

CLEANING AND CONDITIONING OF THE WALLS OF PLASMA DEVICES BY GLOW DISCHARGES IN HYDROGEN

by

F. Waelbroeck, J. Winter, I. Ali-Khan, P. Wienhold,
B. Brandt, K. J. Dietz

Jül - 1692
Dezember 1980
ISSN 0366-0885

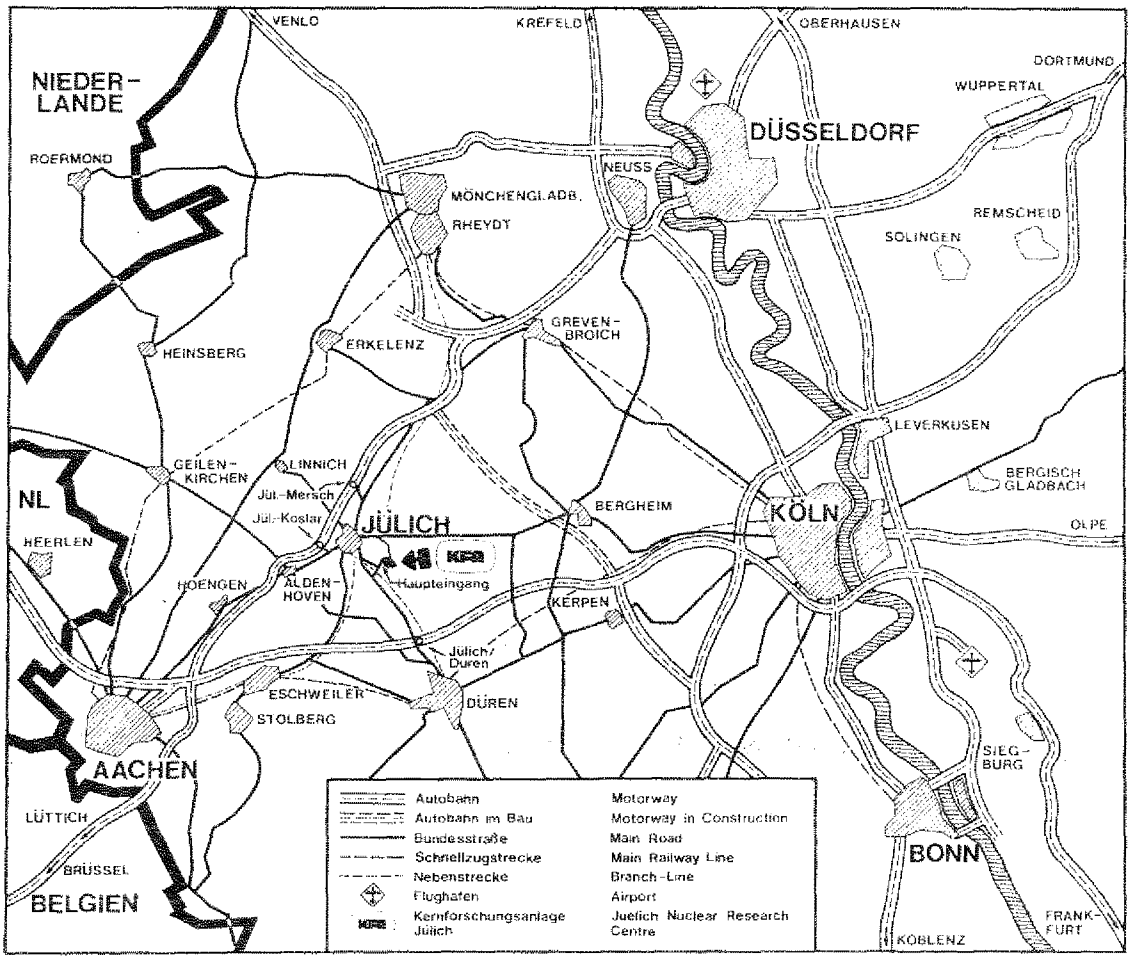

Als Manuskript gedruckt

Berichte der Kernforschungsanlage Jülich – Nr. 1692

Institut für Plasmaphysik Jül – 1692

Zu beziehen durch: ZENTRALBIBLIOTHEK der Kernforschungsanlage Jülich GmbH
Postfach 1913 · D-5170 Jülich (Bundesrepublik Deutschland)
Telefon: 02461/610 · Telex: 833556 kfa d

CLEANING AND CONDITIONING OF THE WALLS OF PLASMA DEVICES BY GLOW DISCHARGES IN HYDROGEN

by

F. Waelbroeck*, J. Winter*, I. Ali-Khan*, P. Wienhold*,
B. Brandt, K. J. Dietz*****

* Institut für Plasmaphysik der Kernforschungsanlage Jülich GmbH, Association EURATOM - KFA, 5170 Jülich, Postfach 1913, FRG

** FOM-Instituut voor Plasmafysica, Associatie EURATOM - FOM, Rijnhuizen, NL

*** The JET Project, Abingdon, UK

CLEANING AND CONDTIONING OF THE WALLS OF PLASMA DEVICES BY GLOW DISCHARGES IN HYDROGEN

F. WAELBROECK, J. WINTER, I. ALI-KHAN, P. WIENHOLD
Institut für Plasmaphysik der Kernforschungsanlage Jülich GmbH,
Association EURATOM-KFA, 5170 Jülich, Postfach 1913, FRG

B. BRANDT
FOM-Instituut voor Plasmafysica, Associatie EURATOM-FOM, Rijnhuizen, NL

K.J. DIETZ
The JET Project, Abingdon, UK

ABSTRACT

The influence of a number of parameters on the cleaning and preconditioning efficiency of a combined rf and glow (RG) discharge is studied experimentally. The emphasis is laid on problems of oxygen removal from the surface. The important parameters are the wall temperature T_W, the pump speed Sp, the current I_{GD} of the glow discharge and the hydrogen pressure P_2. In a device with a ratio $Sp/S = 0{,}1\ ms^{-1}$ (S: inner area), a rapid deoxidation is achieved when $T_W \geqslant 200\ ^oC$. At room temperature, the oxide layer is reduced from a (carbon-free) surface when 1 to 2 % of methane is added to the hydrogen: carbon monoxide is formed and evacuated. Admixture of other gases such as He, Ne do not increase the cleaning efficiency.

An equation derived from a simplified model describes semi-quantitatively the observed parametric dependances.

The tendency for arc spots to occur during the initial phases of the discharge depends on the preconditioning of the wall: a prolonged bake-out at 200 ^oC leads to the non-appearance of arcs in all cases examined.

Problems arise when a quadrupole residual gas analyser is used to measure the partial pressure of water in hydrogen. These are analysed and a conditioning technique is described which has proven to be appropriate in our measurements.

TABLE OF CONTENTS

FIGURE CAPTIONS

PAGE

PAGE

I. INTRODUCTION

The presence of low Z impurities, mostly carbon (C) and oxygen (O), influences strongly the temperature and the confinement of tokamak plasmas. An extensive literature survey is to be found in a recent review paper /1/.

The concentration of C and O in the lattices of the wall materials - usually stainless steels or inconels - generally used in fusion devices is low; it is however well established /2, 3/ that the surfaces of these metals are covered with a layer of C- and O-rich compounds, even after the application of refined UHV cleaning procedures such as etching, electropolishing, ultrasonic rinsing, vacuum outgasing at elevated temperatures... This layer has a thickness of several tens of Å for a well prepared surface and represents thus a (finite) reservoir of C and O, if these substances can be released to the plasma.

Low Z impurities appear early in the plasma discharges, when the ion energy is still low. Hence physical sputtering does not seem to be the main release mechanism. As has been shown previously /4, 5/, chemical reactions between the surface impurity layer and (atomic) hydrogen which has escaped from the plasma lead to the appearance of significant amounts of water, carbon oxides and hydrocarbons. The released gaseous products, dissociated and ionized by the plasma, are probably the dominant origin of the low Z contamination. The chemical reactions occur after the hydrogen has thermally equilibrated with the lattice: the H concentration and the wall temperature are much more important as parameters than the energy at which H penetrates into the lattice /6/. Since the chemical production rates are moreover observed to be large, the early appearances of C and O in the tokamak plasmas is easily understood.

Clearly, in situ prehandling procedures must be applied to remove the surface layers if oxygen and carbon free plasma are to be obtained: the chemical production of volatile substances containing C and/or O atoms must be suppressed or at least considerably reduced. A review /7/ has described the recent developments in this area. The methods applied can be subdivided into gettering and discharge cleaning techniques.

A prominent representative of the first type is titanium (Ti) gettering. It was first applied to the ATC tokamak /8/ and has been utilised since on a number of other toroidal experiments. The method allows to obtain nearly oxygen-free plasmas. The gettering procedure does not remove the contaminants from the system but acts by burying them and by virtue of the very strong chemical bonds which are formed between the impurities and the getter and which cannot be easily re-

duced by the hydrogen. Since the bonding capacity of the film is limited, a frequent deposition of fresh gettering layers is necessary, in particular after each exposure to air or to a vacuum leak. Serious problems are associated with the repetitive use of the method: multiple Ti-layers tend to peel off (flaking) /9/ as had been observed in mirror machines, the hydrogen inventory in a thick Ti coating is large, a problem which will be serious (tritium inventory) in JET or TFTR if the walls, covered by multiple Ti layers, are later exposed to a deuterium-tritium mixture.

Methods based on (physical) sputter cleaning, e.g. on the exposure of the wall to energetic ions of noble gases, are inefficient in the toroidal geometry: the impurity atoms released are not removed from the vessel but redeposited on some other part of the wall just as sparrows chased with stones from a corner of a large wheat field fly off to resume their eating in another corner.

Plasma discharges in hydrogen are well adapted to the cleaning task provided that the plasma temperature and density are maintained at sufficiently low values to avoid an appreciable dissociation and ionisation of the released impurity molecules. Taylor discharge cleaning (TDC) /10/ and glow discharge cleaning (GDC) in a throughflow of hydrogen have been used successfully and led to an important reduction in the low Z contamination of tokamaks discharges. Both lead to appreciable release of hydrocarbons and CO; in TDC, the release of considerable amounts of H_2O has been reported. The conditions under which H_2O is formed and released in GDC are part of an open question. In experiments such as ASDEX /11/ and PDX /12/, the release is practically undetectable, whereas significant H_2O release was reported in simulation experiments /5/ and in TFR 600 /13/.

The aim of this work is to simulate the glow discharge cleaning in experiments like JET and TEXTOR and to study the parametric variation of the cleaning efficiency. Particular emphasis has been laid on the investigation of the deoxidation channel via water formation since it represents the only way to deoxidize a surface which had been decarburized beforehand (case of a tokamak which has been air-flooded after prolonged operation). It is not the aim of this study to investigate the actual surface composition during and after an exposure to a glow discharge in hydrogen /11, 12/ or to atomic hydrogen /14/. The emphasis has rather been laid on the following question: can the vessel surface be so preconditioned by the GDC that it can no longer release C- or O-containing gases even under the subsequent exposure to powerful discharges? At the end of the prehandling

procedure, some metal oxides may remain close to the surface. It is only important that the bonding energies of these residual oxides be so high that the metal-oxygen bond cannot be reduced by H at an appreciable rate: the chemical contamination source can then be deemed to have been eliminated.

As will be shown in the subsequent paragraphs, an important scaling parameter for the effectivity in a system is the ratio Sp/S of the pump speed Sp in the system to the effective area S of the wall to be cleaned. The simulation system has therefore been dimensioned to have approximately the same ratio $Sp/A \approx 0.1\ m\ s^{-1}$ as JET and TEXTOR will have. Another important aspect is the time history of the experiment, i.e. the prehandling of the surfaces before GDC is applied. A strong correlation between the occurence of arc spots and the temperature history of the surface has been observed. Because of the rapid and continous evolution of the system (deoxidation) during a measurement, the separation of the influence of several variables is not easy to make; special methods of evaluation have to be used. Moreover to carry out a systematic study of H_2O release, a reproducible recontamination method had to be developed and applied.

The variables which determine the cleaning effectivity have turned out to be the wall temperature T_W, the glow discharge current density j_{GD}, the pump speed Sp and the hydrogen pressure P_{H_2}. In order to operate a discharge at the desirably low hydrogen pressures, a modified type of glow discharge, the RG-discharge (combined rf- and glow-discharge), has been developed; its characteristic properties had to be investigated; they are described in § III.1.

In the following sections, the experimental set up with its characteristic data will be described first. After the characterisation of the RG-discharge, a discussion on the appropriate handling of the quadrupole by-pass is presented, the temperature manipulations in the system and the reoxidation procedure are outlined. The measurement of the fluxes of particles to the wall are given in an additional paragraph, including measurements on the destruction of gaseous products in the discharge. The cleaning results are discussed in separate sections dealing with the "first clean down" of the system and with later experiments in a decarburized vessel wherein the parametric variation of the deoxidation efficiency was examined, followed by the discussion of the results and the conclusions.

II. DESCRIPTION OF THE EXPERIMENT

The apparatus (fig. 1) consists of a glow discharge vessel (GDV) and a quadrupole by-pass (QBP). They are evacuated by separate turbomolecular pump units (TMU 1 and 2) but joined via the connection tube (CT) with the throttle valve (TV 2). The total inner area and volume of the GDV, including the fifteen appended sidearms and portholes, are $2.98 \times 10^4 cm^2$ and $2.16 \times 10^5 cm^3$ respectively. The inner area, neglecting portholes, usually exposed to the glow-discharge, is $2.01 \times 10^4 cm^2$. The GDV and QBP can be heated up to 600 °C and 400 °C. During the measurements reported here (except for the first clean-down of the apparatus) the temperature of each porthole was ca. 200 °C (cf. § III.4). The only part of the apparatus which was not heated up is the gate valve (GV) of the GDV.

The radio frequency generator (RFG), operating at 13,6 MHz at a power $W_{rf} \leqslant$ 100 Watt, is matched to the radio frequency coil (RFC), consisting of 5 1/2 windings of 5 cm diameter. The coil length is 7 cm. The material is stainless steel (naked, i.e. in direct contact with the plasma). The radio frequency system allows to initiate and maintain an rf plasma discharge in H_2 at low pressures. A dc voltage ($\leqslant$ 1500 V) can be applied by the generator (DCG) between the RFC and the vessel walls. This modifies the rf discharge into a hollow cathode glow discharge (RG discharge). The virtual anode is the plasma within the rf coil. When the current in the discharge is large, the RFC might be overheated; this is avoided by diverting part of the anode current into an auxiliary electrode (AE).

The throttle valve (TV 1) allows to reduce the pump speed in the GDV by a factor of up to about 2 for H_2 and 4 for H_2O. The specific pump speed for H_2O (and CO_2) in the GDV can be increased by use of a cryopump (CF). This consists of a liquid nitrogen (LN_2) cooled finger with an area of 600 cm^2. A lamellar grid system (venetian blind) protects that part of the cold surface which protrudes into the GDV from the RG discharge. This avoids the ion-induced reevaporation of condensed gases. The outer area (exposed to the discharge) of the venetian blind is 630 cm^2.

A squirrel cage array (SC) of tungsten filaments (cf. [5,9]) allows to compare the H_2O, CH_4, CO... production rates achieved using either rf or RG plasmas with those which result from low energy (0.2 eV) hydrogen atoms produced by contact dissociation [15-17] of H_2 on a hot (2100 K) tungsten surface (total area = 1,5 - 9 cm^2).

Hydrogen is stored in an iron-titanium flask. It is fed into either the GDV or directly into the QBP through appropriate inlet valves (E 1 and E 3) after having passed over LN_2 traps. Other gases (He, NH_3, CH_4, H_2O, Ne, N_2, Ar or CO_2) can additionally be introduced into the GDV through another valve E 2. Whenever possible, these additional gases were further purified by an LN_2 trap.

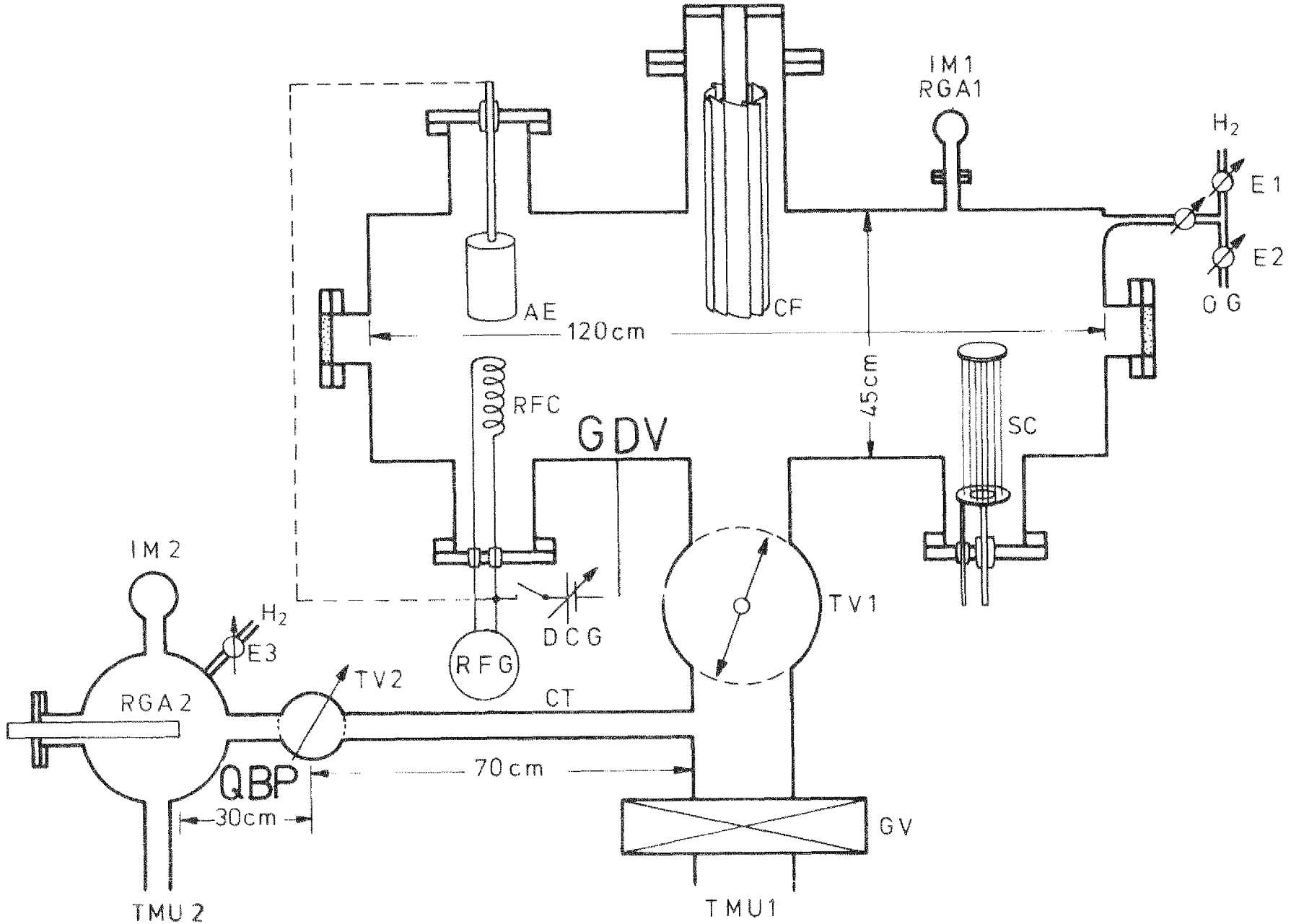

Fig 1. Experimental apparatus: GDV: glow discharge vessel; QBP: quadrupole By-pass.
RFC: radio frequency coil; RFG: radio frequency generator; DCG: d.c. power supply; AE: auxiliary anode; SC: squirrel cage
CF: cryopump; TV1, TV2: throttle valves; CT: connection tube;GV: gate valve; TMU 1, 2: turbomolecular pump units;
E1, E2, E3: gas inlet valves; RGA1, RGA2: residual gas analyzers; IM1, IM2: ion manometers

Additional instrumentation in the GDV includes an ion manometer (IM 1), a quadrupole residual gas analyser (RGA 1) and a Langmuir electrostatic probe to measure the floating potential of the plasma.

The instrumentation within the QBP comprises an ion manometer (IM 2), a quadrupole residual gas analyser (RGA 2) (Balzers, type QMG 511) and the H_2 inlet valve (E 3). A residual gas spectrum of the QBP is shown in fig. 2. The walls were at room temperature and the base pressure was 1×10^{-9} torr. The H_2 peak is not shown on the figure. CO, CO_2, hydrocarbon of the methane, ethane and propane groups and traces of water can be seen. Also Cl (m = 35,37), K (m = 39,41) and F (m = 19), probably from the filament, are detected.

Table I summarizes some of the main parameters of the pump system for various gases:

- The pump speed $(Sp)_j$ in the GDV, with TV 1 and GV open, for the gas of mass m_j,
- the relative calibration of the partial pressures in the GDV as measured by the RGA 2 (in QBP) at some fixed sensitivity (2×10^{-10} A) and for the throttle factor of TV 2 used in our experiments and
- the relative calibration of the partial pressures in the QBP for the same setting of the RGA.

The pump speed $(Sp)_j$ in the GDV is plotted as a function of the molecular mass m_j on fig. 3.

The variation of $(Sp)_2$ versus hydrogen pressure is illustrated on fig. 4. The diameter of our pump port is 15 cm; the pump speeds for H_2 and for traces of impurity gases are then practically equal when $p \geqslant 3 \times 10^{-3}$ torr.

The apparatus allows to vary and to measure practically independently of one another:

- the temperatures of the walls of the GDV and of the QBP as well as those of the portholes and of the connection tube,
- the pump speed by using TV 1 in general and the cryopump CF in the particular case of H_2O (and CO_2),
- the power of the rf discharge,
- the current of the RG discharge,
- the pressure of H_2 in the GDV (via E 1) and when needed in the QBP (via E 3),
- the partial pressure of admixed gases (via E 2).

Summing up the resulting parametric variations allows to assess and optimize the glow discharge cleaning systems foreseen for TEXTOR and JET.

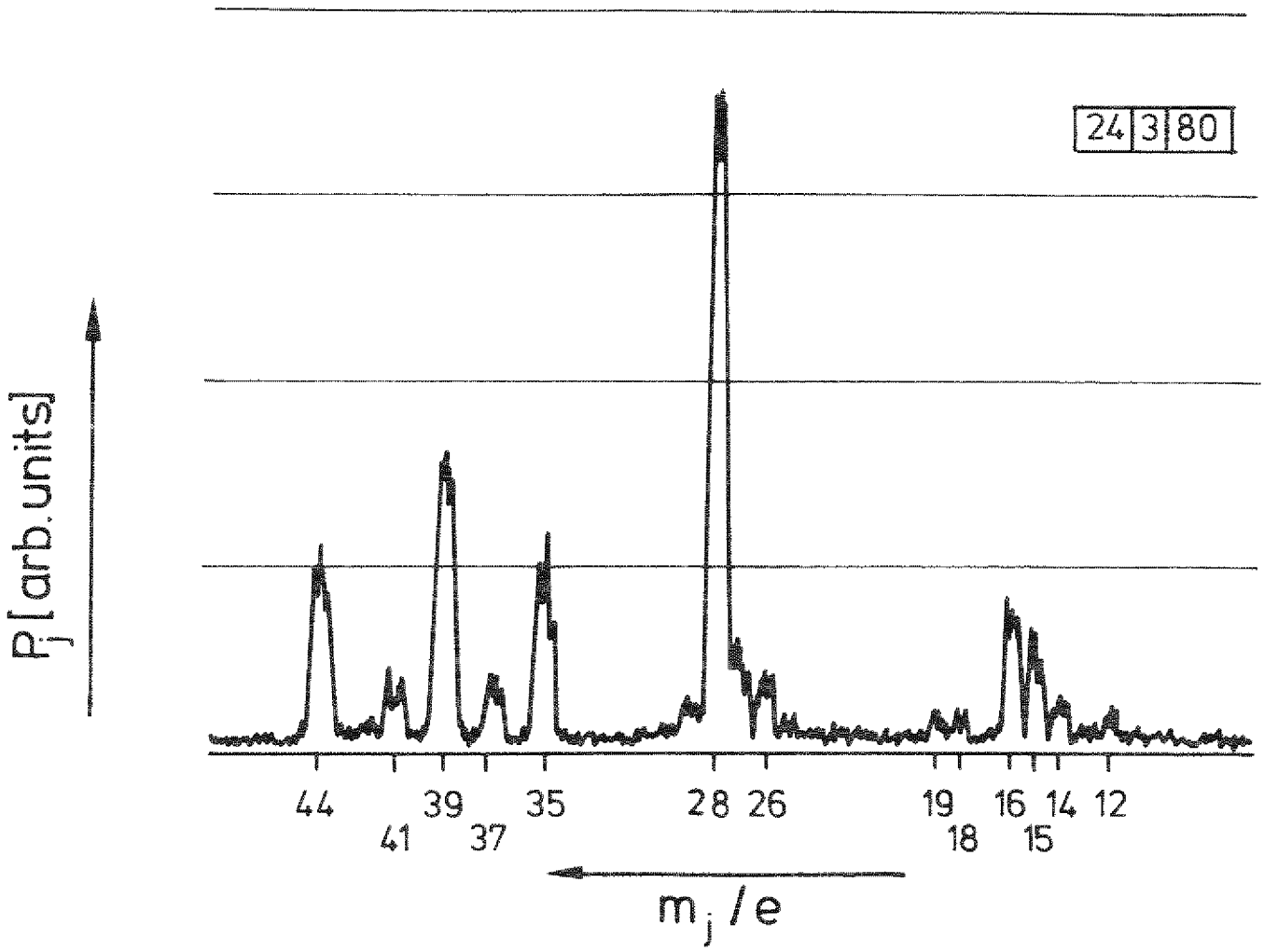

Fig 2.
Residual gas spectrum in the QBP; T_W = 30 ^{o}C, P_{tot} = 1 x 10^{-9} Torr,
the partial pressure of CO (largest impurity peak) is 1.7 x 10^{-11} Torr.

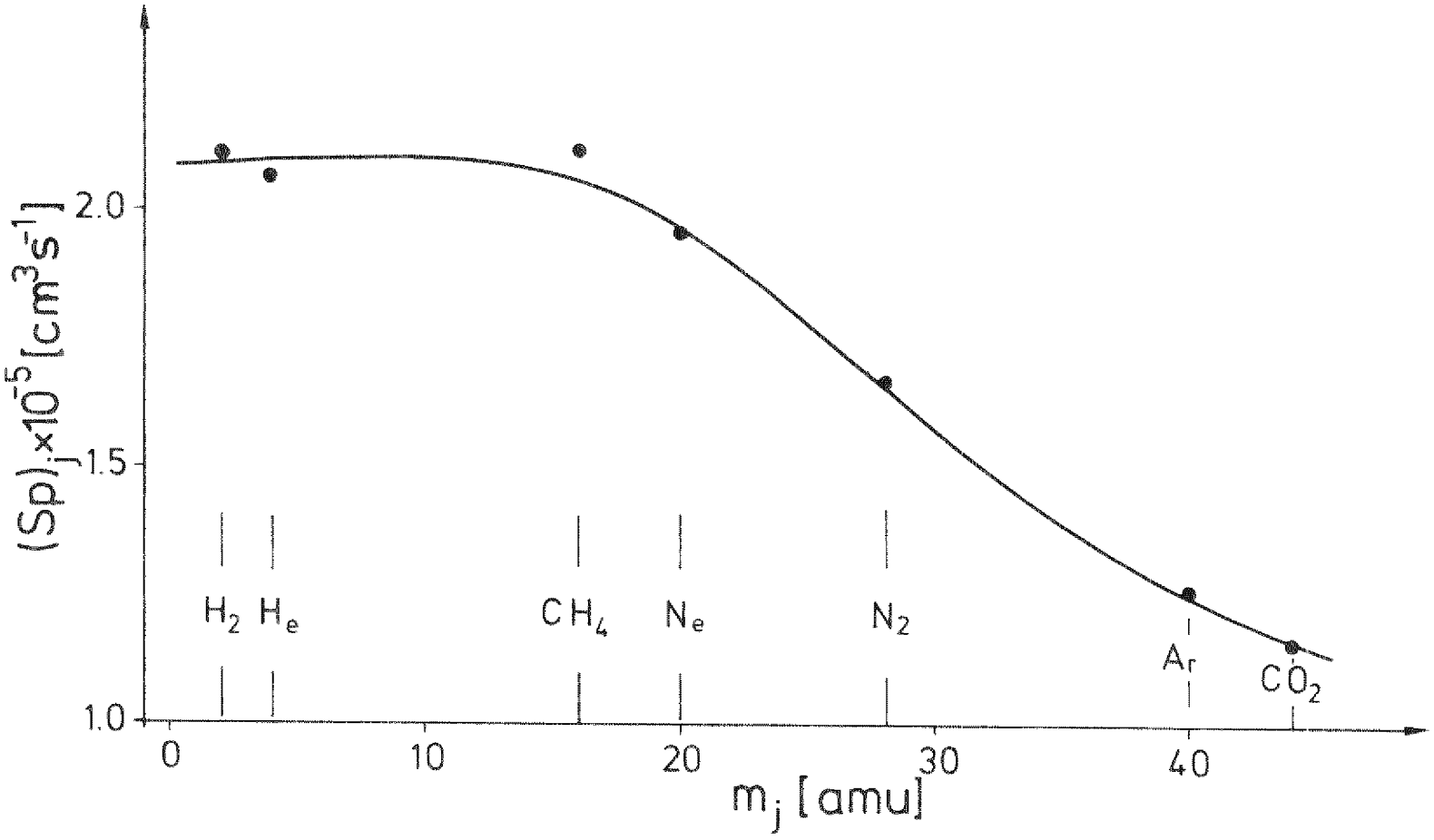

Fig 3.

Pump speeds $(Sp)_j$ for gases of different masses m_j at 200 °C and at $P_j = 6{,}6 \times 10^{-2}$ Pa

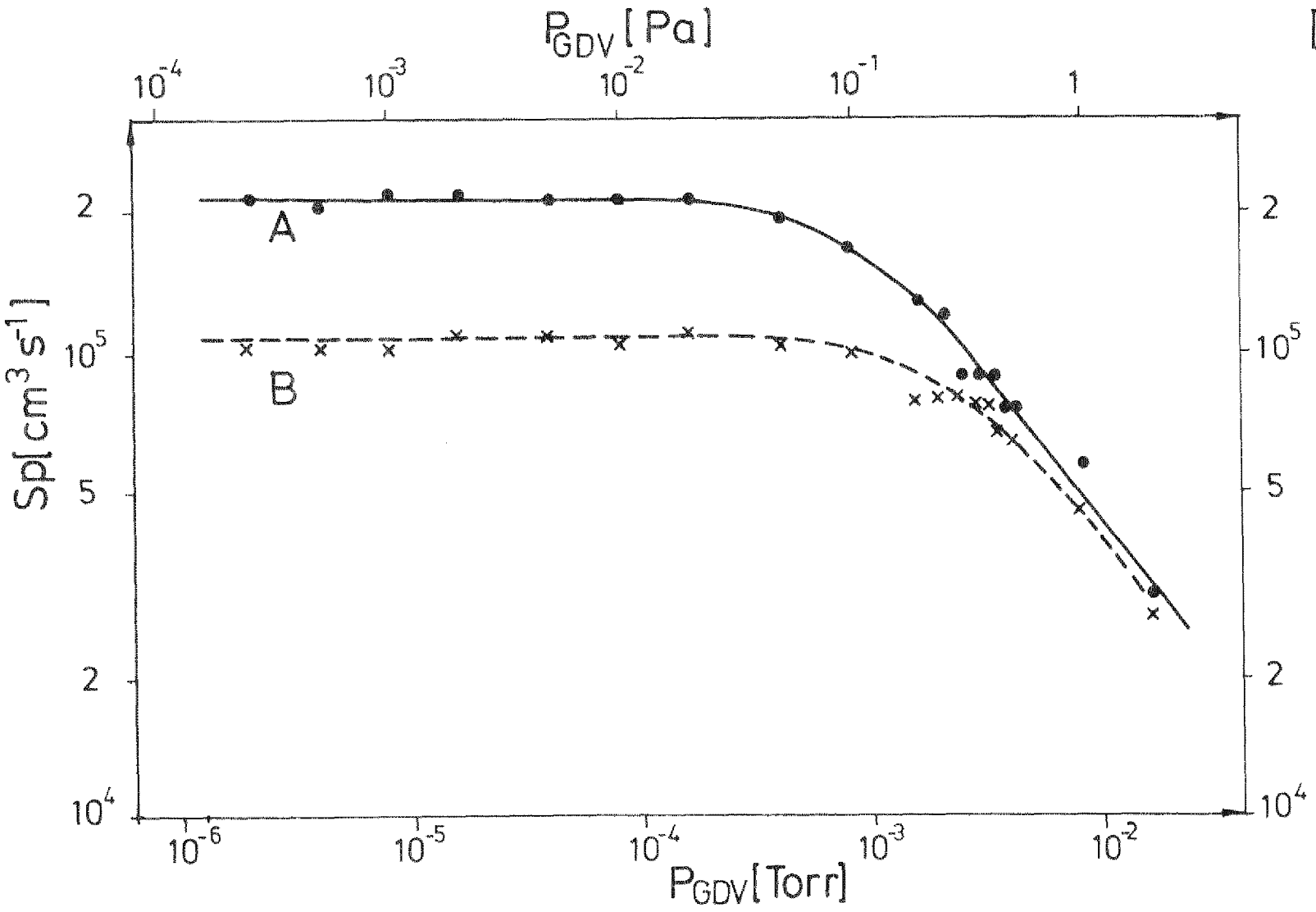

Fig 4.

Pump speed for H_2 as a function of pressure

A: TV1 open B: TV1 closed

Table 1. Pump speeds $(Sp)_j$ and calibration factors K_j

Substance j	$(Sp)_j$ (cm^3s^{-1})	K_j (Torr/Scale unit)	
		GDV	QBP
H_2	$2{,}12 \times 10^5$	$9{,}1 \times 10^{-8}$	$9{,}0 \times 10^{-10}$
He	$2{,}07 \times 10^5$	$4{,}3 \times 10^{-7}$	$4{,}0 \times 10^{-9}$
NH_3	$(2{,}08 \times 10^5)$	$4{,}1 \times 10^{-7}$	$1{,}6 \times 10^{-9}$
CH_4(m = 15)	$2{,}12 \times 10^5$	$4{,}6 \times 10^{-7}$	$1{,}7 \times 10^{-9}$
H_2O	$(2{,}06 \times 10^5)$	$3{,}5 \times 10^{-7}$	$1{,}3 \times 10^{-9}$
Ne	$1{,}96 \times 10^5$	$1{,}1 \times 10^{-6}$	$5{,}1 \times 10^{-9}$
N_2	$1{,}33 \times 10^5$	$3{,}8 \times 10^{-7}$	$1{,}2 \times 10^{-9}$
Ar	$1{,}26 \times 10^5$	$3{,}0 \times 10^{-7}$	$1{,}0 \times 10^{-9}$
CO_2	$1{,}16 \times 10^5$	$3{,}7 \times 10^{-7}$	$1{,}1 \times 10^{-9}$

K_j was measured for the various substances with the same sensitivity of the RGA in the QBP. The measurements relating to the GDV were made with a throttle factor of 100 for H_2 over TV 2. The values of $(Sp)_j$ were measured at a pressure of $\approx 3 \times 10^{-4}$ torr and at T_W = 200 °C. For NH_3 and H_2O, interpolated values are given in brackets.

III. EXPERIMENTAL PROCEDURES

III.1. Rf and RG discharges in hydrogen at low pressures

The cleaning efficiency of a glow discharge decreases rapidly when the hydrogen pressure is increased above a few mtorr (cf. § VI. 5 and 6 and § VII). This results to a large extent from the reduced pump speed. Hollow cathode discharges with plain metal anodes are initiated,in vessels of the size of TEXTOR and JET, when the hydrogen pressures reaches a few times 10^{-2} torr. Once a plasma has been produced, the pressure can be reduced down to about 10^{-2} torr, after which the discharge quenches. The relatively high operating pressure limits the pump speed when turbomolecular pumps are used.

When [4, 5a] a naked radio frequency coil is used as anode, the minimum pressure at which the discharge can be initiated is lowered. The RG discharge can moreover be maintained at much lower pressures without quenching. The available pump system is used more efficiently.

Operation at low discharge currents and measurements in the absence of any discharge current (pure rf plasma) become possible. The extended operation range facilitates the interpretation of the observed phenomena. In what follows, we briefly summarize some characteristic properties of such rf and RG discharges.

III.1.a. The rf discharge

The minimum pressure P_I at which the rf discharge can be initiated and the pressure P_Q at which it quenches are plotted on fig. 5a as functions of the applied rf power W_{rf}. Investigations at hydrogen pressures as low as one millitorr are possible in a broad rf power range even in our relatively small vessel (radius 22,5 cm). Low rf powers (a few Watt) suffice to maintain the discharge in this pressure domain. An increase of W_{rf} beyond a few tens of Watt does not extend the range of working pressures further downwards.

Fig. 5b shows how the floating potential U_{fl} of the rf plasma and the product of the sticking factor α times the flux density φ_i of hydrogen to the wall vary at $P_2 = 2.8 \times 10^{-3}$ torr as functions of the applied rf power. The method to measure $\alpha\varphi_i$ is described in § IV. 1.

The floating potential, of the order of 7 to 13 volts, depends weakly on W_{rf}. It decreases slowly with increasing pressure. Sputtering of wall material by gas ions accelerated in the voltage drop should be negligible. Some sputtering is however expected at the rf coil where high rf voltages are applied.

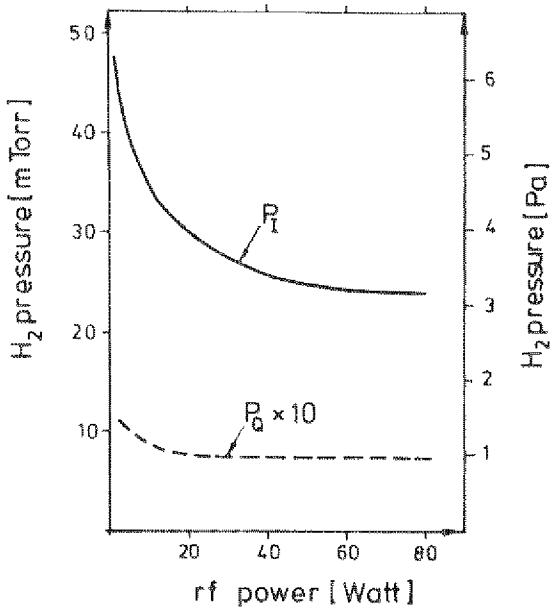

Fig 5a.

Lowest pressures P_I and P_Q at which hydrogen plasmas can be ignited and sustained respectively, using rf power only.

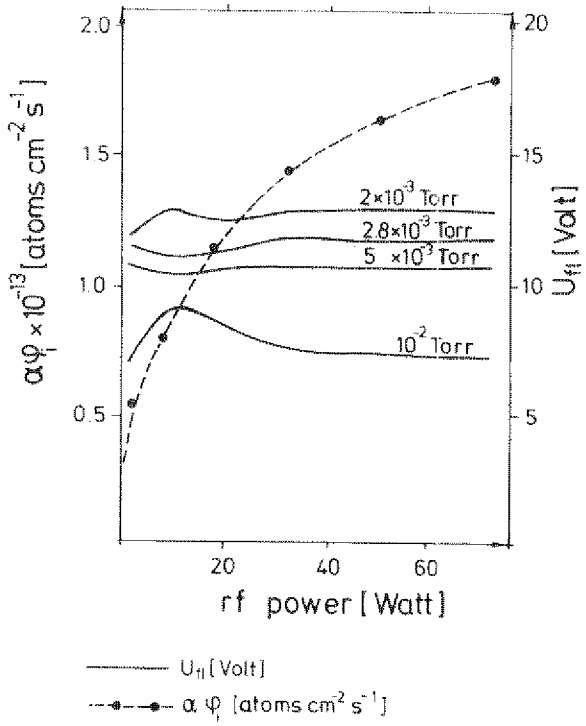

Fig 5b.

Floating potential U_{fl} and flux density of hydrogen into the wall as a function of the rf - power W_{rf} of the radiofrequency discharge

As will be discussed in § VII, the rates at which oxides and carbides are transformed into gaseous products increase rapidly with the flux density $\propto \varphi_i$ of hydrogen penetrating into the material. This flux density becomes larger when the rf power is increased (approximately proportional to $W_{rf}^{1/2}$). Operation with large rf power appears thus to be advantageous if a pure rf cleaning of the wall is aimed at. The effect is however partially compensated by an increased destruction of the gaseous products in the plasma (§ IV.2).

The mean free paths are large in the low pressure domain where the highest cleaning rates are obtained; to achieve a more or less uniform cleaning efficiency around the torus by means of rf discharges alone, a considerable number of rf coils should be used. The cleaning of portholes and sidearms, if desired, introduces additional complications. Glow discharges should be better adapted to these requirements.

III.1.b) The RG discharge

i) Initation and quenching pressures

The pressure P_I at which the RG discharge can be initiated is plotted in fig. 6,a as a function of the dc voltage U_a which is initially applied between the RFC and the walls of the GDV. The curves correspond to different power levels W_{rf} supplied by the rf generator. Fig. 6b is a similar plot showing the lowest pressure P_Q at which the discharge can be maintained. For these measurements, the value of the load resistor had been increased to 1 kΩ . For all other measurements a resistor of 250 Ω was used.

The rf discharge allows, already at low power levels, to extend the pressure domain wherein a RG discharge can be maintained down to a few mtorr. This is lower by a factor of more than twenty than in a pure glow discharge (fig. 7). As we shall see in § VI.4, our results suggest that the cleaning discharge should be operated with RG current densities of 10-25 μA cm^{-2}. The latter value corresponds to a total current of 0.5 A for our vessel and to an initially applied voltage of 600 V. An rf power level of 32 Watt has therefore been chosen for all except the first measurements described in the following paragraphs.

Fig. 7) summarizes the P_I and P_Q values measured for this particular condition. The minimum pressure for plasma ignition is low, but still the pressure must be increased during a short time by a factor of five to initiate the discharge. This is achieved by reducing the pump speed, by short puffs of hydrogen or of some inert gas, for instance helium neon or argon.

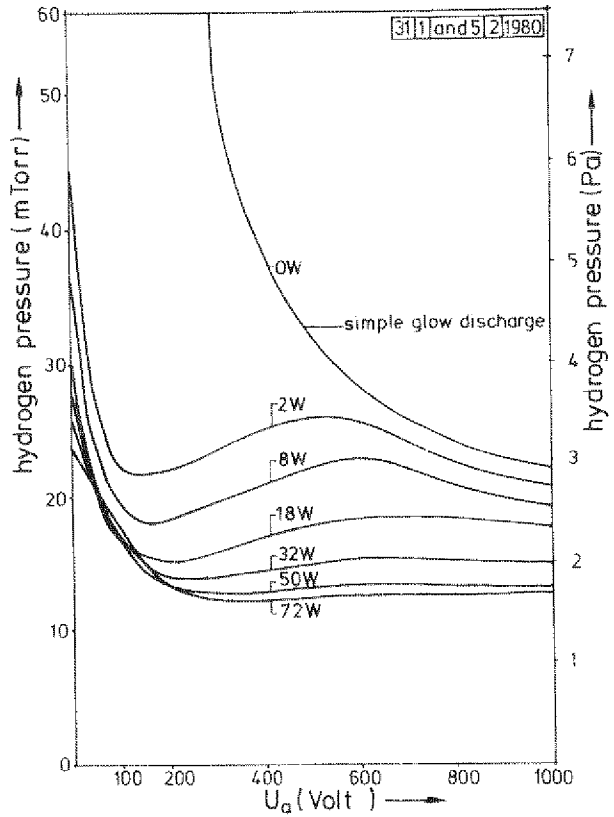

Fig. 6a

Minimum pressure P_1 required to initiate the RG discharge in H_2 as a function of the initially applied dc voltage U_a for different values of the rf power W_{rf}

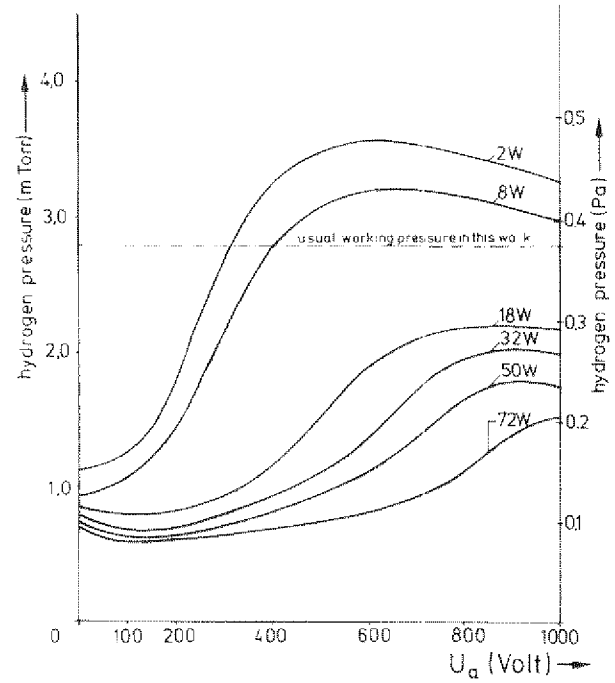

Fig. 6b

Minimum pressure P_Q at which an RG plasma can be sustained, as a function of the initially applied voltage U_a (load resistor 1 KΩ) for different values of the rf power.

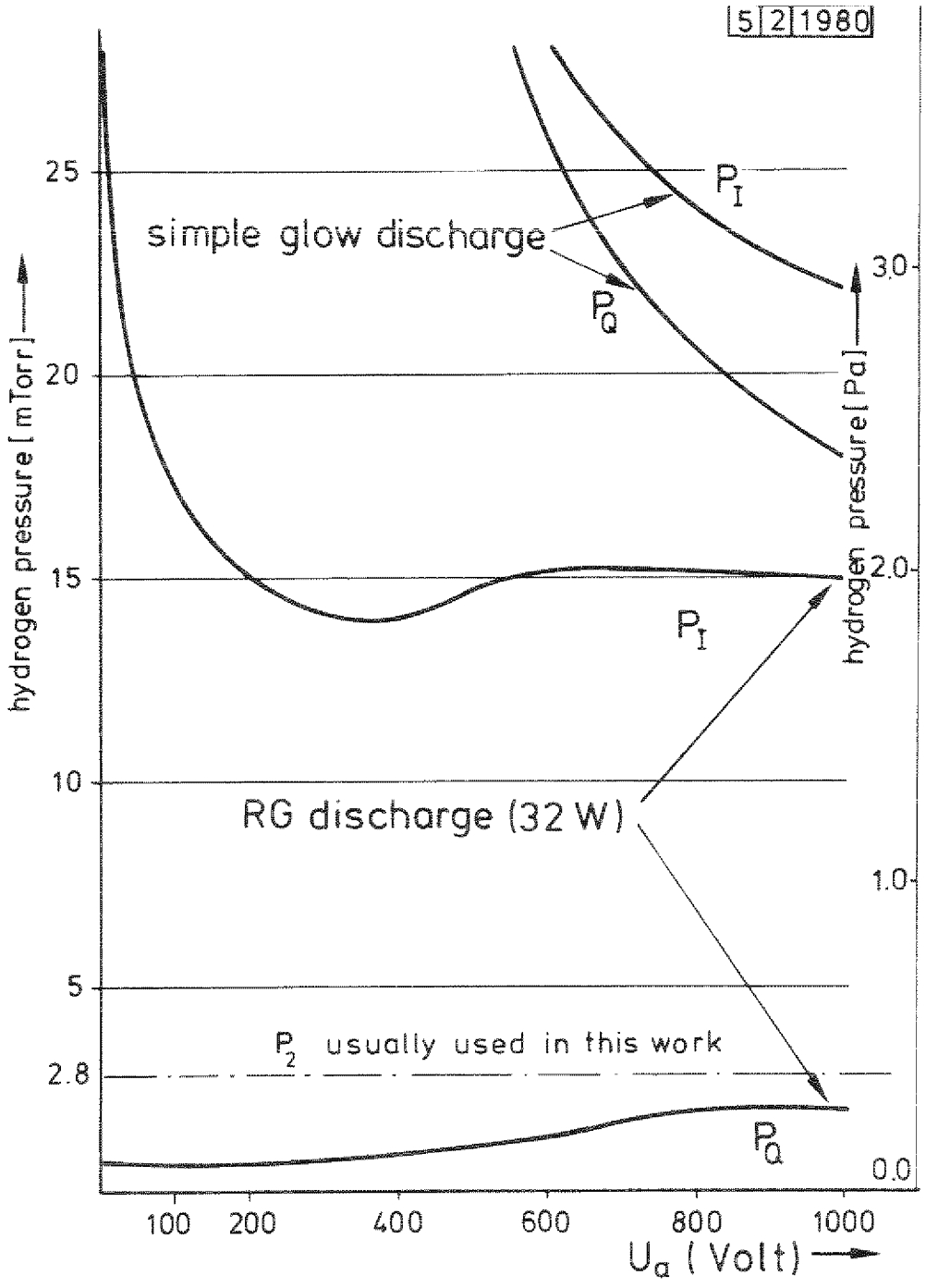

Fig 7.

Lowest pressures P_I and P_Q at which a plasma can be initiated and sustained respectively in a simple glow discharge and in an RG discharge with 32 W of rf power. The abcissa is the dc voltage U_a initially applied across the discharge (load resistor 1 kΩ).

ii) Influence of the rf power level

The current-voltage characteristics of the RG discharge and the floating potential U_{fl} of the plasma at a hydrogen pressure of 4×10^{-3} torr are shown on fig. 8 for different power levels W_{rf}. Additional measurements with W_{rf} = 18 and 8 Watt have not been plotted here to avoid overcrowding the figure; they fall smoothly between the curves obtained with W_{rf} = 32 and 3 Watt. The inset picture describes how U_{GD} and U_{fl} vary with W_{rf} at this pressure when I_{GD} = 0,5 A.

Except in the domain of very low discharge current (< 50 mA) and at very low pressures, the following behaviour is observed:

- U_{GD} and U_{fl} increase slowly from 350 V to 500 V when I_{GD} is increased from 0.1 to 1.8 A,
- the difference U_{GD}-U_{fl} is usually equal to 20 V or smaller, showing a pronounced sparing of the anode by using the RF plasma as virtual anode; it increases to 50 V at low W_{rf} values,
- the variation of U_{GD} and U_{fl} as a function of W_{rf} is small (< 10 % when W_{rf} increases from 3 to 72 Watt): increased rf powers do not lower the plasma potential, i.e. reduce the sputter yield.

iii) Influence of the pressure

The current-voltage caracteristics of the RG discharge and the variation of U_{fl} with I_{GD} are plotted on fig. 9 for different values of the hydrogen pressure at a rf power level of 32 Watt:

At the lower pressures, as expected from fig. 6b, the discharge quenches when a limiting current is reached. In this pressure range, U_{GD} and U_{fl} are higher than at moderate pressures. The potential difference U_{GD}-U_{fl} is large (large anode potential drop), due to the small anode area.

From 3×10^{-3} torr upwards, the full available range of currents can be explored: the shape of the I-U-characteristics varies little with pressure but U_{GD} and U_{fl} decrease when the pressure is raised. The difference U_{GD}-U_{fl} decreases also with increasing pressure; it changes sign when $P_2 > 2 \times 10^{-2}$ torr.

The floating potential of the plasma decreases by 15 % when the pressure is raised from 3×10^{-3} to 8×10^{-3} torr. This should reduce the sputter rates v_{sp} from the vessel walls. The pump speed is however higher at lower pressures (fig. 4), decreasing (§ VI, 6) the clean-down time τ_{cd} during which the wall has to be exposed to the accelerated ions of the RG discharge. The contamination (e.g. of the windows) by sputtering during the discharge is reduced when the product $v_{sp}\ \tau_{cd}$ is minimized. This is best achieved at the lower pressures.

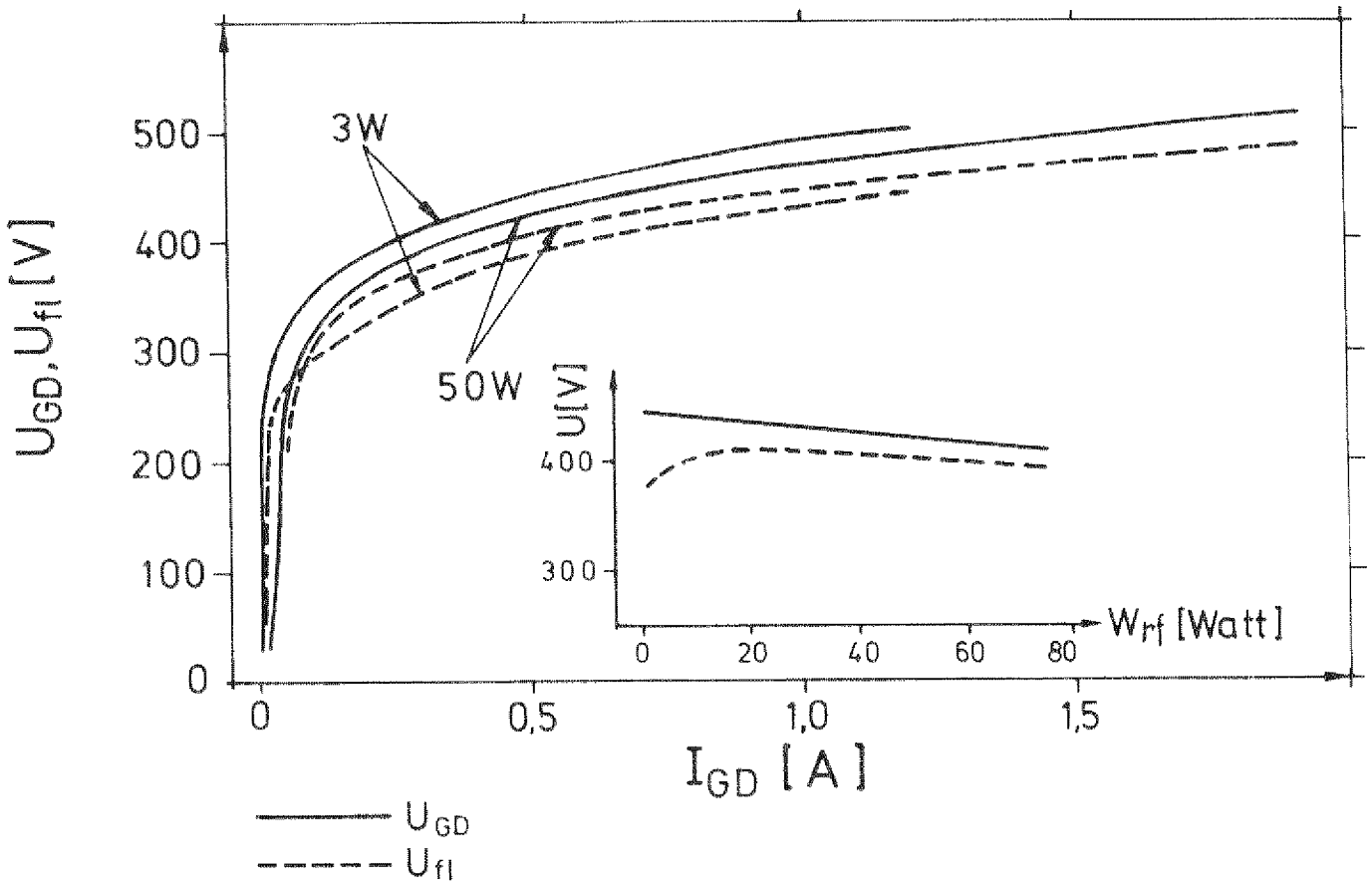

Fig 8

Voltage (U_{GD}) - current (I_{GD}) characteristics and floating potential (U_{fl}) at $P_2 = 4 \times 10^{-3}$ Torr for two typical values of the rf power W_{rf}
insert variation of U_{GD} and U_{fl} as a function of W_{rf} for $I_{GD} = 0.5$ A

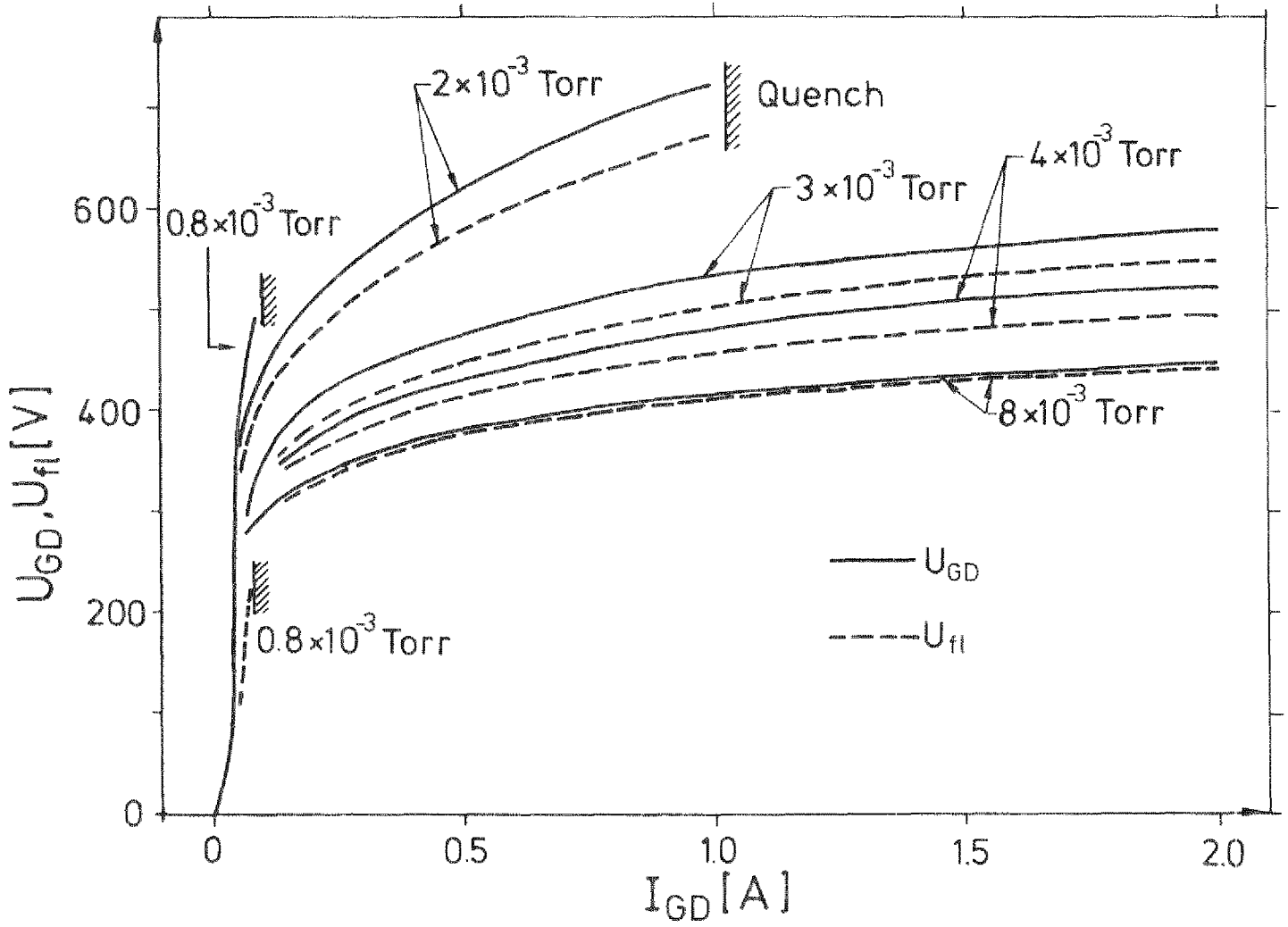

Fig.9.

Voltage (U_{GD}) - current (I_{GD}) characteristics and floating potential (U_{fl}) for RG-discharges at W_{rf} = 32 Watt and various H_2 pressures (load resistor 250 Ω)

iv) Comparison of RG and simple glow discharge and effect of admixed inert gases.

The current-voltage characteristics (and floating potential curves) measured at higher pressures in a simple glow discharge in H_2 are compared in fig. 10 with those observed in a typical RG discharge. Here again, unless a large effort is devoted to optimize the pump system, the product $v_{sp}\ \tau_{cd}$ is larger when the simple glow discharge is used.

The current-voltage characteristics of the RG discharge and its floating potential have also been measured when noble gases such as He or Ne are added to the hydrogen (see e.g. fig. 11). They differ little from the pure H_2 case. Sputtering, in particular in the case of admixed neon, could raise serious problems as already pointed out in [7].

III.1.c) Cleaning of the ports and side-arms

Under the usual RG discharge conditions described in § II.2.b, the plasma is concentrated in the main volume of the GDV. The discharge can be extended into the narrower channels offered by the ports and side-arms: when the pressure of H_2 is increased to several times 10^{-2} torr, it reaches the larger (15 cm diameter) portholes; at 10^{-1} torr it penetrates into the portholes of 6 cm diameter. For this it is advantageous to increase I_{GD} up to 1.5 A and to use the LN_2 cryopump, in order to maintain a large pump speed for H_2O.

§ III.2. Temperature of the quadrupole by-pass and of the connection tube

It is difficult to measure quantitatively the concentrations of gaseous species such as water, hydrocarbons and carbon oxides in a background of hydrogen when a residual gas analyser (RGA) is used. This results [4, 5] from the dissociation of hydrogen molecules on the hot filaments of the RGA and of the ion manometer; the resulting H-atoms, impinging onto surrounding walls, produce gaseous impurities by chemical reactions with the surface contaminants. These impurities, created in situ within the QBP, must be distinguished from the ones which originate from the reaction chamber (GDV or a toroidal vessel) and which stream into the analyser. The problem is serious since, in order to keep the pressure in the QBP sufficiently low for the RGA to operate properly, a throttle ratio of about 150 must be established over TV 2. Increases of the partial pressures of H_2O, CH_4 or CO of, say, 10^{-8} torr in the QBP can then be erroneously attributed to increases of 1.5×10^{-6} torr in the GDV!

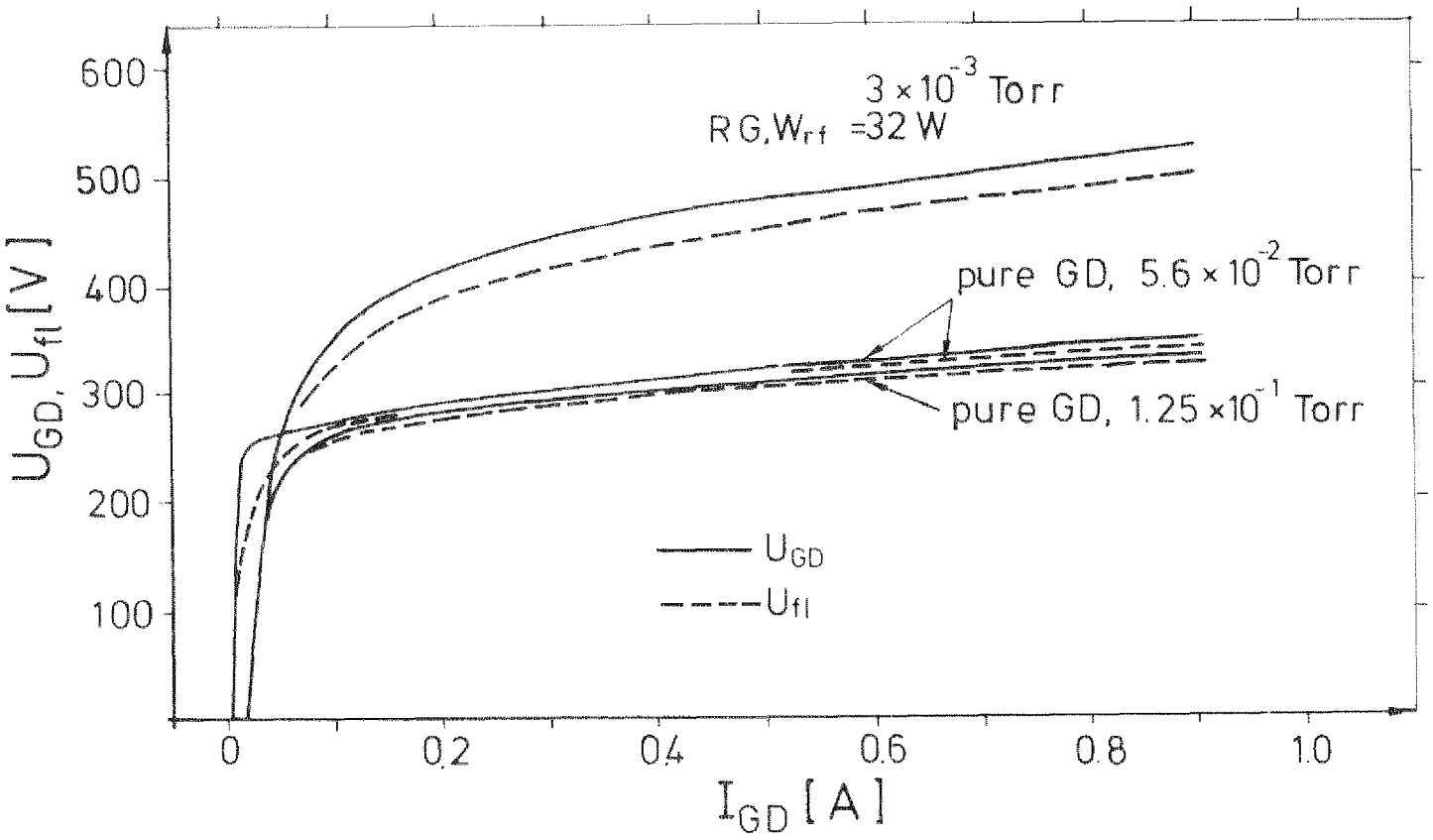

Fig 10.

Voltage (U_{GD}) - current (I_{GD}) - characteristics and floating potential (U_{fl}) of RG discharge and of a pure glow discharge (at higher pressures)

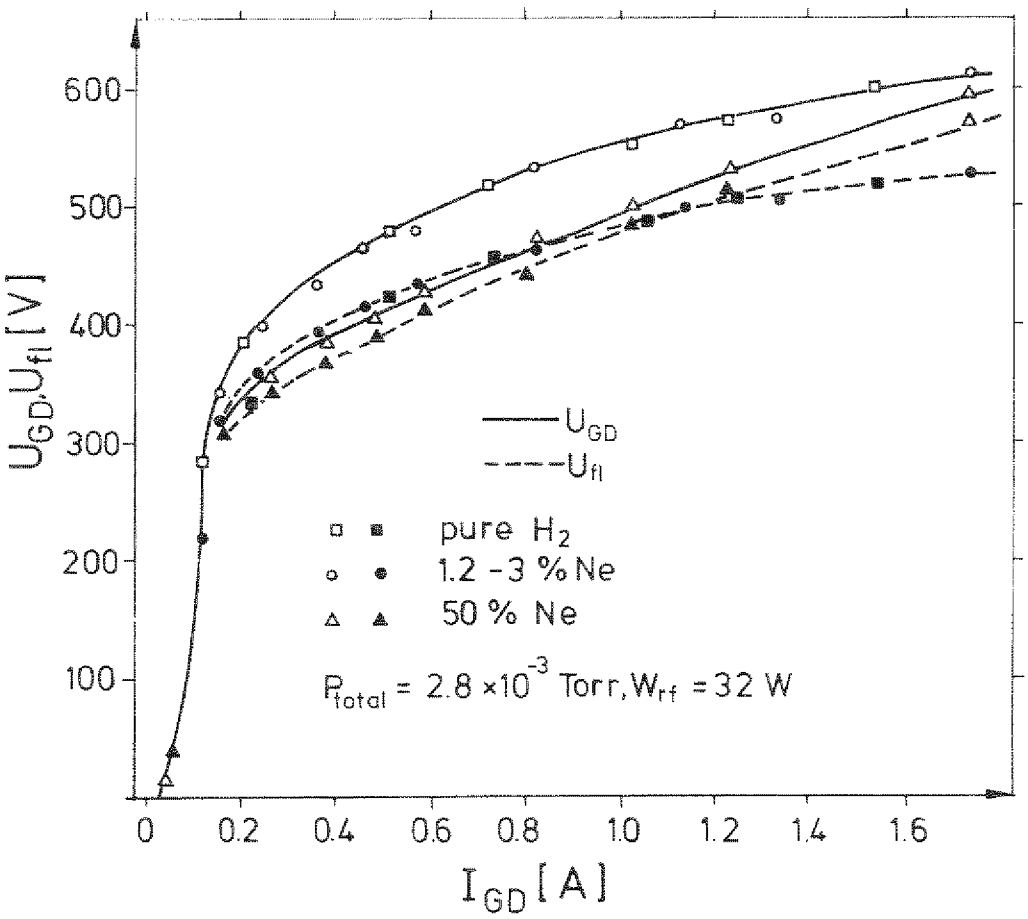

Fig 11.

Voltage (U_{GD}) - current (I_{GD}) - characteristics and floating potential (U_{fl}) for RG discharges with various H_2-Ne mixtures

In the case of H_2O, a further problem is encountered, particularily when the walls of the QBP and of the CT are at low (e.g. room) temperature: rapid variations of the water pressure P_{18} cannot be followed accurately. This results probably from the adsorption-desorption equilibrium between the H_2O vapour and the partly oxidized surface layers of the QBP and CT; an increase of P_{18} increases the amount of water adsorbed; a decrease of P_{18} would decreases it. The resulting time lag buffers out the rapid variations of P_{18}. This phenomenon, which in this interpretation would be analogous to the one which occurs along a gas chromatographic column, makes accurate measurements of rapid P_{18} changes in the reaction chamber impossible.

III.2.a) Effect of the hydrogen pressure in the QBP

Fig. 12 illustrates the temporal variations of the partial pressures of water (P_{18}), methane (P_{15}) and CO (P_{28}) which arise at room temperature when hydrogen is introduced directly into the QBP: P_{15} increases quasi-instantaneously by a factor of 30 and remains almost constant thereafter; P_{28} increases by a factor of 6 within one minute; a further slow increase (10 %) is observed during one or two hours. In the case of H_2O, the effect is more serious: P_{18} increases at first rapidly by a factor of 8; it continues to increase slowly thereafter, towards an asymptotic value which is approximately one hundred times larger than the initial outgasing value; the characteristic (exponential) equilibration time is about 4 hours. The same phenomena had been observed [4] with a quadrupole analyser and an ion manometer surrounded by metallic walls at higher temperatures. The equilibration time is much shorter at higher temperatures: values of the order of 2 minutes have been measured at 300 ^{o}C.

In selecting the working temperature of the QBP, it appeared important to ensure that wall oxidation effects discussed in § VII be kept at a low level; this has led us to choose a temperature of ca. 160 ^{o}C for the measurements. The resulting response of the RGA to the introduction of pure H_2 is shown on fig. 13. About 30 minutes are necessary for the H_2O signal to reach 95 % of its stationary amplitude.

III.2.b) Temperature of the connection tube

At the beginning of the experiment shown on fig. 14, H_2O has been introduced into the QBP via TV 2. The quadrupole by pass and the connection tube were at room temperature; P_2 was negligibly small. The signal rose at first rapidly to about 35 % of its final value; thereafter a slow exponentiation towards the final equilibrium value occurred. The exponentiation time is 75 minutes. Most of the time lag appears to result from phenomena occuring on the walls of the QBP itself:

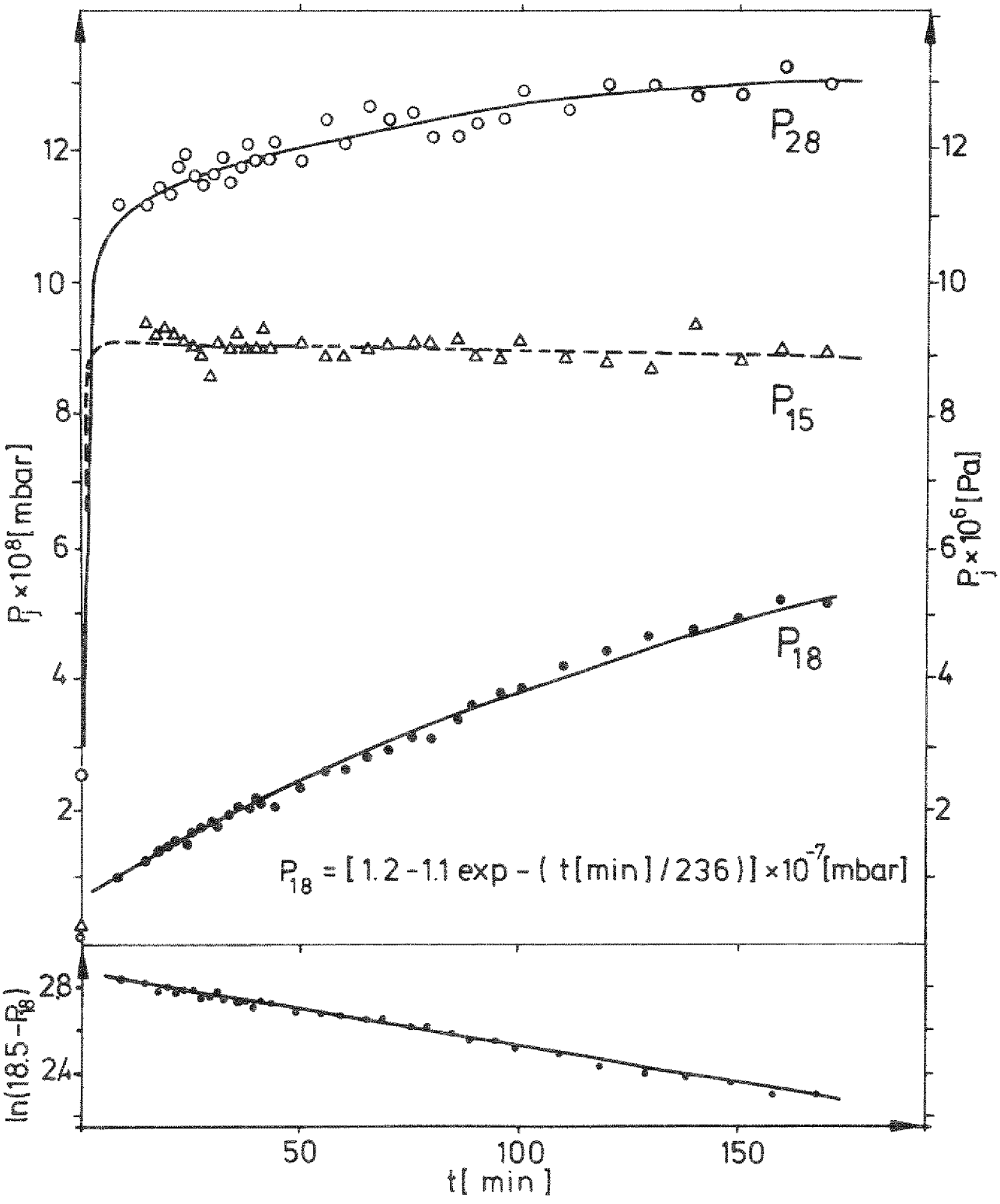

Fig 12.

Evolution of the partial pressures of methane (P_{15}), water (P_{18}) and CO(P_{28}) after direct admission of pure H_2 in the RGA
T_W = 35 °C, P_2 = 1.62 x 10^{-5} mbar (21/1/80).

21 1 80

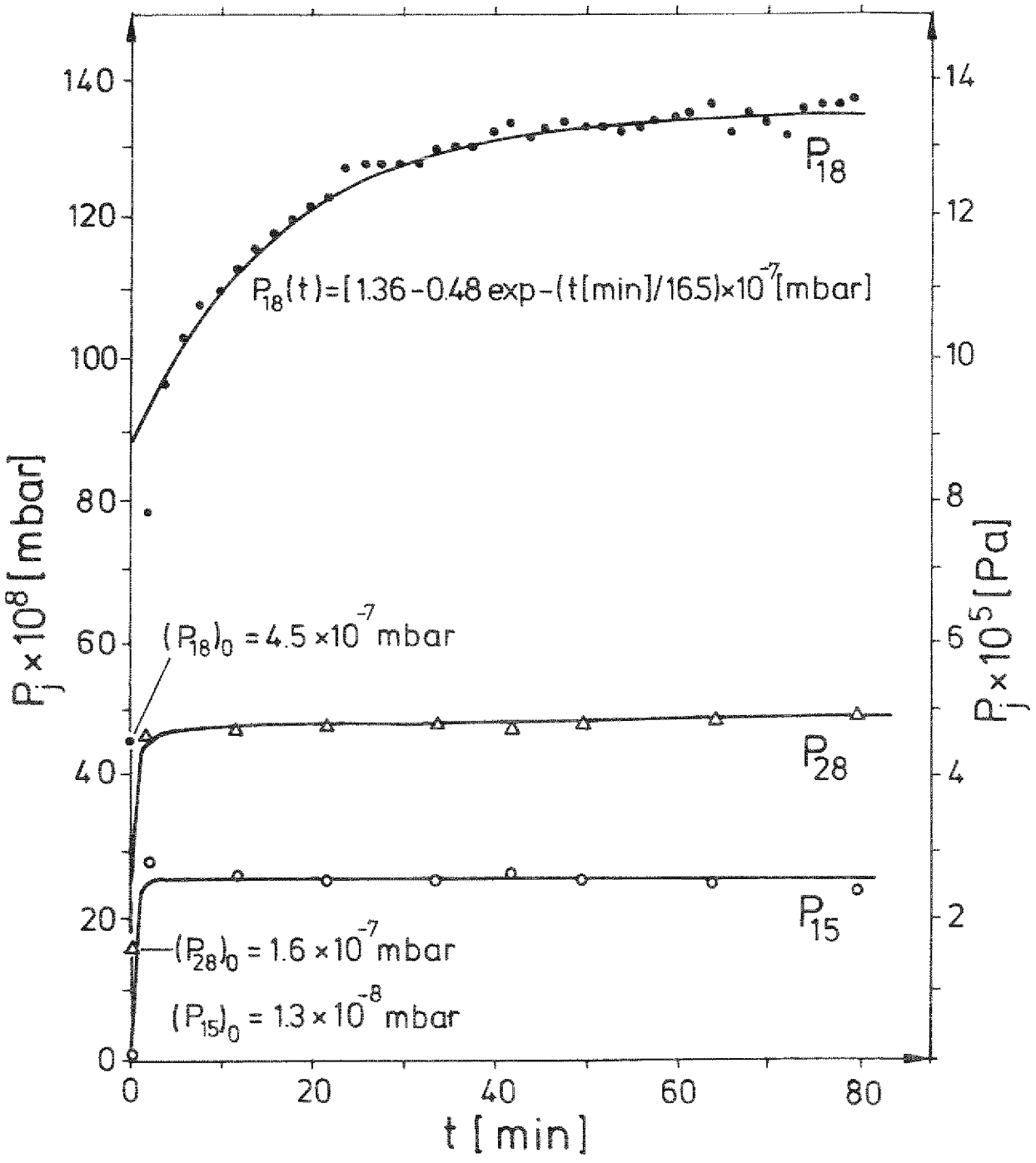

Fig 13.

Evolution of the partial pressures of methane (P_{15}), water (P_{18}) and CO(P_{28}) after direct admission of pure H_2 in the RGA T_W = 160 °C, P_2 = 1.62 x 10^{-5} mbar

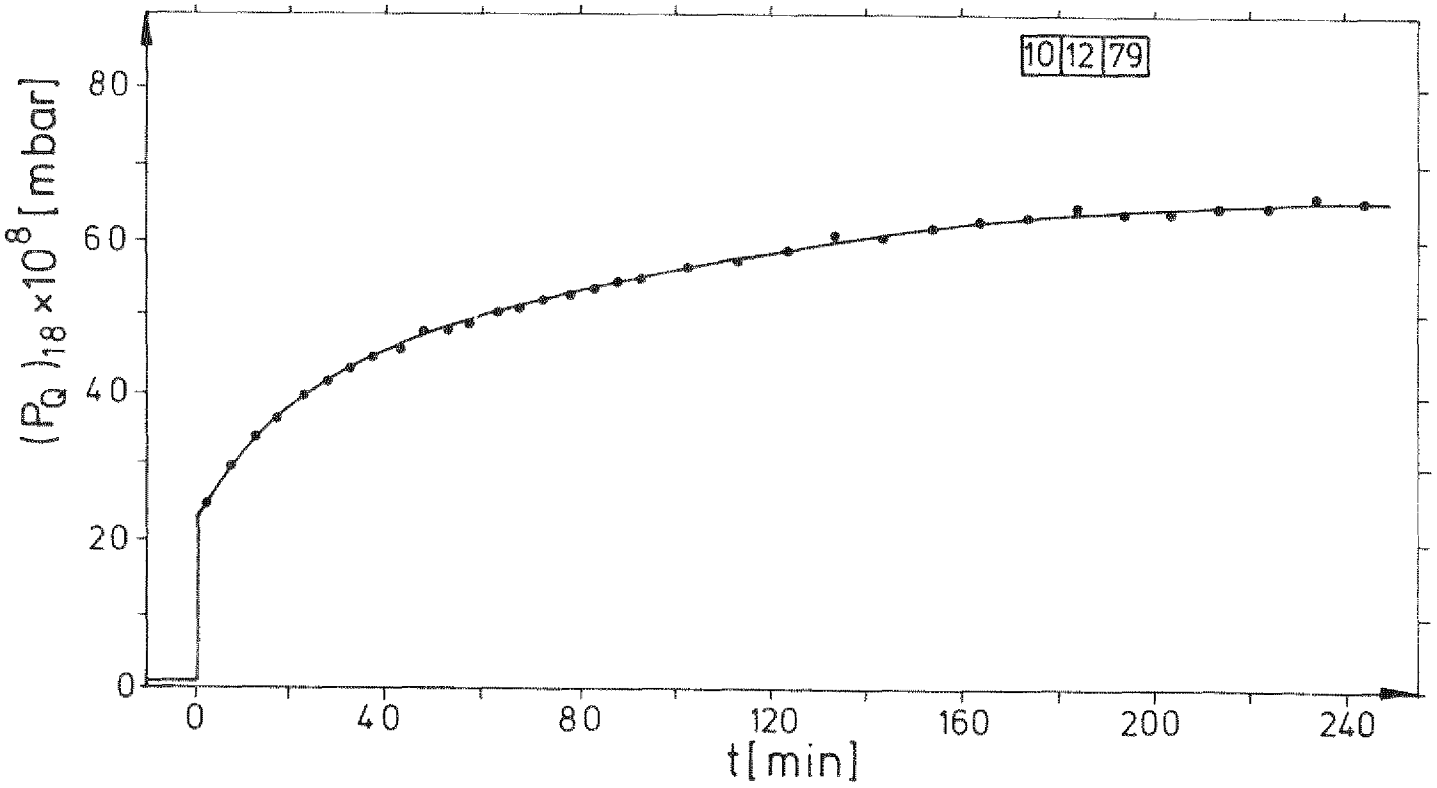

Fig 14.

Variation of the H_2O signal in the RGA after introduction of H_2O vapour at constant inlet pressure through TV2 (P_2 = 3.4 x 10^{-9} mbar). QBP and CT at room temperature

When the temperature of the quadrupole by-pass was raised to 160 °C, the exponentiation time τ_e was reduced to three minutes, although the 70 cm long connection tube CT was still at 40 °C. Still, if one accepts that accurate measurements can first be made after times longer than 3 τ_e, phenomena evolving on a time scale shorter than 10 minutes cannot be followed quantitatively when the CT is at that temperature; τ_e decreases when the temperature of the CT is raised (fig. 15). For our measurements, we have limited (again in order to reduce oxidation effects) the value of T_{CT} to 180 °C. This leads to τ_e = 0.9 minutes. Phenomena which change with characteristic times of 2 1/2 minutes can then be followed. Fig. 16 shows how a rectangular pulse of P_{18} applied just below TV 1, is transmitted to the QBP. Even with "improved" conditions, rapid variations are strongly distorted.

III.3. Beginning and end of a cleaning run

As discussed above, the gaseous impurities set free by the glow discharge must be distinguished from those which are released in the QBP when hydrogen is introduced into it. The time lags in the evolution of the water signals (figs. 13 and 16 for example) must be minimized. Finally, the effect of the short pressure rise produced in the GDV to ignite the dicharge (§ III.1.b,i) must be suppressed: The resulting increase of the hydrogen pressure in the QBP, if TV 2 is partly opened, and if the filaments in the QBP are hot, produces a short but large increase of the impurity release in the by-pass which could mistakenly be attributed to phenomena occuring within the GDV.

The procedure used to minimize these effects has been to maintain the QBP and connection tube at 160 °C and 180 °C respectively during the measurements. The residual gas spectra are first measured in the GDV and QBP. Keeping TV 2 closed, pure hydrogen is then introduced directly via E 1 and E 3 into the two parts of the apparatus at the pressures later required for the cleaning phase (e.g. 2.8×10^{-3} and 1.6×10^{-5} torr respectively); after about 30 minutes (cf.fig 13), the residual gas signals in the QBP have become constant; these values are used as the true zero signals of the QBP.

Within a few seconds E 3 is closed and TV 2 opened in such a way that hydrogen leaks into the QBP over the GDV at the same pressure as before. After a few minutes (cf. fig. 16), a new stationary mass spectrum is obtained, from which the outgasing rate in the GDV is deduced.

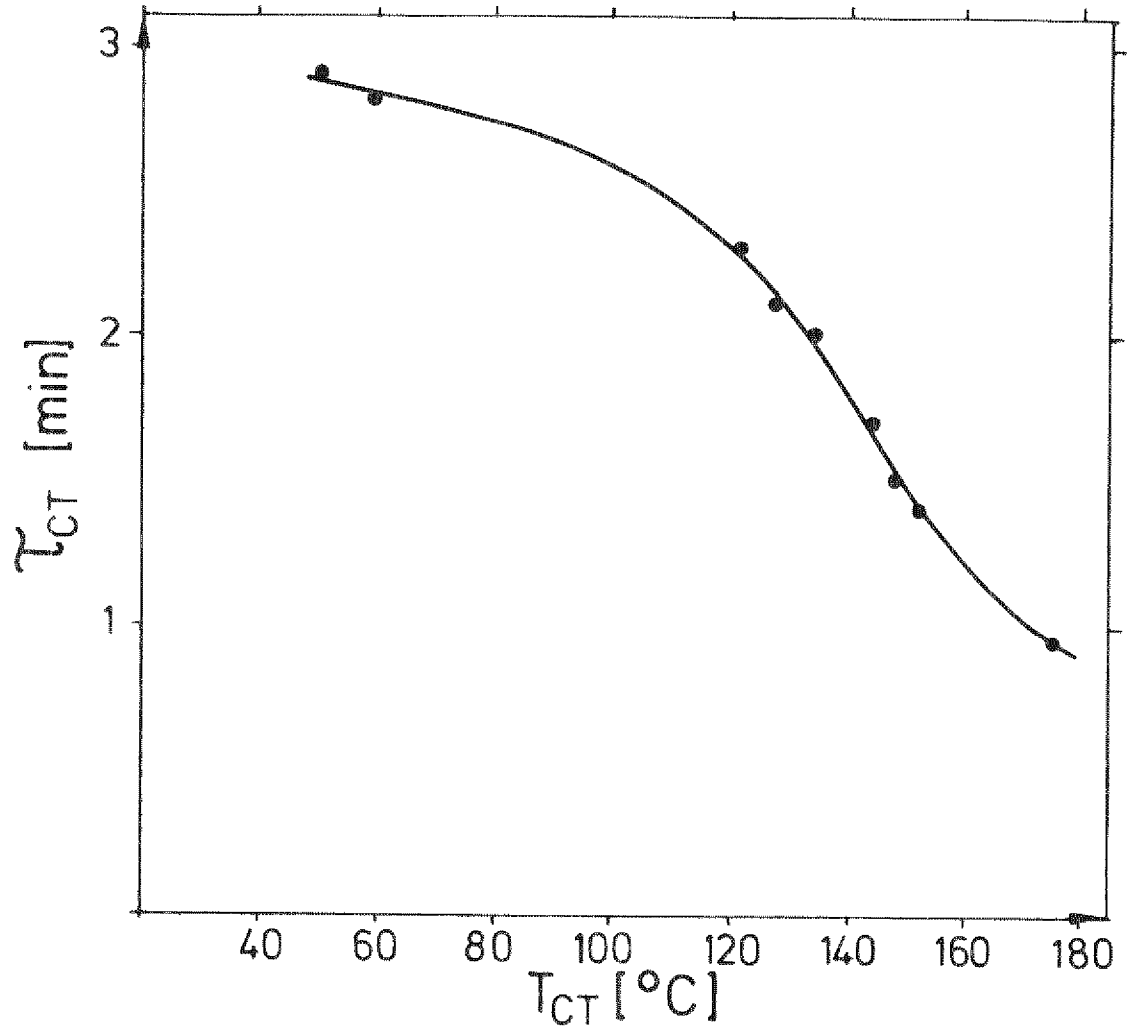

Fig 15.

Variation of the charcteristic time τ_{CT} for water vapour transfer across the connection tube CT as a function of its temperature T_{CT}

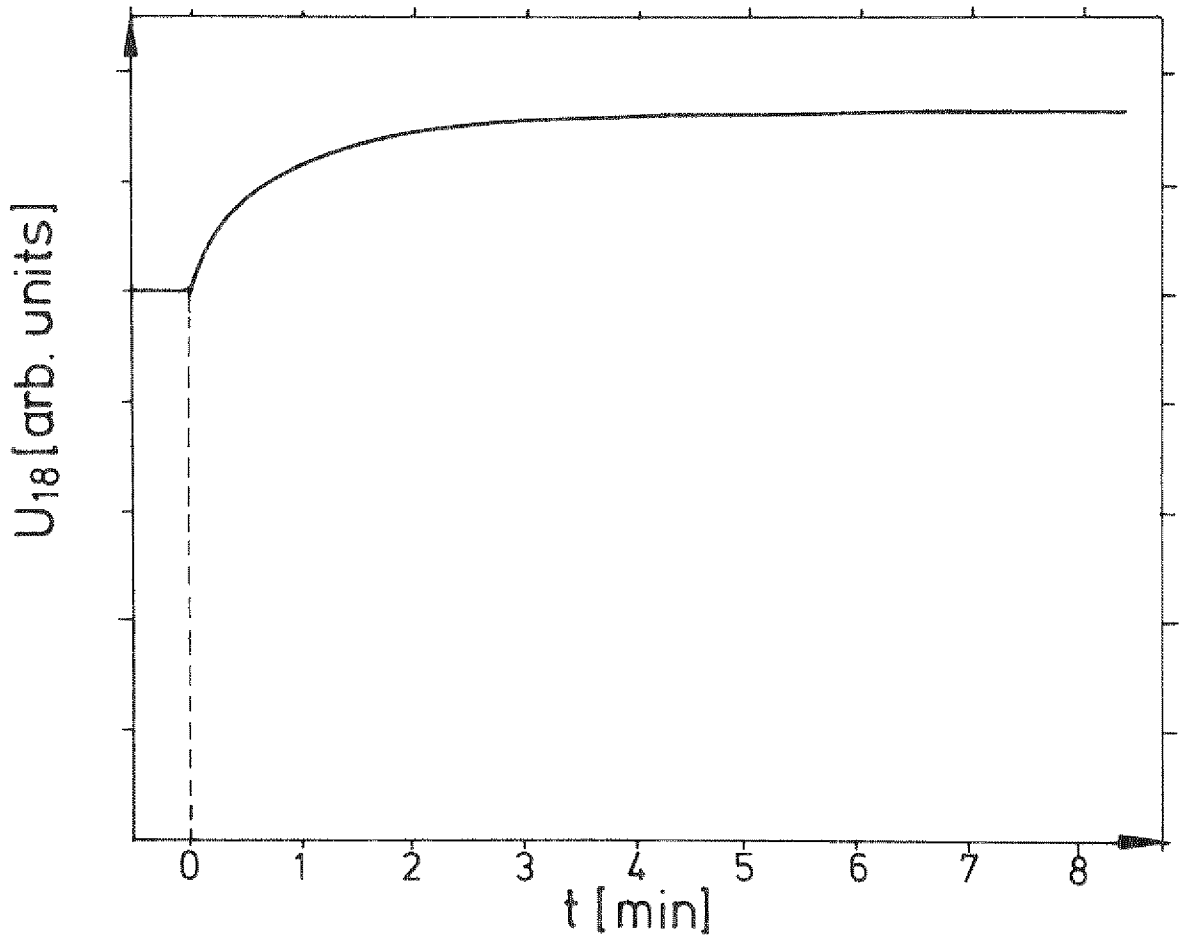

Fig 16.

Variation of the water signal U_{18} in the RGA after a rapid variation of U_{18} in the GDV at t=0. T_{QBP} = 160 °C, T_{CT} = 180 °C, $P_2 \approx 10^{-8}$ mbar.

Just before igniting the discharge, the filaments of the ion manometer and of the residual mass analyser in the quadrupole by-pass are switched off. The gate valve of the glow discharge vessel is closed. The hydrogen pressure increases until ignition occurs, at which time the gate valve is reopened. Some twenty seconds after the start of this sequence, the pressures within the GDV and the QBP have returned to their initial values and the filaments in the QBP are again switched on. The evolution of the H_2O, CH_4, CO... signals can be followed. Tests made without rf power (no ignition) have shown that this sequence of operation does not introduce noticeable errors into the measurements.

At the end of a cleaning run the glow discharge voltage and the rf power are switched off (simultaneously or one after the other). Residual gas spectra are taken. TV 2 is then closed and E 3 opened, introducing anew the same pressure of hydrogen directly into the QBP. The difference between the two last spectra yields the outgasing rates at the end of the cleaning procedure. Finally the two inlet valves E 1 and E 3 are closed, and the outgasing spectra in the absence of hydrogen are obtained.

This sequence of operations is easy to transcribe into the general steering routine of a tokamak. This should allow to start and terminate discharge cleaning operations at preselected times during the night, even in the absence of operators.

§ III.4. Temperature of the portholes and sidearms

Towards the end of the first clean-down phase, the only significant partial pressure in the GDV, except for hydrogen, was that of water (P_{18}). This was high, of the order of 10^{-6} torr in the presence of the RG discharge and at a wall temperature of 400 ^{o}C but it was no longer decreasing with time. In order to ascertain the degree of wall cleanliness already achieved, the discharge was switched off and on and the resulting variation of P_{18} measured. This was small, i.e. P_{18} was large in the absence of the discharge. This led to the suspiscion that some cooler surfaces were involved, which had not been "seen" by the glow discharge. Water, of which the partial pressure had risen to high values in the early phases of the cleaning run, could have been ad- and absorbed by these surfaces. After the end of the cleaning procedure, a slow release (outgas) from these surfaces would now be taking place and a recontamination of the freshly deoxidized surfaces by this H_2O vapour after the end of the cleaning procedure had to be feared. We have therefore tried to minimize the condensation of water on such hidden surfaces during the cleaning phase.

The most likely water-trapping surfaces were thought to be the portholes and side-

arms of which the extremities had remained almost at room temperature whilst the GDV was first cleaned down at 400 ^{o}C. In order to check this hypothesis, the temperature of fourteen of the fifteen portholes were first raised to 200 ^{o}C and the large amount of water released was noted. The fifteenth porthole was then also heated up to 200 ^{o}C and the amount of water desorbed, was measured. This was equivalent to several hundreds of monolayers. For all measurements reported here with the exception of the first clean-down of the vessel, the temperature of each porthole was thereafter maintained at 200 ^{o}C. This should reduce the absorption of water by these surfaces during the deoxidation. In a tokamak, the residual P_{18} level should then become very low when the temperature of the portholes is reduced at the end of the cleaning run. Another advantage resulted from the increased porthole temperatures: as mentioned in § V, 2, arc spots were observed in the cold portholes when the first RG discharges were produced there using the procedure described in § III.1.c). These arc phenomena were suppressed when the temperature of the sidearms was raised to 200 ^{o}C. They did not reoccur even when new windows were built in and discharge cleaned at 200 ^{o}C.

III.5. Reoxidation and outgasing procedures

At wall temperatures higher than 200 ^{o}C, a few hours of RG discharge in hydrogen decrease the release rates of water, hydrocarbons and carbon oxides down to such low values that accurate measurements are no longer possible. When a new discharge is initiated, even one or two weeks later, the amplitudes of the corresponding signals are still negligibly small. In order to study the cleaning efficiency over a broad parameter range, a systematic recontamination procedure had to be applied.

We have chosen the technique previously used by Dietz et al. [5b]: the inner surface of the GDV is exposed to laboratory air at one atomosphere for one hour with the walls at T_w = 200 ^{o}C. The vessel is then evacuated. This simulates a rather serious accident in a tokamak.

On the whole, a fairly reproducible state of surface oxidation results as far as the impurity release is concerned. It is however probable that the surface state is not the same when one or when fourteen hours at T_w = 200 ^{o}C have elapsed after an oxidation procedure. This is mainly a consequence of the diffusion and reactions of oxygen in the surface-near layers. The deoxidation seems to proceed faster when the time since the last oxidation is shorter.

Also different surface oxidation states probably prevail when the surface is kept at 200 ^{o}C after reoxidation, or when its temperature is raised overnight to e.g. 400 ^{o}C. A difficulty is therefore encountered in comparing the absolute am-

plitudes of the signals and their decrease with time (cleaning rates) at different wall temperatures for otherwise identical discharge conditions.

Except for the first clean-down of the apparatus (§ V), no extensive or systematic outgasing procedure was used in this work. As a rule, the surface was oxidized as described above towards the end of the day. After reevacuation, the vessel temperature was adjusted if required to the desired value which was reached in about one hour. Some outgasing occured overnight at that temperature and the glow discharge was initiated in the next morning.

III.6. Measurement of parametric dependances

It would be tedious, time consuming and misleading to investigate the parametric dependance of the cleaning rate ν_{18} by making one deoxidation run for each set of parameters. Uncertainties would result, as pointed out in the preceeding paragraph, from the lack of precise knowledge of the state of oxidation at the start of each run. The calibration of the RGA varies by a few percents from day to day. Finally, as shall be seen in § VI.2.b, at $T_W > 200\ ^{o}C$, the initial value of ν_{18} after an oxidation procedure is more strongly limited by the amount of active H reaching the wall than by other parameter: practically all the H atoms penetrating into the wall return in the form of H_2O molecules.

We have therefore studied the parametric dependances as follows. All parameters but one were frozen for a given run. The rf discharge was started and the RG discharge allowed to burn for about one hour, until ν_{18} varied moderately slowly. The free parameter was then varied at regular intervals. In order to minimize the evolution of the surface between two measurements, these intervals were kept as short as justifiable, usually six to twelve minutes. Schematically, a curve as illustrated on fig. 17 is obtained.

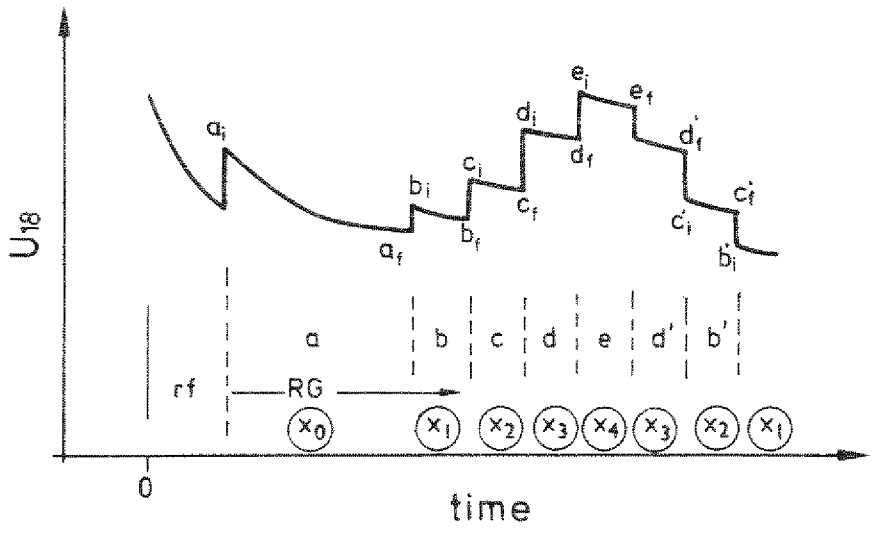

Fig. 17: Illustrating the procedure used to measure the variation of P_{18} as function of a parameter X.

We must correct for the progressive decrease of the amount C_{MO} of oxides in the surface-near layers. To do this, we assume that, at least over moderately short time intervals, ν_{18} is a linear function of C_{MO}. We can then write that, if C_{MO} remained constant, we would have had:

$$\frac{\nu_{18}(x_1)}{\nu_{18}(x_o)} = \frac{b_i}{a_f} \quad , \quad \nu_{18}(x_2) = \nu_{18}(x_1)\,\frac{c_i}{b_f} = \nu_{18}(x_o)\,\frac{c_i\ b_i}{b_f\ a_f}$$

and, in general:

$$\nu_{18}(x_m) = \nu_{18}(x_o)\ \frac{m_i\ k_i\ \ldots\ldots\ c_i\ b_i}{k_f\ j_f\ \ldots\ldots\ b_f\ a_f} \ ,$$

from which the dependance of ν_{18} on the parameter x has been deduced.

A control of the assumption that ν_{18} is proportional to C_{MO} is found in the fact that, whereas both the product Sp n_{18} of the pump speed Sp times the concentration n_{18} of water vapour in the GDV and the slope $d\ln n_{18}/dt$ usually change strongly when a discharge parameter is varied, their ratio remains unchanged - within the limits of experimental errors - in the course of this variation. No evidence of abrupt effects which could result e.g. from a threshold phenomenon, could be detected. Some controls have been made, as indicated on fig. 17 by returning after a time to a previous parameter setting. They have shown that the procedure outlined here is acceptable.

Still the progression evolution of the surface during the measurements limits somewhat the accuracy of the interpretation.

IV. FLUXES TO THE WALL

IV.1. Hydrogen flux; Langmuir effect

It has been reported previously [4, 5,] that the rates at which water, methane, carbon oxides are produced within the surface-near layers of the wall are proportional to the flux density $\alpha\varphi_i$ of hydrogen which penetrates into the lattice from the gas phase; α is a sticking factor.

In the case of atomic hydrogen produced by contact dissociation of molecular hydrogen on hot metal surfaces, the flux density φ_i of atoms to the wall can be evaluated from equations given by Hickmott [16] and Gould [17] ; for this, the temperature and area of the hot metal and the surrounding pressure of H_2 must be known. A second method is to measure the permeation flux of hydrogen through a membrane exposed to H-atoms. If the H-concentration in this membrane is kept low, surface effects are rate determining [18]; the permeation flux density is then practically equal to half the flux density $\alpha\varphi_i$ of atoms sticking to the

wall on the primary side of the membrane (the other half of $\alpha\varphi_i$ recombines to the gas phase on the upstream surface).

A third method, similar to the one used by Langmuir [15], is particularly well adapted to the measurement of $\alpha\varphi_i$ in the present case: when a source leading to hydrogen absorption by the wall, e.g. a hot filament, a rf, glow or RG discharge, is switched on in hydrogen gas, a pressure drop (fig. 18) results which can be correlated with the rate at which hydrogen penetrates i.e. is "pumped" into the wall material. The results of this method, which we shall name "Langmuir effect" in the following, have been found to agree quantitatively with those of the two first. A full description of the technique will be published elsewhere.

We discuss here only the early phases of the phenomenon:

a) The RG discharge in H_2 is suddenly initiated. If the surrounding walls have been deoxidized and well outgased, the fluxes of H_2 or H_2O released from the wall are negligible at the very beginning of the discharge. Let $\mathcal{V}$ be the volume of the vessel, S_o the exposed area, N_2 the total number of H_2 molecules in the vessel and n_2 the concentration in the gas, which is directly related to the H_2 pressure. Immediately after the start of the discharge we have:

$$dN_2/dt = 2\, S_o\, \alpha\varphi_i, \qquad \text{i.e.}$$

$$\alpha\varphi_i = \frac{\mathcal{V}}{2\, S_o}\,\frac{dn_2}{dt} \quad . \tag{IV.1}$$

The factor of 2 emerges because two atoms penetrate into the lattice for each molecule leaving the gas phase.

b) After a long exposure of the wall to the discharge, a state of quasi-equilibrium is reached: the release rate of H_2 from the wall in the presence of the discharge, $v_r^{(I)}$ is practically equal to the rate of penetration $S_o\,\alpha\varphi_i$. When the discharge is interrupted, φ_i becomes abruptly equal to zero. A transient increase of the pressure results of which the initial rate is directly related to $v_r^{(o)}$, the release rate of H_2 in the absence of the discharge. The relation is similar to equation (1):

$$\frac{v_r^{(o)}}{S_o} = \frac{\mathcal{V}}{2\, S_o}\,\frac{dn_2}{dt} \tag{IV.2}$$

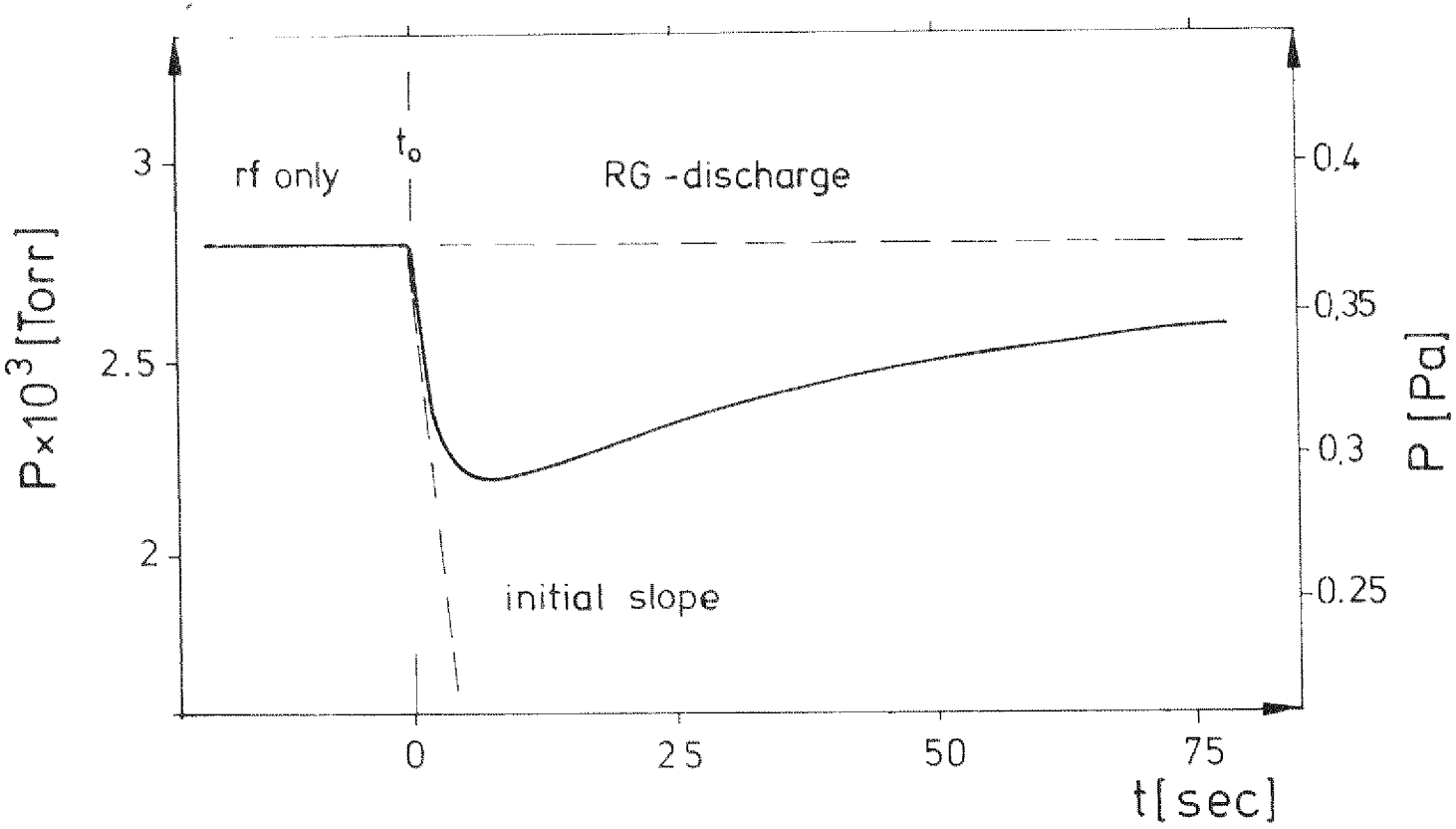

Fig 18.

Observed decrease of the H_2 pressure in the GDV at the start of the RG discharge "Langmuir effect".

If v_r does not change discontinuously when the discharge is interrupted, $v_r^{(o)} \approx v_r^{(I)} = S_o \alpha\varphi_i$ [+]. The phenomenon evolves rapidly; it is important to ascertain that the very early phase of the discharge is measured.

Both methods (a) and (b) have been applied to the case of the RG discharge. Good agreement has been found in the investigated T_W domain between the values of $\alpha\varphi_i$ and $v_r^{(o)}$ determined from eq (1) and (2).

In the case of the rf discharge, only method (b) could be used, since the pressure increase neccessary to initiate the plasma discharges (cf. § III.2.b and III.3) masks the Langmuir effect in case a).

Fig. 19. shows the variation of $\alpha\varphi_i$ measured at 200 °C as a function of the glow discharge current. Measurements made at 130°, 240°, 300° and 400° can be superposed within the limits of experimental errors on the same line.
We obtain:

$$\alpha\varphi_i = (\alpha\varphi_i)_{rf} + A \times I_{GD} = 1{,}4 \times 10^{13} + 6{,}0 \times 10^{18} \times j_{GD} \text{ atoms cm}^{-2}\text{s}^{-1} \qquad \text{(IV.3)}$$

where j_{GD} is the current density expressed in A cm^{-2}.

The number of particles sticking to the wall is close to twice that of the number of charged atoms which strike the surface. Since the potential drop at the cathode is high (450 volts), H_2^+ (or H_3^+) ions should dissociate upon impact with the wall, giving rise to two (or three) atoms which then penetrate into the lattice. Some additional penetration of Frank-Condon atoms resulting from reactions such as

$$H_2 + e \longrightarrow 2\,H^o + e$$

is also expected.

The Langmuir effect has also been used to measure the (partial) flux density of H entering into the wall material in the more complicated situation where the discharge is initiated in mixtures of hydrogen and noble gases.

[+] This is the case when the Langmuir-Hinshelwood mechanism [19] of surface recombination between adatoms governs the release. The Eley-Rideal model, [20] which assumes that the main recombination results from reactions between impinging atoms and ad-atoms, and models [1, 21] according to which surface release is dominated by the ion-induced desorption of hydrogen from trapping centers close to the surface would lead to a discontinuous variation of the release rate when the discharge is interrupted: $v_r^{(o)}$ would be much smaller than $v_r^{(I)}$ and than $S_o \alpha\varphi_i$.

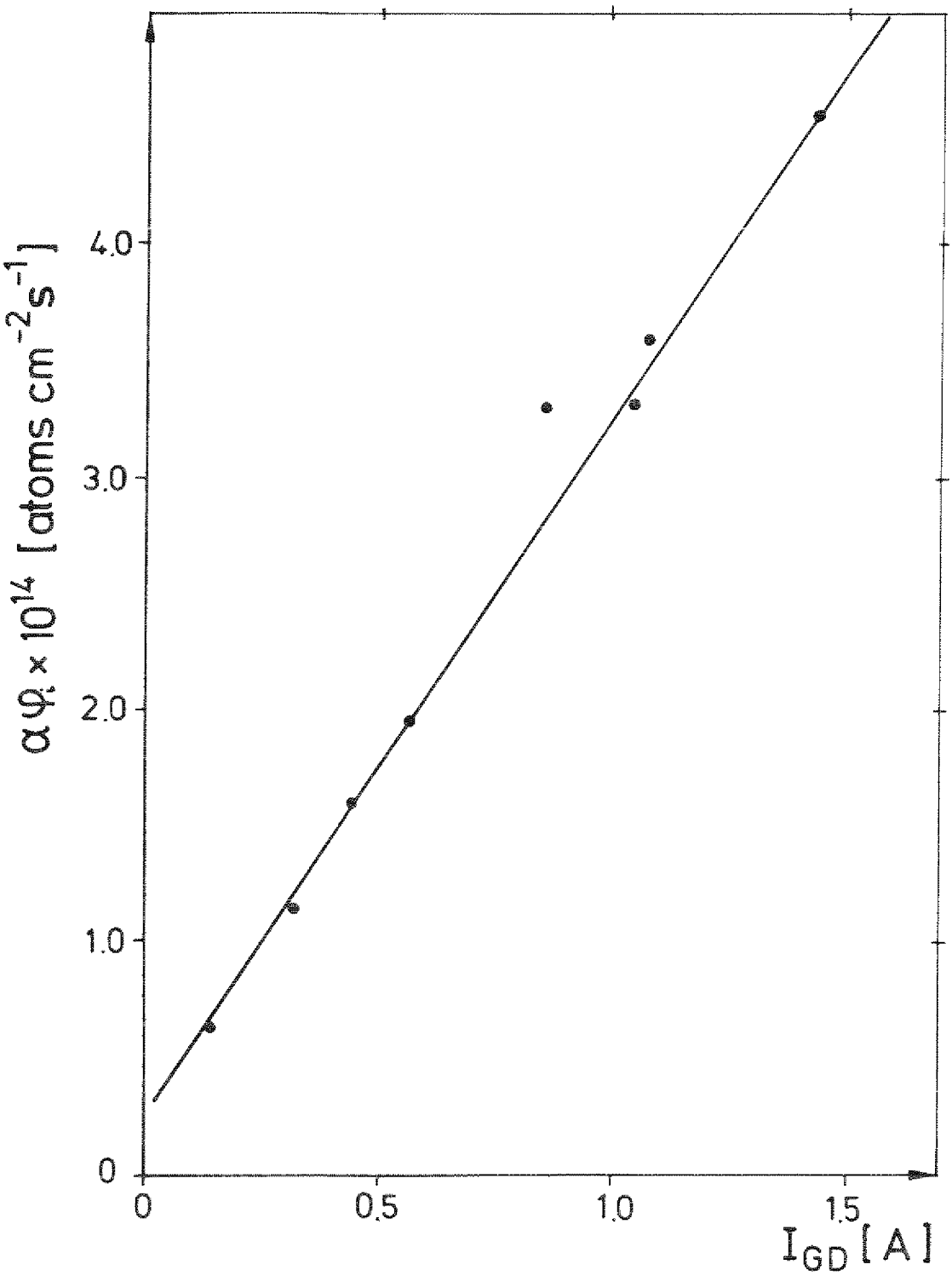

Fig 19.
Flux density $\alpha\varphi_i$ of atomic hydrogen penetrating into the wall as a function of the RG - current

IV.2. Destruction of the reaction products by the plasma discharge

When an RG discharge is initiated in hydrogen to which CH_4 has been added, the methane partial pressure P_{16} is reduced, provided that the walls had been decarburized beforehand. P_{16} decreases further when the RG current I_{GD} increases (see also § VI.8 and fig. 37 and 38): the plasma destroys the methane molecules, probably through the formation of CH_4^+, CH_3^+, CH_2^+...ions; some of these, accelerated by the cathode drop potential, are dissociated back to C and H when they strike the wall.

The methane balance equation can be written, in a first approximation, as:

$$E_{16} = (Sp)_{16}\, n_{16} + K_D\, n_{16}$$

E_{16} is the rate at which methane is introduced via E2 into the vessel, $(Sp)_{16}$ the pump speed for methane, n_{16} the methane concentration in the gas and K_D a phenomenological rate constant for the destruction of methane molecules by the plasma. K_D is expected to depend on the intensity of the discharge and (cf. § VII.3.a) on the plasma density, i.e. on the filling H_2 pressures P_2.

Writing $n_{16}^o = E_{16}/(Sp)_{16}$ for the methane concentration in the absence of the RG discharge ($K_D = 0$), we obtain, at constant P_2:

$$\frac{K_D}{(Sp)_{16}} = \frac{n_{16}^o - n_{16}}{n_{16}} \qquad (IV.4)$$

Fig. 20 shows how K_D varies as a function of I_{GD} in three distinct experimental cases at a pressure $P_2 = 2.8 \times 10^{-3}$ torr. Fig. 21 is a similar plot measured when NH_3 instead of CH_4 was admixed to the hydrogen.

The hydrogen atoms and ions from the RG discharge reduce some of the carbon and of the nitrogen deposited on the wall back to CH_4 and to NH_3. Corrections have been evaluated from the rates at which CH_4 and NH_3 continued to be released from the wall when the CH_4 or NH_3 inlet value was suddenly closed. This is however a fast transient effect which tends to be more strongly underevaluated a) in the case of NH_3 than in that of CH_4, b) when the percentage of admixed CH_4 is low and c) when the wall temperature is high. We believe therefore that K_D should approximately be represented (in the case of CH_4) by an equation of the type:

$$K_D/Sp = k_D(S_o/Sp) \approx 0{,}2 + 4\, I_{GD} \qquad (VI.5)$$

Since the plasma destroys continuously a fraction of the CH_4 and NH_3 gas, it is natural to expect a similar phenomenon also in the case of H_2O. I.e. a

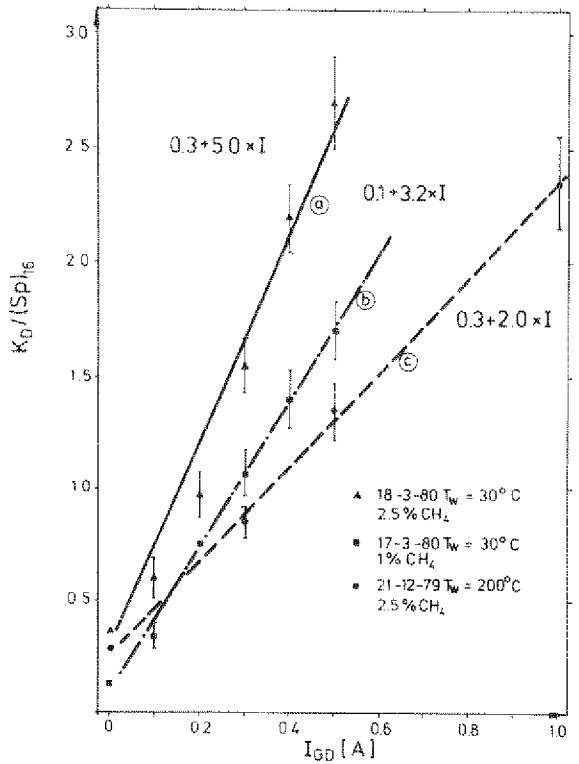

Fig. 20

Rate K_D at which CH_4 is destroyed by the rf and RG discharges. The abscissa is the glow discharge current I_{GD}. $(Sp)_{16}$ is the pump speed for CH_4; P_2 = 2.8 x10^{-3} torr.

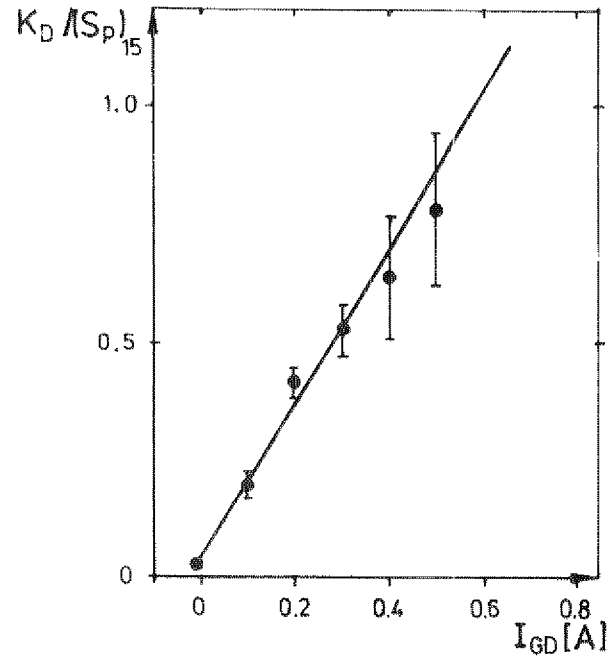

Fig. 21

Rate K_D at which NH_3 is destroyed by the rf and RG discharges. The abscissa is the glow discharge current I_{GD}. $(Sp)_{15}$ is the pump speeds for NH_3; P_2 = 2.8 x 10^{-3} torr.

plasma-induced reoxidation of the wall is expected. This should be particularly pronounced when I_{GD} is large. In what follows, we assume as a first approximation that the value of K_D for water is also given by equ (IV.5).

IV.3 Thermal reoxidation of the wall by H_2O vapour

There is yet another mechanism through which water vapour can reoxidize the wall, and this even in the absence of an RG discharge. We have indeed observed that the rate at which water vapour recontaminates our surface becomes appreciable whenever the wall temperature T_W is higher than 200 °C. The corresponding rate constant increases rapidly when T_W is further raised. Thus, unless the pump speed Sp is very large, part of the oxygen which is released in the form of H_2O by the RG discharge returns to the wall via this reoxidation mechanism instead of being evacuated out of the system.

A way to evaluate the rate at which a gaseous substance j reacts with the walls of the vessel is to evacuate the system at two different pump speeds $Sp^{(o)}$ and $Sp^{(1)}$ ($Sp^{(o)} > Sp^{(1)}$) and to measure the stationary densities $n_j^{(o)}$ and $n_j^{(1)}$ which establish themselves in both cases. Assuming that the inlet (or outgasing) rate E_j of the substance is independent of Sp, we have

$$E_j = Sp^{(o)}\, n_j^{(o)} = Sp^{(1)}\, n_j^{(1)}, \text{ i.e. } \quad n_j^{(1)}/n_j^{(o)} = Sp^{(o)}/Sp^{(1)}, \qquad (IV.6)$$

if the substance j does not react with the wall. This behaviour is observed for most substances (e.g. H_2, CH_4, C_2H_6, He, Ne) in the whole temperature domain explored here. It is also observed for H_2O vapour at lower wall temperature. But at higher wall temperatures, the ratio $n_j^{(1)}/n_j^{(o)}$ is lower than predicted by equ (IV.6).

Denote the release rate of H_2O from the surface by v_{18} and assume that it is unaffected by the pump speed of the system (P_{18} is of the order of 10^{-8} torr here). Let us further assume[+] that we can write, for the oxidation rate:

$$v_{ox} = S\, k_{ox}\, (1 - \theta_o)\, n_{18} = S\, k'_{ox}\, n_{18};$$

k_{ox} is a (temperature dependent) phenomenological constant. The surface (area S) is assumed to be sufficiently deoxidized for the surface coverage fraction θ_o by oxide to have become almost time-independent. When we consider the stationary con-

---

[+] Other dependences of v_{ox} on n_{18} (e.g. $v_{ox} \propto n_{18}^{1/2}$) could be assumed, but this would not affect fundamentally the qualitative conclusions drawn below and in § VII).

centrations of H_2O which establish themselves for the two values of the pump speed, we obtain:

$$0 = \frac{dn_{18}^{(o)}}{dt} = \frac{dn_{18}^{(1)}}{dt} = v_{18} - \left[Sp^{(o)} + Sk'_{ox}\right] n_{18}^{(o)} = v_{18} - \left[S_p^{(1)} + S\ k'_{ox}\right] n_{18}^{(1)}$$

i.e:

$$\frac{n_{18}^{(1)}}{n_{18}^{(o)}} = \frac{Sp^{(o)} + S\ k'_{ox}}{Sp^{(1)} + S\ k'_{ox}} \qquad (IV,7)$$

Accurate measurements are not easy to make. In addition to the oxidation-reduction reactions mentioned above, a considerable amount of H_2O ad/absorption and desorption occurs on the oxidized surfaces which inevitably remain (e.g. in the gate valve and in the neighbourhood of the pump) in the system. This leads to very long measuring times (up to tens of hours) in the lower T_W range and makes a careful control of the temperature homogeneity and constancy along the whole surface indispensible. For the measurements at low T_W, Sp must be determined accurately. Also variations of the oxidation state of the surface must be avoided. Preliminary measurements have however indicated that, at a partial pressure $P_{18} \approx 10^{-8}$ torr, $S\ k'_{ox}$ varies roughly between 40 and 1000 l/sec when T_W is increased from 250 ^{o}C to 400 ^{o}C. The corresponding activation energy of k_{ox} would then be of the order of 10 to 20 kcal.

More important is the fact that, as the temperature reaches about 400 ^{o}C, $S\ k'_{ox}$ becomes equal to or larger than $Sp + K_D$ for $I_{GD} \approx 1$ A, i.e. that above 400 ^{o}C, the surface reoxidation by H_2O vapour should become a dominant effect.

V. FIRST CLEANING OF THE SURFACES

The study of the cleaning of surfaces during their first exposure to an RG discharge presents serious problems (cf. § I,3): the experimental conditions are either such that the decontamination is slow - measurements are inaccurate - or that the release rates of H_2O, CO, CH_4 are rapid - only a limited parameter variation can be made before the surface is cleaned down. Another difficulty was encountered: the optimisation of the apparatus, of the measuring devices and of the discharge itself, the choices of throttling factors, of the pressure in the GDV and of the temperature of the QBP had to be made during the first cleaning phase of the GDV. The sensitivity of the RGA was progressively improved at that time, so that the calibration factors corresponding to the very initial cleaning phase (fig. 22) are not available. We have however tried to gather as much information as possible on this critical phase of the cleaning procedure. Somewhat later, a new surface (cryopump CF) was introduced in the GDV. Results on its conditioning are also presented in this paragraph.

V.1. Time history of the apparatus

The GDV was baked out for one week at wall temperatures T_w of 200° to 450 °C. It was then cooled down to room temperature, exposed to air twice for one hour for minor improvements and reevacuated. A new bake-out procedure was started with 200 °C < T_w < 500 °C for ten days, at the end of which T_w was adjusted to 410 °C. The base pressure (mainly H_2) was of the order of 10^{-7} torr; p_2 was raised to 10^{-2} torr, and a RG discharge (current I_{GD} = 0.58 A, voltage U_{GD} = 350 V) was initiated and maintained for 72 minutes.

The vessel was thereafter maintained at 400 °C for a further fortnight. Short exposures of the walls to RG discharges of various types were made to improve the measuring techniques. During this time, some evolution (discharge cleaning, oxygen diffusion in the lattice) of the walls unquestionably occured.

On the twelfth day, a prolonged (7 hours) exposure to a RG discharge similar to the first one but with I_{GD} = 0,4 A and U_{GD} = 300 V was made.

The glow discharge was thereafter maintained practically uninterruptedly for another fourtyeight hours. Towards the end of this exposure, the hydrogen pressure in the GDV was increased to 10^{-1} and later 2.6 x 10^{-1} torr leading to strongly

luminescent phenomena in the portholes.

The wall temperature was brought down to room temperature, and a RG discharge was produced to check on the possible occurence of arc spots.

V.2 Arc Spots

A striking observation made during this cleaning procedure was for us the absence of any visible arc phenomenon when the first RG discharges were initiated in the GDV.

In all the vessels wherein rf or RG discharges had been until then produced in this laboratory, a multitude of luminous points flickered around the surface of the vessel during the first hours of operation. Their occurence became less and less frequent with increasing time of exposure. In earlier experiments however, the plasma discharge had been first initiated in a vessel of which the walls were at room temperature. When these walls had been previously outgased, then at moderate temperature ($T_w < 200\ ^oC$). The GDV was the first vessel wherein the first RG discharge was initiated with warm walls.

In order to examine the role which T_w might play on this phenomenon, the H_2 pressure was increased to $> 10^{-1}$ torr towards the end of the cleaning run,. The plasma discharge penetrated into the portholes of which the temperature was low ($\approx$ room temperature, § III.4). Arc spots appeared in <u>all</u> the portholes, in particular at the metal-glass junctions of the two larger windows. The resulting evaporation was sufficient to decrease the transparency of one window. When the temperature of the portholes was raised to 200 ^oC, arc spots no longer occured. The windows were later replaced; new glow discharges were initiated with the portholes at 200 ^oC. No evidence of arcing could be found then or afterwards in the portholes.

After the GDV had been discharge-cleaned at elevated wall temperatures, T_w was decreased to room temperature. Glow discharges were initiated and the operating pressure varied in a broad domain. Even then, no arc spots could be observed.

When the cold finger C F was first built into the GDV, every standard UHV procedure (glass blasting, etching, rinsing in distilled water and in alcohol under ultrasonic waves) was used to ensure its surface cleanliness. The RG discharge was started at room temperature. Flickering spots were observed on the whole of the exposed C.F. surface as soon as the discharge was initiated. As usual their frequency of occurrence decreased with time, and increased strongly when the current of the glow discharge was raised. The arcs disappeared definitively after the wall

temperature had been brought up to $T_w > 200\ ^oC$.

The evidence gathered is yet insufficient to draw final conclusions; it seems however likely that arcs can be avoided during the RG discharges when the walls are first conditioned at a sufficiently high T_w ($\geqslant 200\ ^oC$). It has moreover been observed that, once a sufficient degree of wall conditioning has been achieved, no ways could be found to produce again arc spots in our apparatus, except by bringing uncleaned elements into it. In particular, the reoxidation procedure (§ III, 5) used here does not recontaminate the wall in such a way that arc spots reoccur.

V.3. Impurity Release from fresh Surfaces

The decrease of the partial pressures of water and of carbon monoxide during the 72 minutes of the first cleaning run of the glow discharge vessel is shown on fig. 22.

The partial pressure of water was 1.8 times larger than that of CO; both signals decreased at the same rate ($\tau_{1/e} = 75$ minutes).

The further evolution of these partial pressures, measured twelve days later, is illustrated on fig. 23. At that time:

- the ratio of the water pressures of H_2O and CO was again of the order of two,
- the partial pressure of methane was seven times smaller than that of water,
- the three partial pressures decreased proportionally to one another at that T_w,
- although the parameters of this RG discharge were not the optimum for fast cleaning, less than ten hours were sufficient to bring the partial pressure of methane down to a level where the signal to noise ratio limited the measuring accuracy,
- some five further hours were necessary to bring the CO and H_2O signals to the same state.

A strong change in the slope of the log $P = f(t)$ plots took place between the two cleaning exposures. It is unlikely that this resulted from the (short) cleaning tests made in the meantime. Oxygen diffusion in the lattice has probably also played a role here.

Additional information on the impurity release from fresh surfaces was gained when the cold finger (LN_2 cryopump CF) was built into the GDV:

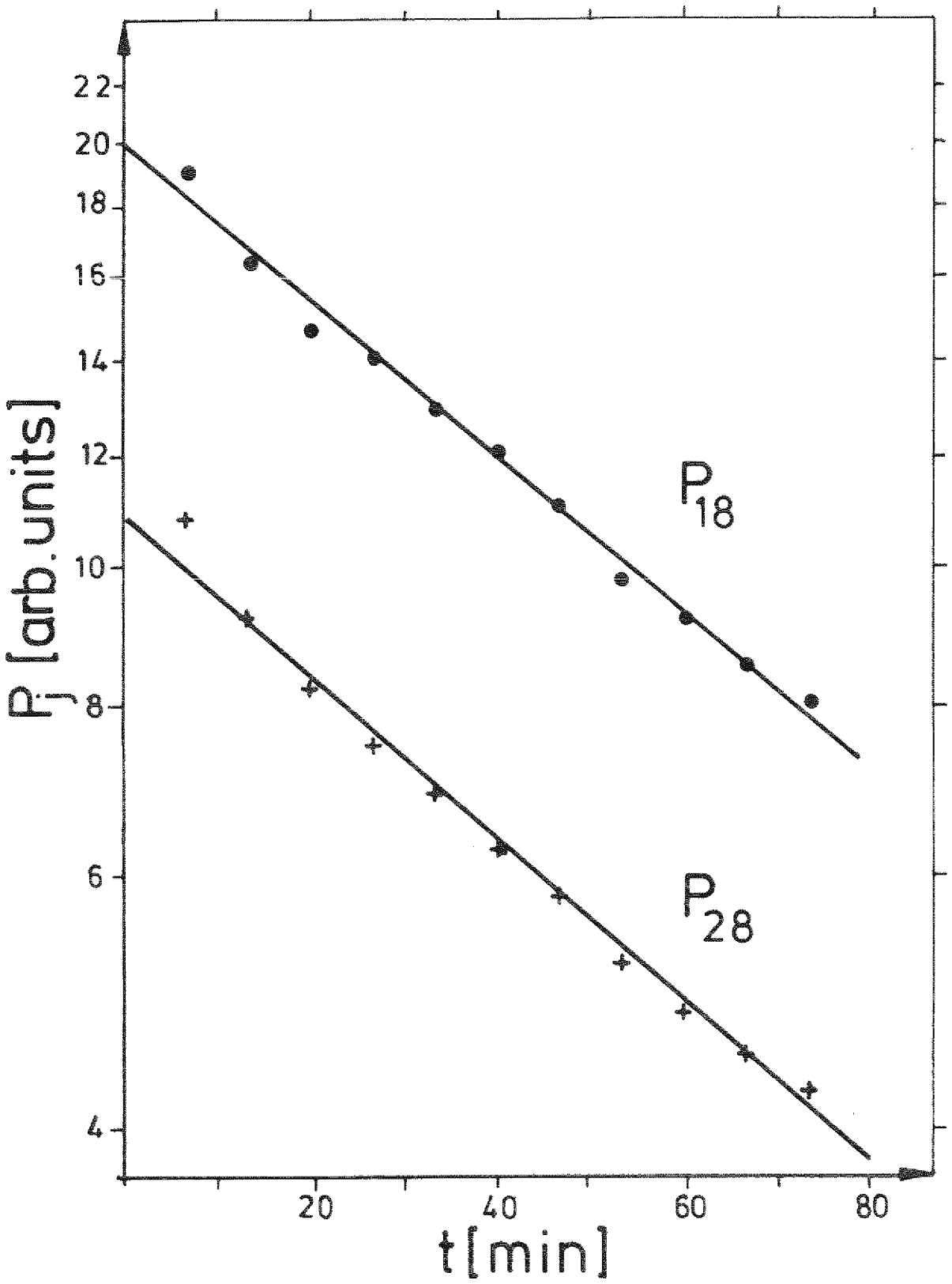

Fig 22.

First clean-down of the GDV: decrease of water (P_{18}) and CO(P_{28}) partial pressures. T_W = 410 °C, I_{GD} = 0.58 A, $P_2 \approx 10^{-2}$ torr, U_{GD} = 350 V.(31/8/79).

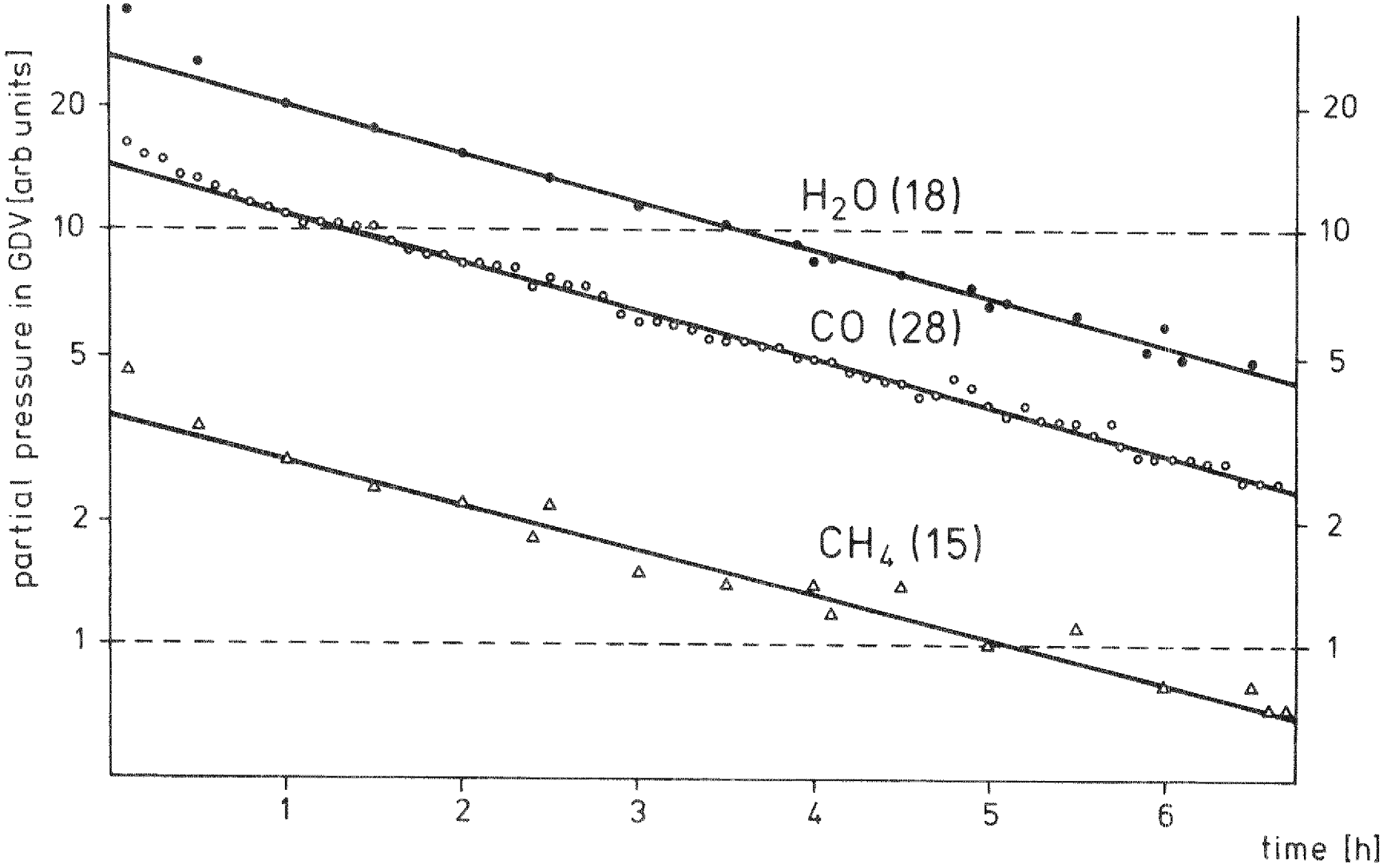

Fig 23.

Impurity release at the end of the first clean-down of the GDV by a RG discharge.
T_W = 400 ^{o}C, I_{GD} = 0.40 A, P_2 = 3 x 10^{-3} torr, U_{GD} = 300 V (10/9/79).

- At room temperature, only CH_4 and CO were produced by the discharge.
- At 100 ^{o}C (fig. 24a) the removal of CO and CH_4 became rapid even when only the radio frequency discharge was used. The amplitudes of these signals decreased rapidly with time. They increased when the current of the RG discharge was raised. The release of H_2O by the discharge became large enough to be measured. In contrast to those of CH_4 and CO, the water signal increased at first monotonously with time; P_{18} became equal to P_{15} after about 40 minutes; it remained however smaller than P_{28}.
- On the next day, the wall temperature was 200 ^{o}C. When the discharge was initiated (fig. 24b), the partial pressures of CO, CH_4 and H_2O were larger by a factor of more than 10 than the ones measured at 100 ^{o}C. All three signals decreased for a given condition with increasing time and increased when the RG discharge current was increased. Discharge cleaning was applied (partly with an admixture of neon) for about one hour on the same day.
- Fig. 24c) shows the initial evolution of the partial pressures of H_2O, CO and CH_4 observed when a new RG discharge in H_2 was initiated two days later, again at 200 ^{o}C.

We conclude that, at room temperature, the only gaseous products which can be released from the surface by the RG discharge in hydrogen are hydrocarbons and CO. This agrees with observations of other authors [11, 12]. At 100 ^{o}C, the release of H_2O is observable, but smaller than that of CO. When present, the decrease of P_{18} with time is slower than that of P_{15} and P_{28}. At 200 ^{o}C the partial pressure of H_2O is the largest. Again the H_2O signals decrease more slowly than the others. Only at temperatures of $\approx$ 400 ^{o}C we do obtain similar cleaning rates for H_2O, CO and CH_4. (figs. 22, 23). At the lower temperatures, it is the reduction of the surface oxides via the H_2O reaction channel which limits the rate of surface decontamination. We have therefore concentrated on this rate in the following chapters.

The abcissa of figs. 24 gives the cleaning rates in monolayers removed per hour. The normalisation factor is the total internal area of the GDV. For the measurements plotted here the source of methane and carbon monoxide was however limited to the venetian blind of the cryopump CF, of which the area is only one fourtieth of that of the GDV. Adding the amounts of CH_4 and CO removed at room temperature and during intermediate experiments to those shown on the figure, the total amount of carbon removed from these limited surface is a few hundred monolayers in agreement with measurements of other authors [12].

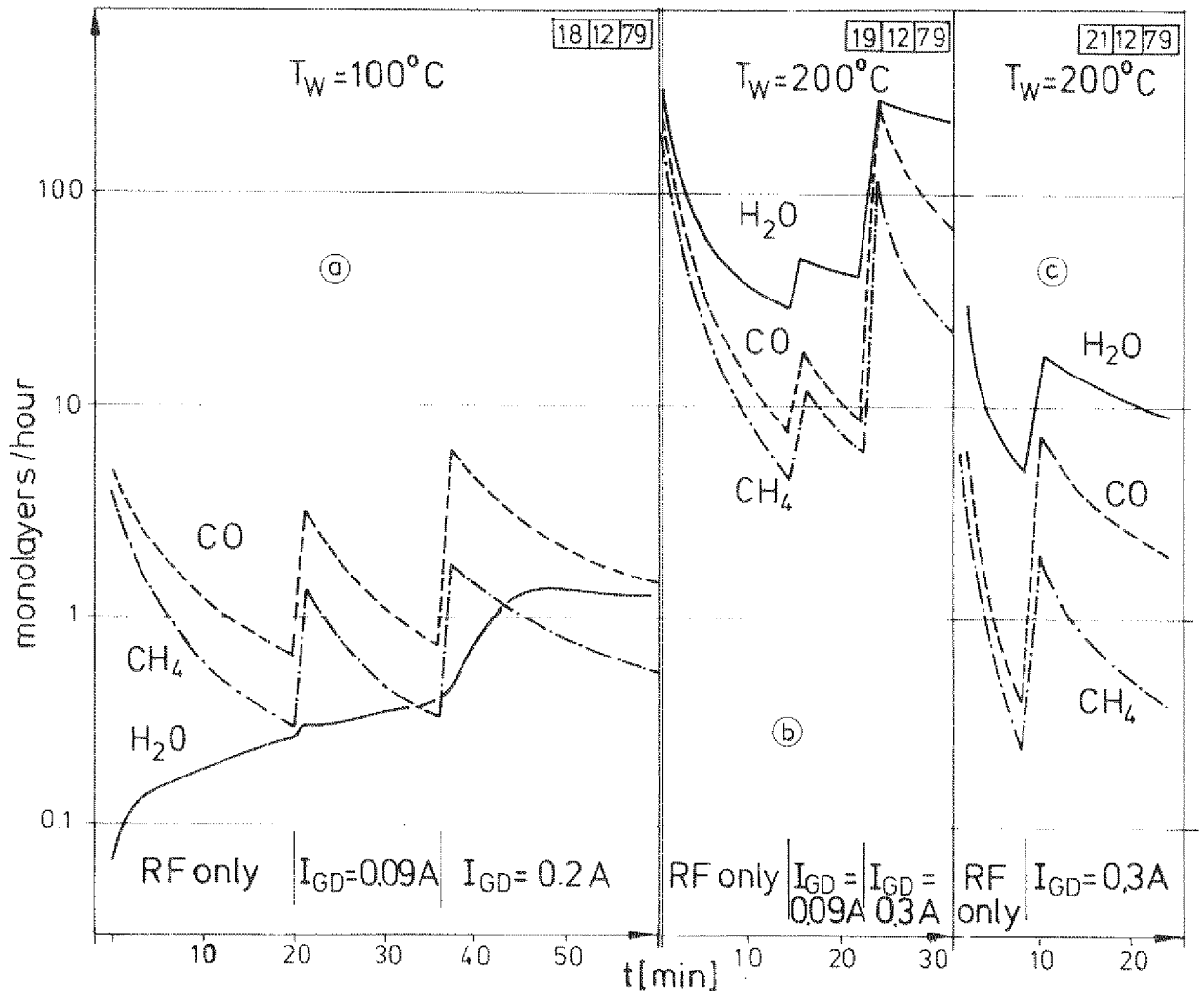

Fig 24.

Release of impurity gases in an RG discharge after the introduction of a new element (CF) into the GDV. (See § VII.4. and /4/ for a discussion of the H_2O behaviour at T_W = 100 °C)

VI. SURFACE DEOXIDATION BY RF AND RG DISCHARGES IN HYDROGEN

VI.1 Description of a typical experiment

a) Sequence of operations

The vessel has been oxidized according to the procedure outlined in § III.5. Immediately after evacuation, its temperature was raised to 300 ^{o}C; this temperature was reached in about one hour.

On the next morning, the preconditioning procedure for the residual gas analyser (§ III.3) was started. The residual gas spectra measured before, and thirty minutes after the introduction of pure H_2 (P_2 = 1.6 x 10^{-5} torr) into the quadrupole by-pass are shown on fig. 25a and b. Meanwhile another throughflow of H_2 had been established through the GDV, at a pressure of 2.7 mtorr.

After spectrum b had been obtained, the inlet valve for H_2 into the QBP (E3) was closed and TV 2 immediately opened until the H_2 pressure within the QBP reached again 1.6 x 10^{-5} torr. Thirty minutes later, the spectrum of fig. 25.c was measured.

The rf discharge was initiated (§ III.5). A typical spectrum, obtained ten minutes later, is shown on fig. 25.d. After 30 minutes, a RG discharge current of 500 mA was established. Fig. 25.e illustrates the spectrum obtained, again ten minutes after this operation.

The spectrum obtained after 240 minutes of RG discharge cleaning has been compared with the one resulting from the pure outgasing of the quadrupole by-pass: the results corresponding to that time are shown in the form of short horizontal bars on fig. 25.b.

After 250 minutes of glow discharge, liquid nitrogen was poured into the LN_2 cryopump. These results will be presented in § VI.6.b.

b) Discussion of the mass spectra - identification of the gaseous products

As mentioned in § III.2.a and discussed in[4], the introduction of H_2 into the quadrupole leads to a pronounced enhancement of the observed impurity peaks (compare spectra a and b, see also fig. 12). On the basis of the cracking patterns, we have ascribed the peaks at m = 17 and m = 18 to H_2O. Because of the overlap of O^+(from H_2O) and CH_4^+, the interpretation of the m = 16 peak is ambiguous. The peak at m = 15, due to CH_3^+ (hydrocarbons), has been taken as a measure of the methane partial pressure. This explains why, in this report, the subscript 15 (and not 16) is used to characterize the peak amplitude U_{15}, the concentration n_{15} and the partial pressure P_{15} of methane.

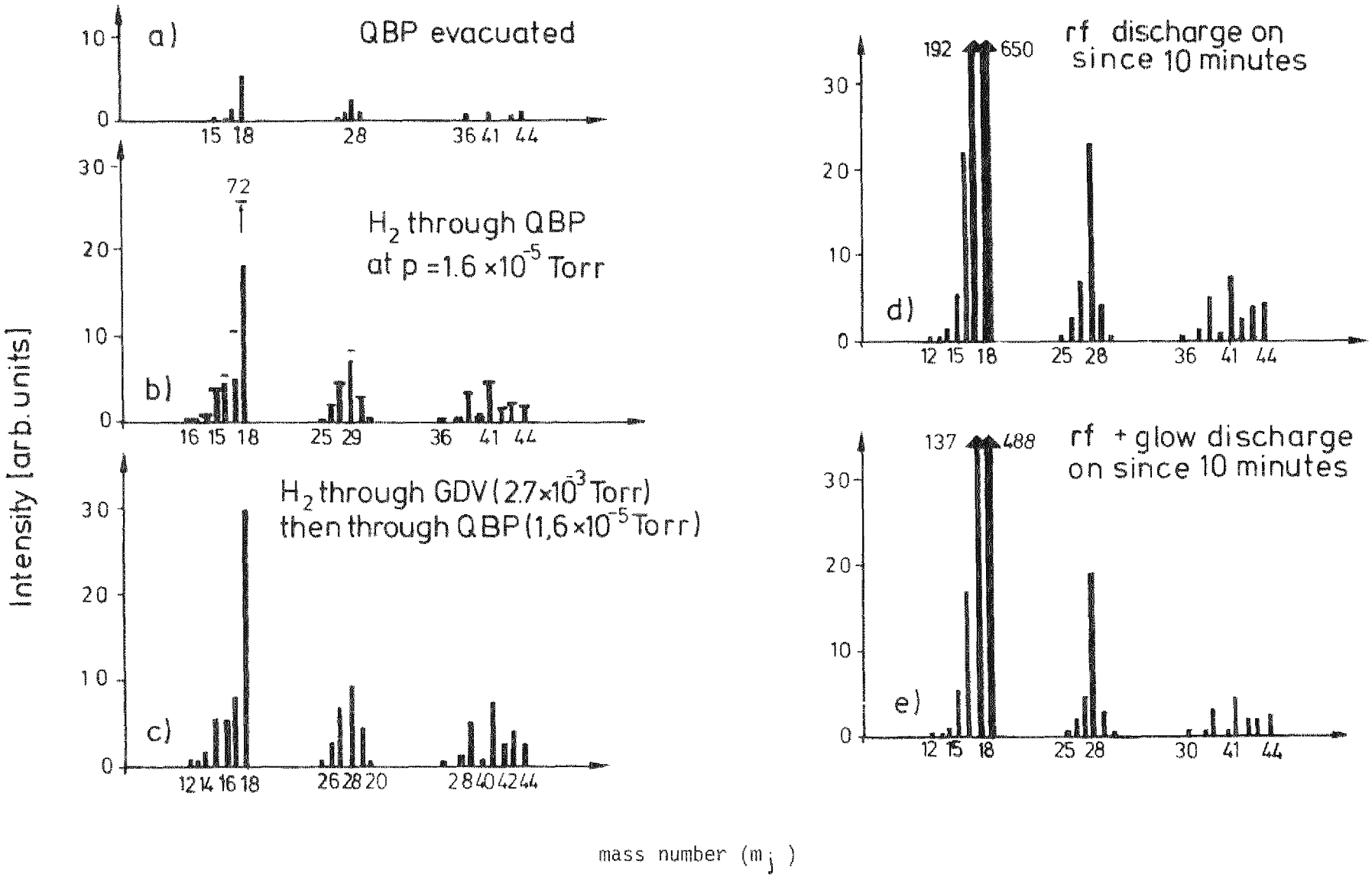

Fig 25.

Evolution of the residual gas spectra during the successive phases of an experiment (24/1/80)

The peaks observed between m = 25 and 30 result from hydrocarbons and CO (m = 28). An unique assignment on the basis of spectrum b cannot be made; the later development of the spectra (d and c) shows however that only CO (m = 28) increases. The analysis of the m = 14 peak shows that the contribution of N_2 to the latter peak is negligible.

The mass peaks from m = 38 to 43 are also due to hydrocarbon. The assignment of m = 44 is again ambiguous. Fig. 25.d and e show that no important release of CO_2 (m = 44) occured during this cleaning run.

The outgasing of water from the walls of the GDV after the oxidation procedure is appreciable (compare spectra b and c). Taking into account the throttle factor (θ_F = 150), the H_2O partial pressure in the GDV is $P_{18} = 8 \times 10^{-7}$ torr; the other partial pressures are much lower.

A large increase in the peaks corresponding to H_2O (m = 16, 17, 18) is observed when the rf discharge is started. At the time when spectrum d was taken, we evaluate $P_{18} = 9{,}4 \times 10^{-5}$ torr. The smaller increase of the CO peak corresponds to a partial pressure $P_{28} = 1 \times 10^{-6}$ torr. Qualitatively the spectrum does not change when the RG current of 500 mA is switched on.

The amplitudes of the other peaks fall, during the cleaning run, rapidly back to the background values of the spectrometer (fig. 25.b): The release of these substances from the GDV is negligible.

c) Evolution of P_{18} and P_{28}

The rf discharge in hydrogen produces (fig. 26) an increase of the water pressure P_{18} in the GDV by more than a hundredfold; P_{18} reaches 2×10^{-4} torr and decreases thereafter by a factor of six during the following thirty minutes.

A second sudden rise of P_{18}, by a factor of 3,4, occurs when the RG discharge current I_{GD} is established. Again a rather rapid decrease follows. The slope $d\ln_{18}/dt$ changes also by a factor of ≈ 3.4 when I_{GD} is switched on.

Except for the discontinuities which are associated with changes of I_{GD}, n_{18} decreases smoothly and continuously. The slope $d\ln n_{18}/dt$ decreases also slowly with time; it tends to become constant after about two hours of RG discharge cleaning. The partial pressure of water in the discharge decreases down to 6×10^{-6} torr during the first four hours.

28 1 80

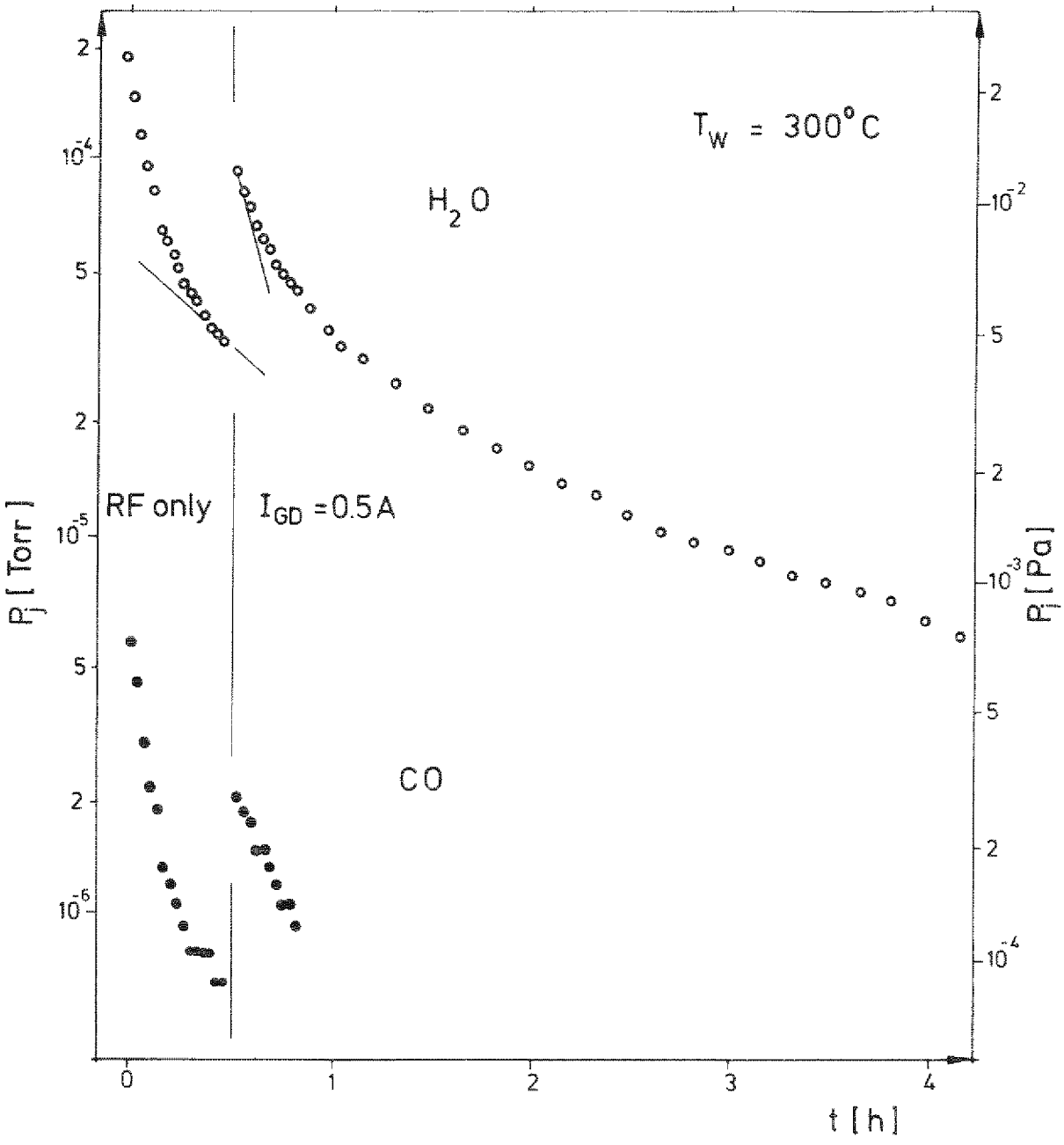

Fig 26.

H_2O and CO release from a freshly oxidized SS surface in a RG discharge

Fig. 27) illustrates the last phase of a cleaning run started under similar conditions: the walls had been oxidized and exposed to ten hours of glow discharge (I_{GD} = 0.5 A) in H_2 at 200 °C. When the discharge is reinitiated, P_{18} increases back to the value attained at the end of the previous exposure (10^{-6} torr in this case). A quasi exponential decrease follows during thirteen hours at the end of which $P_{18} = 1 \times 10^{-8}$ torr in the glow discharge vessel in the presence of the RG discharge.

The initial evolution of the partial pressure of CO, P_{28} is plotted on fig. 26; P_{28} behaves similarily to P_{18} but it is fourty times smaller. After an hour of RG discharge cleaning, the signal to noise ratio becomes too small to track the signal further. This holds for all other peaks including those of methane, and of CO_2, during the whole discharge, as can be deduced from fig. 25.

VI.2 Comparison with other cleaning runs; initial clean-down rate and clean-down time τ_{cd}

As was the case for new surfaces (§ V), rf and RG discharges in hydrogen do not release measurable amounts of water when the reoxidized walls are at room temperature. The evolutions of P_{18} observed above 100 °C are qualitatively similar to those shown on fig. 24, 26. and 27.

a) The rf discharge causes an initial rise of P_{18} to 1×10^{-6} torr at 100 °C, to 6×10^{-5} torr at 200 °C and to 2×10^{-4} torr when $T_W \geq 250$ °C. The flux density $d\varphi_i$ of hydrogen sticking to the wall during the rf discharge was measured to be $\alpha\varphi_i = 2 \times 10^{13}$ atoms cm^{-2} s^{-1} for the experiment at T_W = 300 °C shown on fig. 26. The P_{18} value expected, if all the hydrogen sticking to the wall returns as H_2O molecule, is $P_{18} \approx 2.10^{-4}$ torr. Thus the fact that the initial P_{18} value in the rf case does not rise above 2×10^{-4} torr is not surprising: the rate at which water is released from the wall is limited (see also[5.b]) by the flux of hydrogen which sticks to the surface.

b) We have always observed, as described under § VI.1c), that the relative variation of P_{18} which occurs when I_{GD} is changed is equal to that of the slopes $d\ln P_{18}/dt$ before and after the change. This is expected if the cleaning rate is related linearly to the concentrations c_{MO} (atoms cm^{-2}) of the reducible oxides which are still present in the surface-near layers. We can then write as a first approximation for the cleaning rate v_{cd}:

$$v_{cd} = S_o \frac{dc_{MO}}{dt} = S_o \frac{c_{MO}}{\tau_{cd}} = Sp\, n_{18} \; ; \qquad \tau_{cd} = \left[\frac{d\ln c_{MO}}{dt}\right]^{-1} \approx \left[\frac{d\ln n_{18}}{dt}\right]^{-1}$$

τ_{cd} is the characteristic time for the decrease of P_{18} and S_o the geometric area of the GDV.

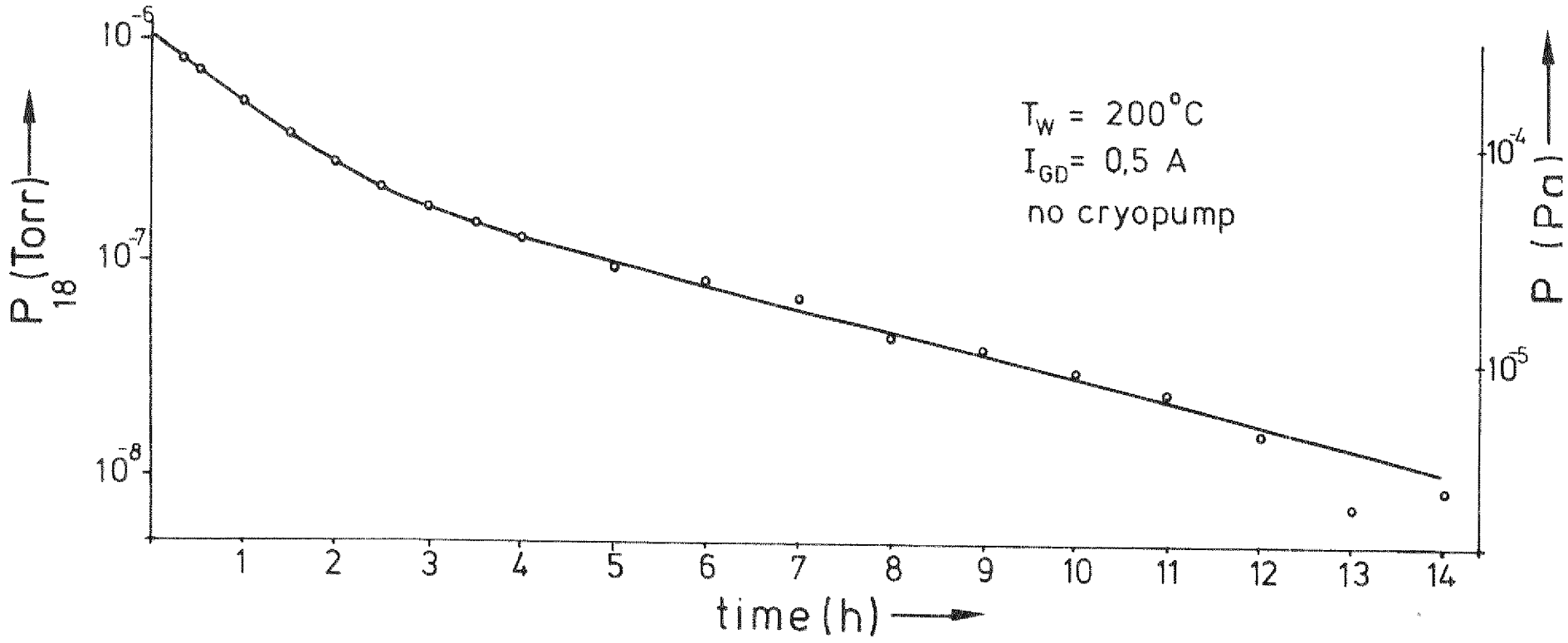

Fig 27.
Final clean down phase of the vessel at T_W = 200 °C

VI.3 Variation with the wall temperature T_W

The rate at which stainless steel surfaces are deoxidized depends strongly on their temperature: As mentioned earlier, no water release by the discharge could be detected at room temperature; P_{18} (cf. fig. 28) increases rapidly between 100° and 350 °C and starts decreasing beyond 400 °C. This agrees with earlier observations of Dietz et al [5b] on the deoxidation of SS by hydrogen atoms produced by contact dissociation on a tungsten filament.

The cleaning rate at 300 °C is eight and a half times larger than at 100 °C; at 400 °C, the ratio is twelve and a half. Thus if it takes (cf § VI.1) about 10 hours to deoxidize a wall at 300 °C, the time would be reduced to seven hours at 400 °C; the improvement is not very significant. But is takes ≈four days of continuous discharge cleaning to achieve the same results if the wall temperature cannot be raised above 100 °C. Other means (see § VI.7.) must be used to remove the oxide layer from a previously decarburized wall if T_W cannot be raised above room temperature.

The reduced clean-down times at higher T_W limit moreover the sputter effects during the phase of glow discharge as discussed in § 1.b.iii.

Of the measurements presented in § VI, that of the variation of P_{18} vs. T_W is most subject to error: the procedure (cf § IV.6) has been to - (a) glow discharge the vessel at a given T_W for 26 minutes, (b) stop the RG discharge and let the GDV outgas at that T_W for thirty minutes, (c) increase T_W to a new value (30 minutes) and let the GDV further outgas at that temperature (a further 30 minutes). A new RG discharge was then initiated. The amount of H_2O released during each phase, expressed in equivalent monolayers, is plotted on the inset of fig. 28). We see in particular that 1.6 and 2.4 monolayers of water have been released from the walls as T_W was raised from 100° to 200 °C and from 200° to 300 °C respectively. Most of the removal (55 monolayers in total) occured however during the phases of glow discharge. The error which results from the unavoidable transition phases from one temperature to the next are therefore probably not too serious.

VI.4 Effect of the current I_{GD} of the glow discharge

The rate of deoxidation increases when a glow discharge current flows (fig. 29). At our normal operating pressure , 100 mA of glow current double the cleaning rate with respect to its value in the rf plasma alone. The rate becomes larger when the current is further increased but a tendency towards a saturation is observed. This holds for freshly oxidized walls (curve a) as well as for materials which have been preexposed to H_2-RG discharges (curve b).

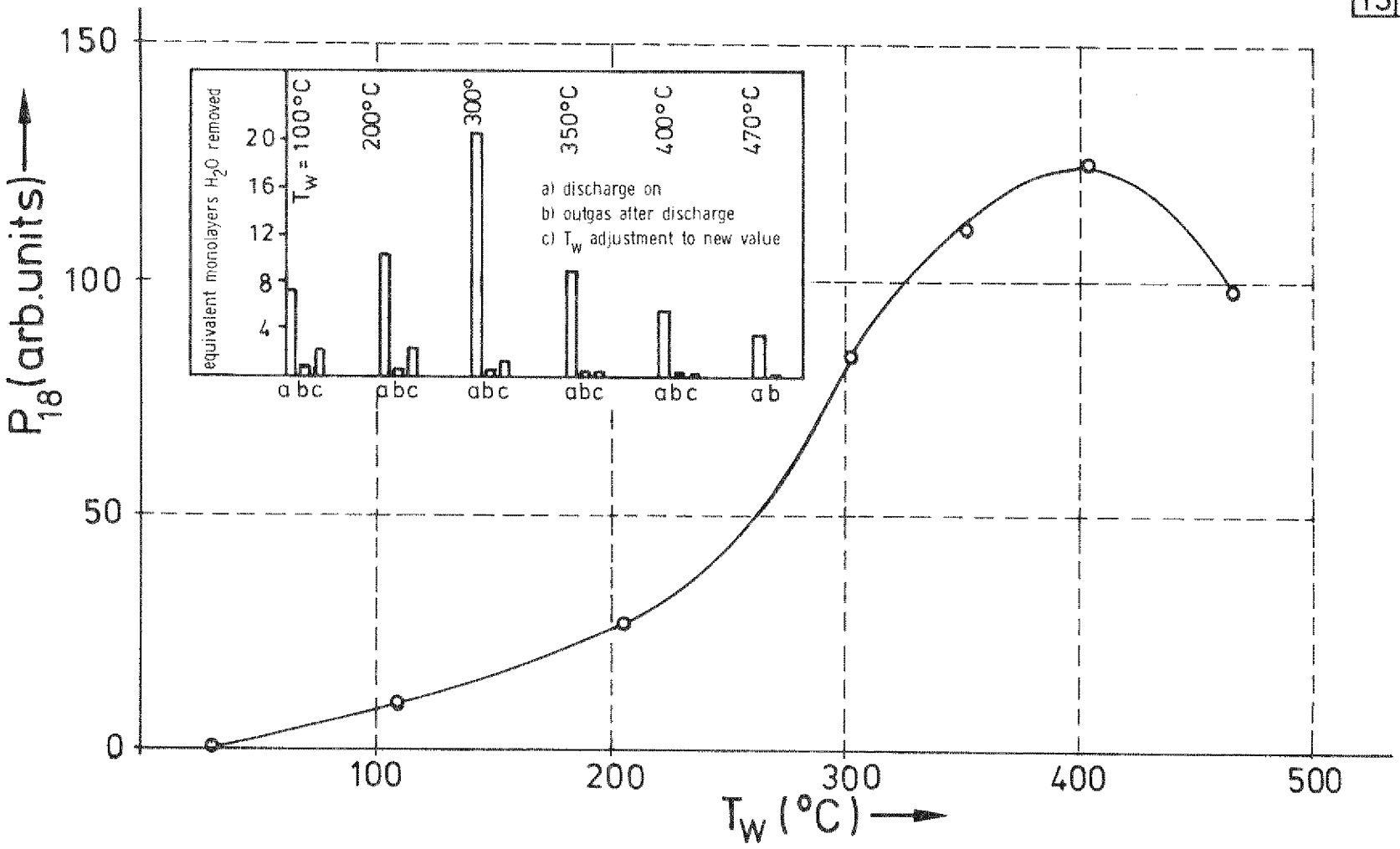

Fig 28.

Variation of the partial pressure P_{18} of water in the RG discharge as a function of the wall temperature T_W; P_2 = 2,8 x 10^{-3} torr, I_{GD} = 0,5 A, W_{rf} = 32 W. Insert: equivalent number of monolayers of H_2O released during the successive steps of the procedure. Most of the release occurs during the discharge phases; a considerable evolution of the oxide layer takes place during the experiment. It has been indespensible to utilize here the procedure outlined in § III.6. to evaluate the values of P_{18} presented

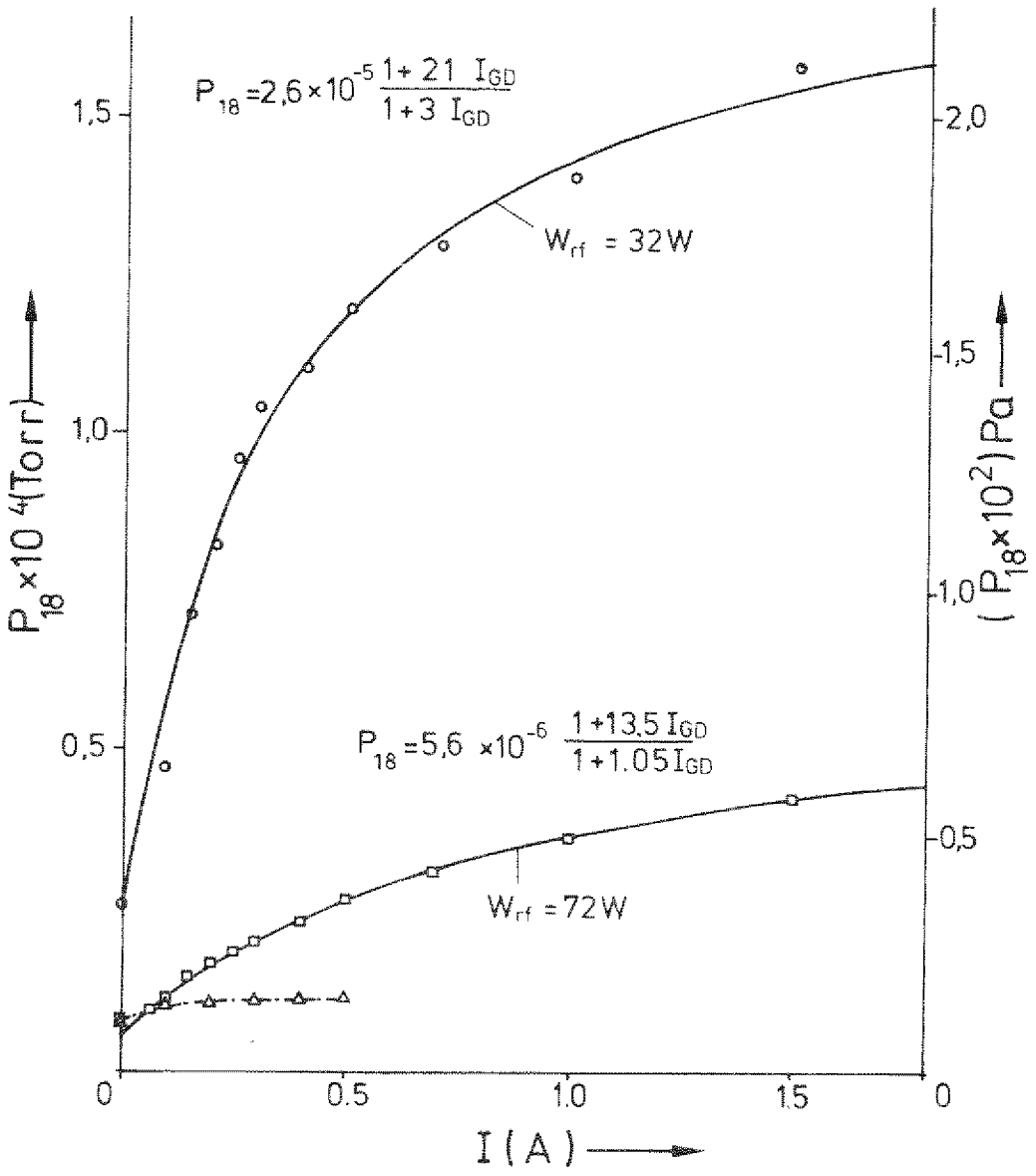

Fig 29.

Variation of the partial pressure of water P_{18} as a function of the glow discharge current I_{GD}. T_W = 200 °C.

- o 11.1.1980, freshly oxidized walls, $P_2 = 2.8 \times 10^{-3}$ torr
- □ 23.11.1979, partly deoxidized walls, $P_2 = 2.8 \times 10^{-3}$ torr
- Δ 15.2.1980, partly deoxidized walls and $P_2 = 1.2 \times 10^{-2}$ torr

When $P_2 = 1.2 \times 10^{-2}$ torr (curve c), the glow discharge no longer increases the deoxidation rate significantly; I_{GD} was not increased here beyond 0.5 A to avoid a possible extention of the RG discharge into the portholes (§ III.1.c).

At still higher pressure (and low I_{GD} values), the partial pressure of water (outgas) decreases when the discharge is initiated! Such observations have also been made in ASDEX and DITE (private communications).

The inverse of the cleaning rate gives a measure of the time τ_{cd} necessary to achieve a certain degree of deoxidation. If we normalize τ_{cd} to 10 hours at a current density of 25 μA cm^{-2} (I_{GD} = 0.5 A), it increases to fourteen hours, i.e. by fourty percent only when the current density is lowered down to 10 μA cm^{-2} (I_{GD} = 0.2 A). But τ_{cd} reaches 20 hours at a current density of 5 μA cm^{-2} only and 45 hours in the case of an rf plasma.

On the other hand, an increase of the current density beyond 25 μA cm^{-2} does not reduce τ_{cd} much: Even with a current density of 100 μA cm^{-2}, τ_{cd} is decreased by less than 30 %, down to 7 hours. This does not seem to compensate the increased power consumption and the risk that the discharge might become unstable at very high currents.

Thus current densities lying between 10 and 25 μA cm^{-2} appear to be best adapted for the procedure (See however § VII.3.d) and fig. 40).

VI.5 Influence of the hydrogen pressure in the RG discharge on the partial pressure of water

The concentration n_{18} of water in the RG discharge decreases when the hydrogen pressure P_2 in the GDV is raised. The experimental results, plotted on fig. 30, were obtained as follows: P_{18} was first measured in our standard experimental conditions, i.e. a RG discharge with I_{GD} = 0,5 A and P_2 = 2.8 mtorr. The wall had been partly deoxidized.

The throttle factor θ_2 of TV 2 was then increased, leading to the expected decrease of the m = 18 signals of RGA 2 ($U_{18} \propto \theta_2^{-1}$).

The inlet rate of H_2 into the GDV was increased half a minute later, increasing P_2 in the GDV and bringing the H_2 pressure in the QBP back to its initial value (1.8×10^{-6} torr). A deconditioning of the quadrupole (§ III.2) was thereby avoided. A decrease of the water signal resulted from this operation. The procedure was repeated to obtain the measurements plotted on the figure until the pressure in the GDV reached 1.2×10^{-2} torr. This limit was set by the fear that the cleaning of new surfaces in the portholes (§ III.1.e) might affect the measurements if the pressure were further increased.

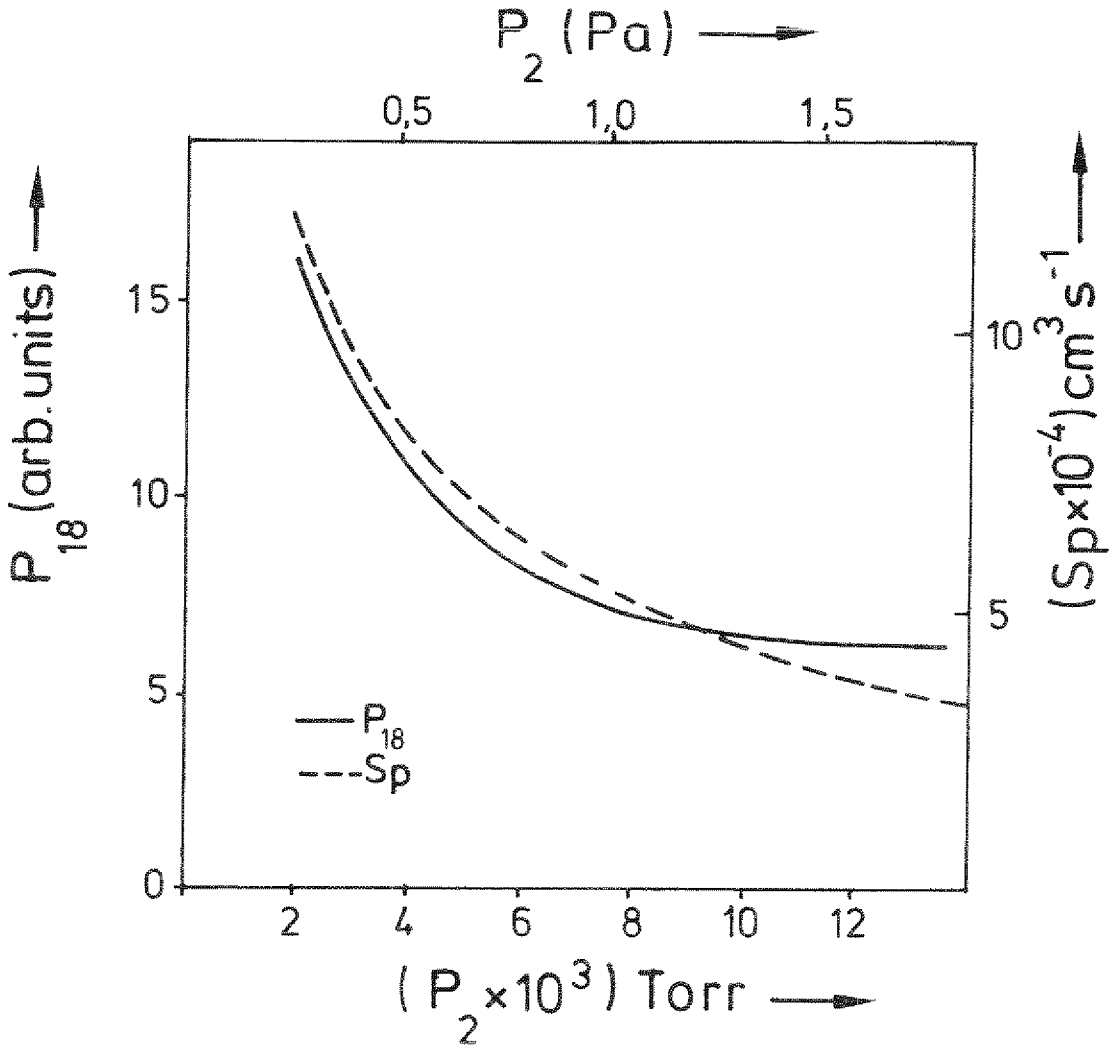

Fig 30.

Variation of the partial pressure of water P_{18} in the GDV and of the pump speed Sp with the hydrogen pressure P_2 in the RG discharge.
T_W = 200 ^{o}C

Thus, when the partial pressure in the GDV is increased, both P_{18} (fig. 26) and the pump speed (fig. 4) decrease. The resulting effect is almost multiplicative[+]. This leads to the conclusion that the cleaning rate (Sp n_{18}) decreases strongly when the pressure in the GDV is raised.

VI.6 Influence of the pump speed Sp

VI.6.a Experiments using the throttle valve TV 1

The results of these measurements show that a kind of water vapour pressure equilibrium tends to establish itself in the GDV at moderately high wall temperature and glow discharge currents. The water release rate v_{18} from the wall is practically fully balanced by the reoxidation rates of the wall by thermal (v_{ox}, § IV.3) and plasma-induced (k_D, § IV.2) effects. Phenomena associated with the pump speed become then second order effects. The results are easy to understand starting from the simple "Gedankenexperiment" shown fig. 31.

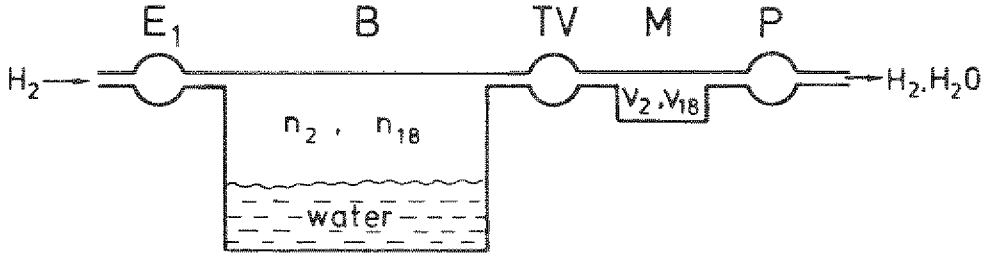

Fig. 31: "Gedankenexperiment" illustrating measurements with the throttle valve TV1

A vessel B, at constant temperature, contains some water. Hydrogen is forcibly introduced at a constant rate E through the inlet valve E_1 and evacuated together with some water vapour by the pump P with constant pumping speed Sp. The concentrations of H_2 and H_2O in B are n_2 and n_{18} respectively and we have $n_2 \approx n \gg n_{18}$ ($n = n_2 + n_{18}$). Between B and P we have intercalated:

- a two-position valve TV which limits the pump speed at the vessel B to the values $S^{(1)}$ (TV open) and $S^{(2)}$ (TV partially closed), and
- a small volume M where the concentrations ν_2 and ν_{18} of H_2 and H_2O can be measured.

Consider first the stationary throughflow rates of H_2. The fluxes streaming through E_1, TV and P are equal. With TV open we have: $E = S^{(1)} n_2^{(1)} = Sp\ \nu_2^{(1)}$, and with TV partially closed: $E = S^{(2)}\ n_2^{(2)} = Sp\ \nu_2^{(2)}$. Thus, since E and Sp are constant:

$$\nu_2^{(1)} \Big/ \nu_2^{(2)} = 1 \qquad \text{(VI.1)}$$

The stationary concentration of H_2 in M is independent of the setting of TV. On the other hand, the stationary concentration of H_2 in B is larger when TV is

[+] The streaming regime in the pump port varies in this pressure domain. A simple multiplicative relation might therefore not be justified.

partially closed: $n_2^{(2)}/n_2^{(1)} = S^{(1)}/S^{(2)}$.

Consider next the transient phase for H_2:

Immediately after closing TV the H_2 concentration in B is still $n_2^{(1)}$, i.e. low. The flow through TV is reduced ($S^{(2)} n_2^{(1)} < S^{(1)} n_2^{(1)}$) and the concentration v_2 in M decreases. A rapid increase of n_2 to its new stationary value $n_2^{(2)}$ follows, accompanied by a corresponding return of v_2 to its original value. Thus a negative spike in v_2 arises whenever TV is (partially) closed. Similarly, a positive spike in v_2 accompanies the opening of TV. The expected variation of v_2 and n_2 are schematically shown in fig. 32.

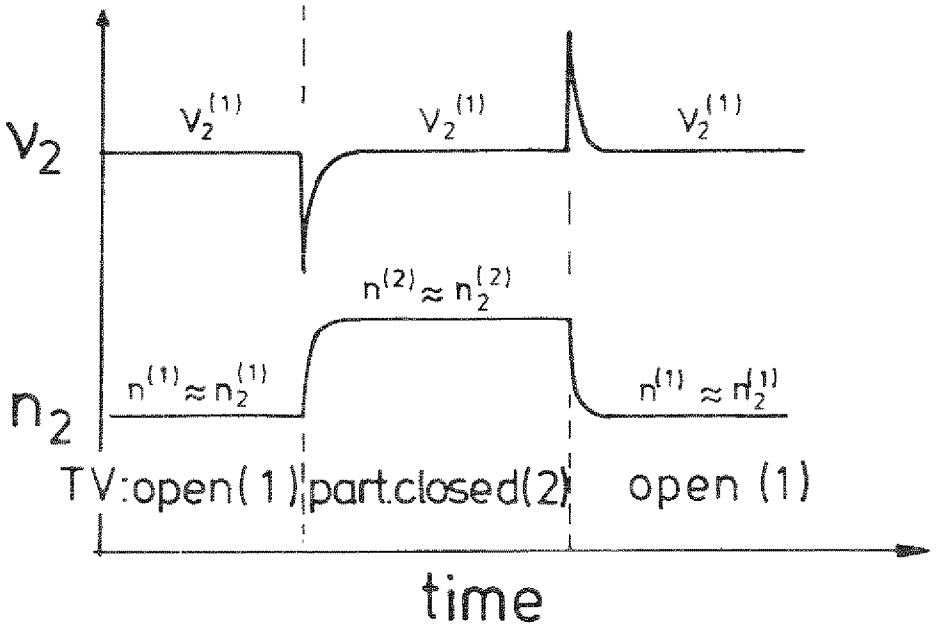

Fig. 32: Expected variations of the hydrogen concentrations n_2 in B and v_2 in M.

Gases which do not significantly react with the wall should exhibit this behaviour.

We turn now to the behaviour of the water vapour.

In the limiting case where the rates of water evaporation and condensation in B are much larger than that at which it is evacuated through TV, we can write: $n_{18}^{(1)} \approx n_{18}^{(2)} \approx n_{18}^{eq}$ where n_{18}^{eq} is the equilibrium concentration of the water vapour in vessel B. In the stationary case, the flow of water vapour through TV and P are again equal. We obtain (stationary flow):

- with TV open: $S^{(1)} n_{18}^{eq} = Sp\ v_{18}^{(1)}$, and
- with TV partially closed: $S^{(2)}\ n_{18}^{eq} = Sp\ v_{18}^{(2)}$.

Thus: $$\frac{\nu_{18}^{(2)}}{\nu_{18}^{(1)}} = \frac{S^{(2)}}{S^{(1)}} < 1 \qquad \text{(VI.2)}$$

The expected behaviour is shown in fig. 33.

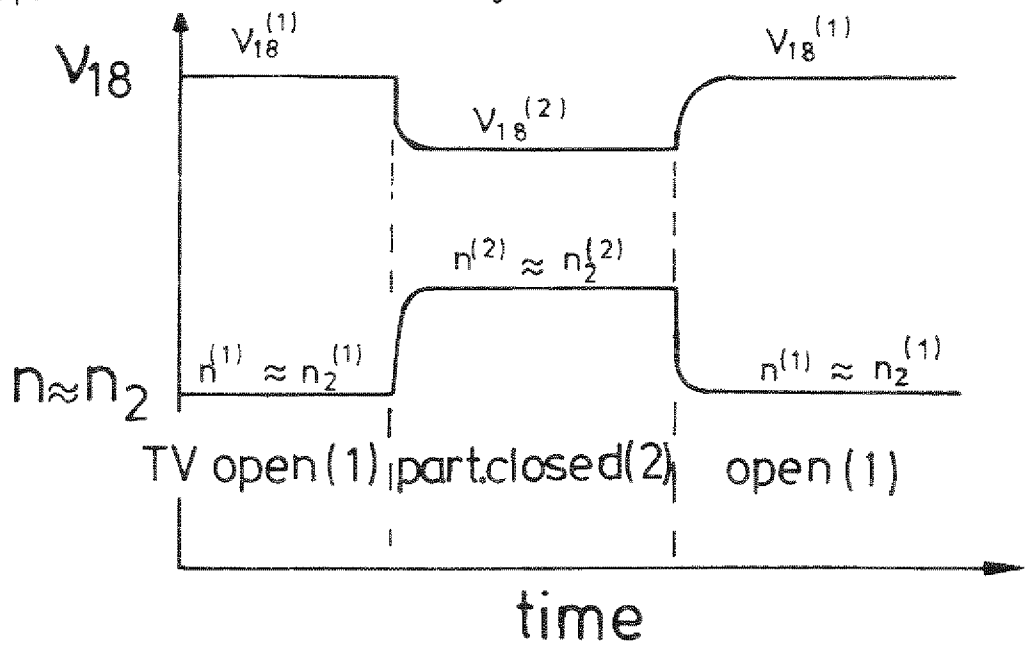

Fig. 33: Expected variation of the water concentration ν_{18} in M and of the total concentration $n \approx n_2$ in B.

Let, in the general case, V_{eV} be the evaporation rate and $V_{cond} = K_{cond} n_{18}$ the recondensation rate of water in B. The water-balance requires that:

$$V_{eV} - K_{cond} n_{18}^{(1,2)} = S^{(1,2)} \; n_{18}^{(1,2)}, \text{ and}$$

$$S^{(1,2)} n_{18}^{(1,2)} = Sp \; \nu_{18}^{(1,2)}.$$

Solving the first of these equations for $n_{18}^{(1,2)}$ and inserting into the second gives

$$\frac{\nu_{18}^{(1)}}{\nu_{18}^{(2)}} = \frac{S^{(1)}}{S^{(2)}} \; \frac{K_{cond} + S^{(2)}}{K_{cond} + S^{(1)}} \qquad \text{(VI.3)}$$

In the limiting case where K_{cond} is much smaller than $S^{(1,2)}$, we obtain equation VI.1. In the opposite limit ($K_{cond} \gg S^{(1,2)}$) equation VI.2 is found. We conclude that in such a system, when the ratio $\nu_j^{(2)}/\nu_j^{(1)}$ differs from 1 for a substance j, some mechanism exists through which this substance recondenses onto the wall of vessel B.

It is easy to see from fig. 1 that our system is equivalent to the "Gedanken-experiment" discussed above. The GDV corresponds to vessel B, TV 1 to TV and the

QBP to the measuring device in M. The evaporation rate of water is replaced by the chemical production rate of H_2O from the wall. The condensation mechanism consists of two processes: reoxidation of the wall by the water vapour (§ IV.3) and destruction of the water vapour by the plasma (cf. § IV.2).

The experimental results agree with the model as shown on fig. 34 (left hand side): The vessel walls had been partially deoxidized at 300 °C. The glow discharge current was 0.5 A. The ratio $S^{(1)}/S^{(2)}$ is 1.25 for H_2 and 2.03 for H_2O (interpolated from measurements in CH_4 and Ne). The variation of the total pressure in the GDV and that of the H_2 pressure in the QBP are shown in fig. 34c and a, respectively. The features are those expected from fig. 32. The full line in fig. 34.b is the water signal measured in the QBP. The broken line has been calculated from equ. VI.2, i.e. assuming that the condensation rate of water is much larger than the evacuation rate. The right hand side presents similar measurements made with liquid nitrogen in the cold finger.

Water recondensation phenomena set thus a serious limit to the achievable cleaning rate. The QBP gives the partial pressure of H_2O immediately above TMU 1 where the pump speed is independent of the setting of TV 1; the results show therefore that moderate changes of the pump speed at the vessel decrease significantly the rate at which H_2O is eliminated (factor of 2 in this case).

VI.6.b) Influence of the cryopump CF

The cleaning rate should increase when the pump speed is increased, i.e. when the cryopump, which eliminates rapidly the water vapour, is activated. Fig. 35 shows that when LN_2 is poured at time t_o into the cold finger CF, a quasi-instantaneous drop of P_{18} results at first: this results from the increased pump speed. But at later times, the slope of $d\ln P_{18}/dt$ remains markedly larger (factor of two and a half at T_W = 200 °C) than without CF: the rapid condensation of the water vapour onto the cold surfaces reduces strongly the rate at which the walls are continuously being reoxidized by H_2O.

Another example of the effect of the CF is shown on fig. 36. This is the continuation of the experiment described in § VI.1.a), the beginning of which is shown on fig. 26. The wall temperature is 300 °C in this case and I_{GD} = 0.5 A. When the CF is activated after about 4 hours of RG discharge, the rapid drop of P_{18} and the later increased slope $d\ln P_{18}/dt$ are again evidenced. Within about one hour, P_{18} has decreased by a factor of five.

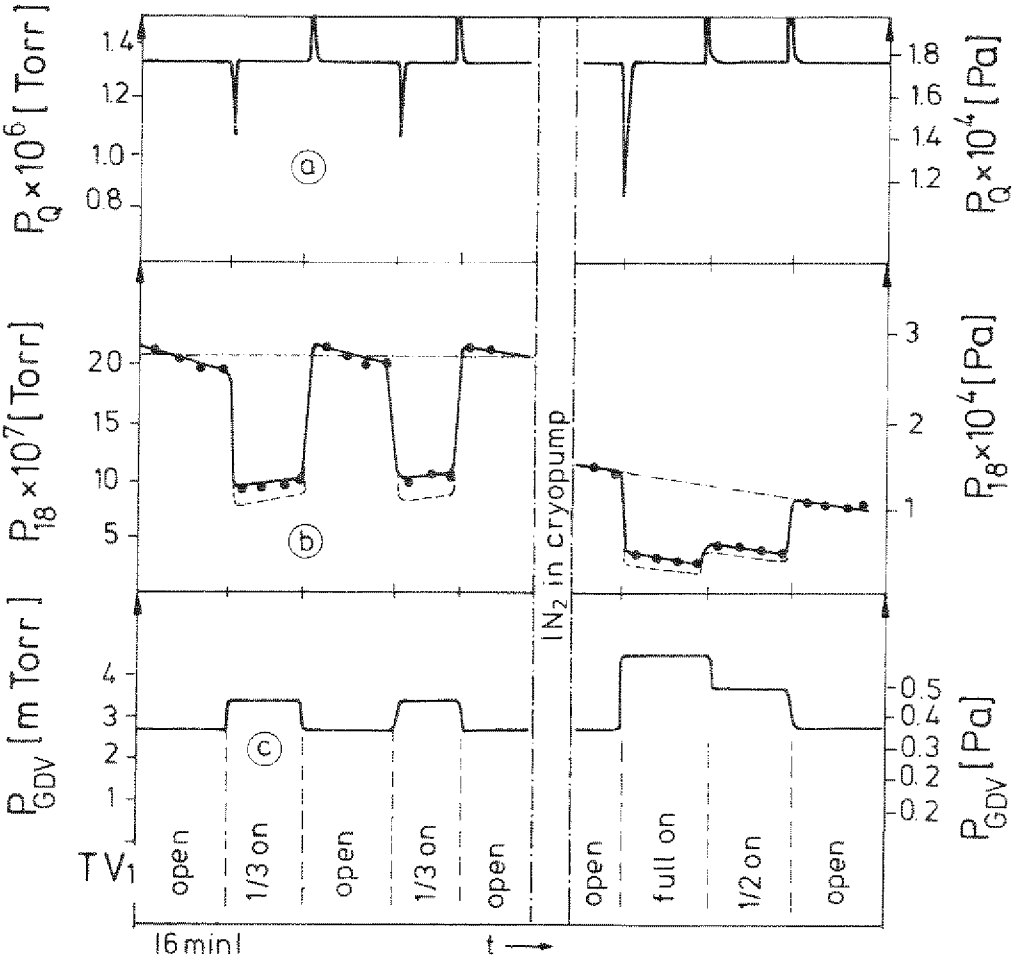

• P_{18} measured just below TV1 –•–•– values expected if P_{18} in GDV constant

– – values expected if P_{18} in GDV is inversely proportional to the roughing speed

Fig 34.

Influence of the pump speed on the elimination rate of water
T_W = 300 °C, I_{GD} = 0.5 A, partly deoxidized walls

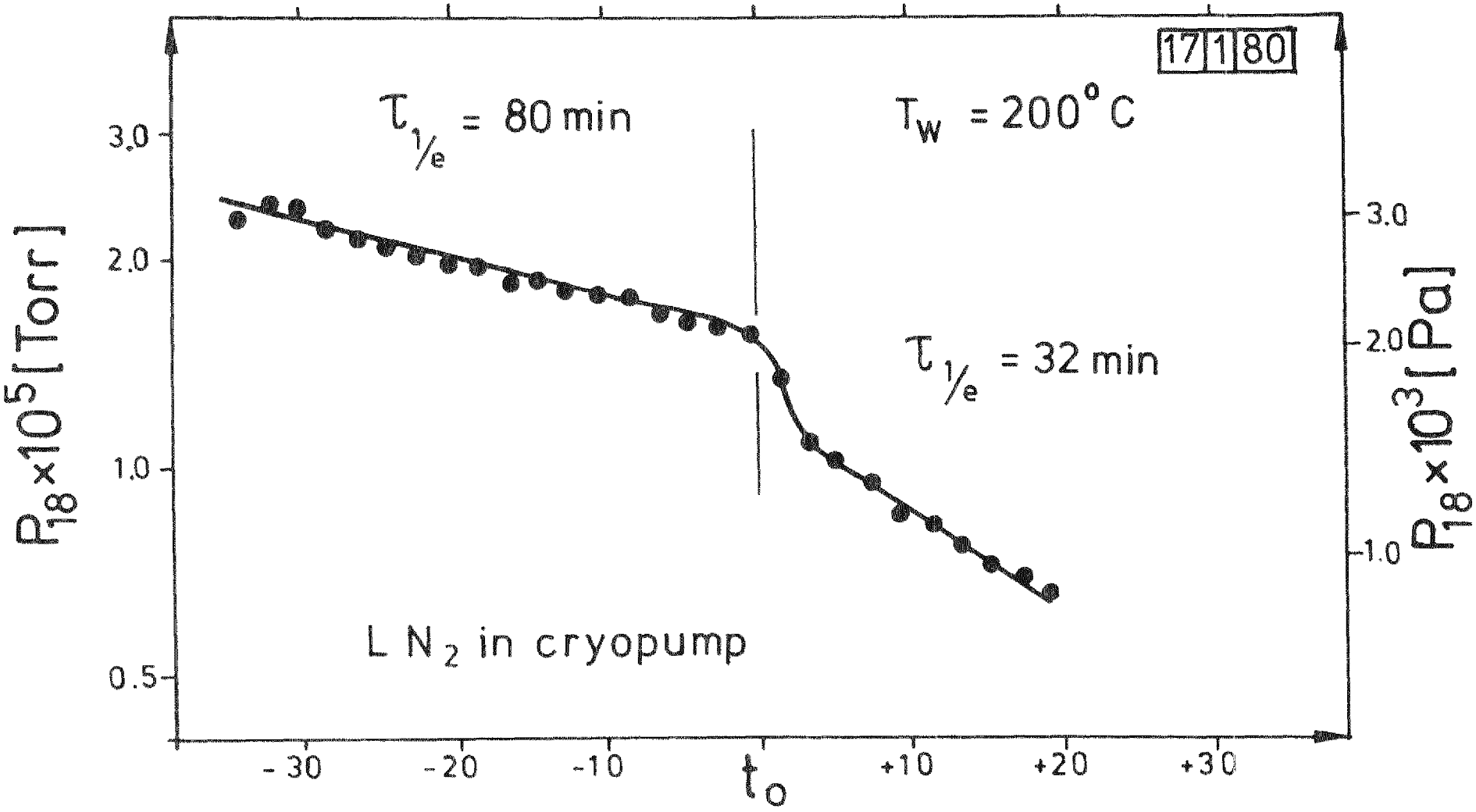

Fig 35.

Effect of the LN_2 cryopump on the elimination rate of water during a cleaning run

P_2 = 2.8 x 10^{-3} torr, I_{GD} = 1.0 A

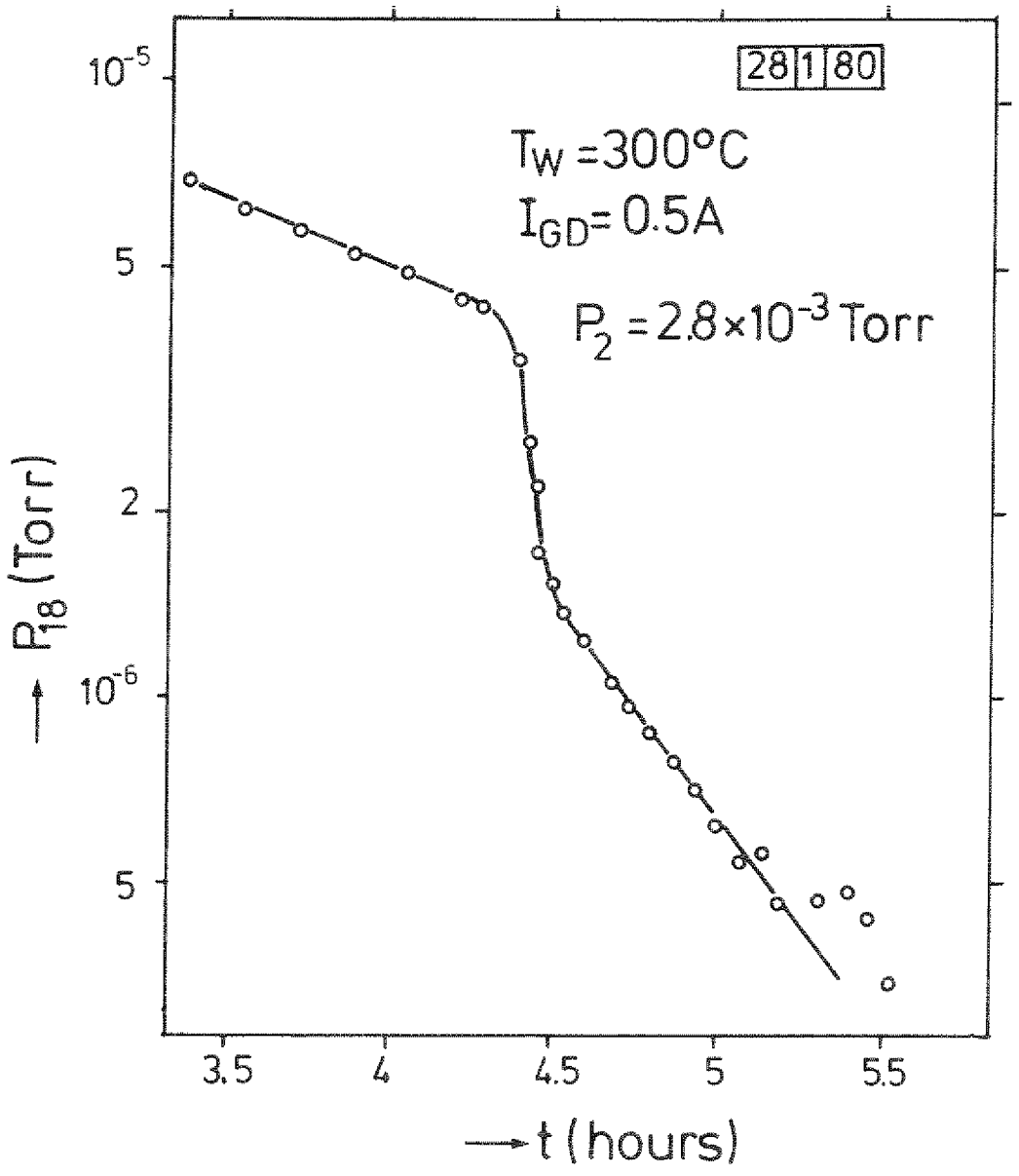

Fig 36.

Effect of the LN_2 cryopump on the elimination rate of water at the end of the cleaning run illustrated on fig. 26

In a tokamak device such as TEXTOR or JET, the cold finger should be withdrawn behind a gate valve before one lets it return to room temperature. This ensures that the water evaporation occurring at that time does not recontaminate the freshly deoxidized surfaces.

VI.7 Admixed noble gases

The addition of helium or neon to the hydrogen of the RG discharge leads, at 200 °C, to a certain decrease of the H_2O release rates. This decrease is practically proportional to the decrease of $\alpha \varphi_i$ which is measured when the methods of § IV.1 are used.

When a fresh surface (9 V.3) is exposed to a mixed H_2 + Ne (2 - 5 %) RG discharge, the release rate of CH_4 is decreased, with respect to the pure H_2 case, by about the same ratio as that of H_2O. On the other hand, the amount of CO is larger by a factor of about two than in the absence of neon.

In pure neon discharges, the release rates of water and methane from this fresh surface vanish completely, whereas the release of CO remains high, an effect which is also observed when neon is replaced by helium.

When the surface has been previously decarburized, (but reoxidized), neither the neon nor the helium addition to the RG discharge increase the release rate of CO above noise level.

VI.8. Admixed methane

Attempts to release measureable amounts of water by the rf or RG discharge have failed whenever the walls were at room temperature. CH_4 and CO are produced whenever significant amounts of surface carbon are still available. But, as mentioned in the introduction, the deoxidation of surfaces which have been previously decarburized and later exposed to air, as will occur in TEXTOR when internal diagnostics are modified, raises a problem. The admixture of small amounts of methane to the hydrogen of the cleaning discharge has been found to be a rather efficient method to deoxidize the surface when this cannot be warmed up. This is illustrated by the experiment which are summarized on figs. (37) and (38):

A routine oxidation procedure was applied to the walls on the preceding evening; the wall temperature was decreased overnight to room temperature. Pure hydrogen gas was introduced into the GDV and the partial pressures of methane, water and carbon monoxide were measured in the rf and for various currents of the RG discharge. After this run, 1 % of methane was added to the hydrogen and the same

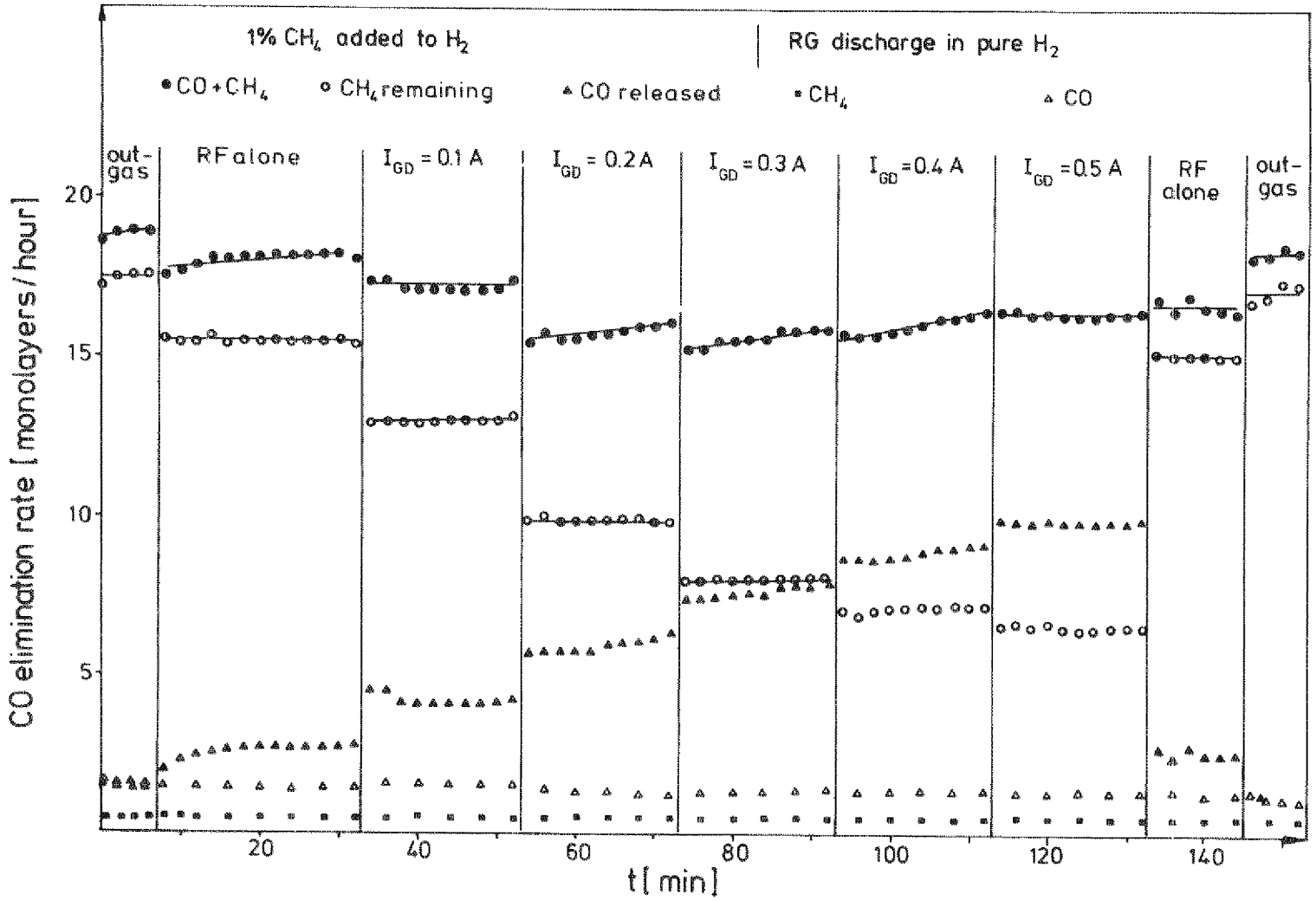

Fig 37.

Cracking of CH_4 in a RG discharge and corresponding appearance of CO with walls at room temperature: 1 % CH_4; 99 % H_2.

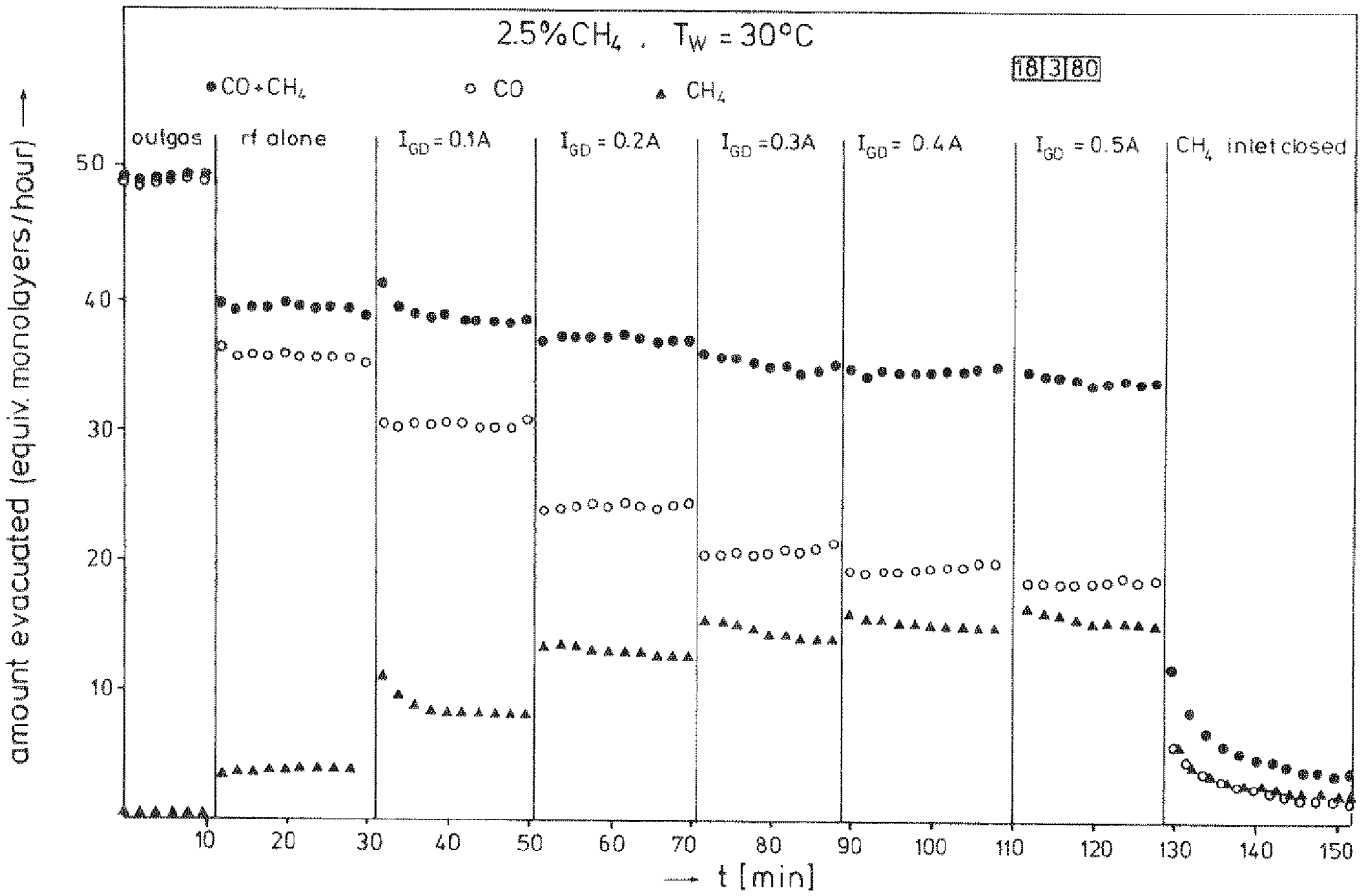

Cracking of CH_4 in a RG discharge and corresponding appearance of CO with oxidized walls at room temperature: 2,5 % CH_4 + 97,5 % H_2

procedure was repeated. On the following day (without intermediate oxidation) these experiments were reproduced using 2,5 % of methane in the mixture.

No relevant variation of the partial pressure of water was observed in any of the runs. The P_{18} signals are therefore not shown.

The RG discharges in pure hydrogen did not release measureable amount of CH_4 or CO; this is not surprising since the walls had been submitted during the previous months to numerous cycles of strong oxidations and deoxidation; the reducible carbon layers had thereby probably been fully removed.

When 1 % of methane is present in the RG discharge, a dissociation of CH_4, leading to surface deposition is observed (cf also § V.2). Most of the carbon returns rapidly to the gas phase, either in the form of CH_4 (re-reduction by the discharge) or in that of CO: as shown on fig. 37, the sum of the CO and CH_4 partial pressures remains practically constant when I_{GD} is changed. We also note that the production rate of CO (i.e. the elimination rate of surface oxygen) is rather high, of the order of 10 equivalent monolayers per hour, even though considerably lower than that of H_2O at higher wall temperature. When the methane introduction is interrupted, the further RG discharge in H_2 liberates only traces of methane. This indicates that the surface contamination by carbon is not serious when this percentage of CH_4 is admixed.

When 2,5 % of methane were added to the H_2 (fig. 38), the production rate of CO was increased by 50 % with respect to the values obtained at the 1 % level. The progressive reduction of the surface oxygen during the cleaning operation may however have masked a possibly faster removal rate. The sum of $P_{15} + P_{18}$ is no longer constant indicating a net deposition rate of carbon on the surface. This is confirmed by the observation that, when the valve letting CH_4 in is closed, the RG discharge in pure H_2 now release quantities of CH_4 and CO which can easily be detected. A further check was made by raising the wall temperature to 200 ^{o}C, starting a new discharge. Very large amounts of water were observed (as usual at that temperature) but in addition, the CH_4 and CO signals were, although not very large, still appreciably more important than in usual cases.

One should finally note that

- although only CH_4 was let in, at values of I_{GD} = 0.35 A, the partial pressure of CO became larger than that of CH_4.

- the same effects have been observed at higher temperatures (e.g. during the experiments of curve c on fig. 20a).

- the complicated chemistry which occurs at the wall may partly explain the difference between the measurements of the K_D values for methane which have been presented in § V.2.

VI.9. An optimized cleaning run

Fig. 39 shows the evolution of P_{18} as observed under the following experimental conditions: wall temperature T_W = 300 °C, RG current I_{GD} = 0.5 A, hydrogen pressure $P_2 = 2.8 \times 10^{-3}$ torr; liquid nitrogen was poured into the cryopump twelve minutes after the start of the discharge; i.e. the conditions are close to the ones which other measurements have indicated to be best appropriate for rapid deoxidation of the wall. The discharge was interrupted after four hours, the GDV was evacuated, closed and the pressure rise caused by the evaporation of the H_2O condensed on the CF was measured (the amount of CO_2 condensed was very small).

During the two minutes following the initiation of the discharge, the partial pressure of water in the GDV increased (from $\approx 10^{-7}$ torr) up to $P_{18} = 4 \times 10^{-4}$ torr; this corresponds to a removal rate of more than 5 equivalent monolayers of O per minute from the exposed surfaces and to a pressure ratio P_{18}/P_2 of $\geq$ 0.14 in the GDV.

When LN_2 was introduced into the CF, P_{18}, as observed by the RGA in the QBP, decreased by a factor of three as a consequence of the increased specific pump speed for water. Simultaneously the total pressures in the GDV dropped abruptly by $\approx$ 5 %. It recovered slowly towards its initial value during the following hours. Since the number E_2 of H_2 molecules entering into the GDV via the inlet valve E_2 must be equal to the sum of the number of H_2 molecules which are evacuated and of H_2O molecules which are produced (and condensed on the cryopump), it is easy to deduce from the variation of the total pressure curve in the GDV the rate of water production and the corresponding partial pressure. The values of P_{18} thus evaluated are plotted as solid triangle or fig. 33, agreeing nicely with the values deduced from the RGA signal.

Four hours after the initiation of the RG discharge P_{18} is still $\approx 1.5 \times 10^{-6}$ torr, but continues to decrease steadily[+]; the experimental results

[+] Fig. 27 illustrates how P_{18} evolves overnight in a similar RG discharge, without cryopump.

can be fitted from the 12th to the 240th minutes by the empirical equation (plain curve): $P_{18} = 1.15 \times 10^{-3} / [\, t(min) \,]^{1,2}$.

The amount of water collected on the CF during the four hours corresponding to the exposure of fig. 39 was equivalent to 110 monolayers of O removed from the exposed surface. To this number should be added $\approx$ 50 monolayers removed during the twelve minutes preceding the start of the cryopumping procedure, and ca. 25 monolayers evacuated by the turmolecular pump system during the phase where CF was active. Thus we can evaluate that about 200 equivalent monolayers of oxygen have been removed during this exposure of four hours.

VII DISCUSSION OF THE RESULTS

VII.1. Sputtering, arcs and carbon removal

As pointed out in the introduction, discharge cleaning procedures are applied to minimize the amount of impurities which can later be released from the wall during hot plasma discharges. They should be applied in such a way that vulnerable parts of the apparatus such as windows and appendages are as little affected as possible.

Only one serious alteration of our windows occurred and this at an early time of operation when, as mentioned in § V.2, the glow discharge penetrated into cold portholes. Serious arc spots developed at the metal-glass junctions and a significant darkening of the windows resulted. After the replacement of these windows and further prolonged operation (about five hundert hours of RG discharge) with warm portholes, only a very thin, quasi transparent film could be detected on the glass surfaces. It is not possible to specify what fraction of this - probably sputtered-on - deposit resulted from prolonged sets of measurements made with neon and argon plasmas of which the sputtering coefficients are much greater than that of hydrogen. Brushing the windows with a soft cloth allowed to remove effortlessly the deposit which was not implanted into the glass.

Prehandling procedures cannot affect significantly the later contamination of confined plasmas which results from the wall bombardment by energetic atoms and atomic ions, leading to sputtered atoms. The main aim is therefore to convert chemically the low Z contaminants - present in the form of carbon and oxides in the surface-near layers - into volatile components such as hydrocarbons, water and carbon oxides, to ensure that these are released from the wall and eliminated from the vessel via the pump ports.

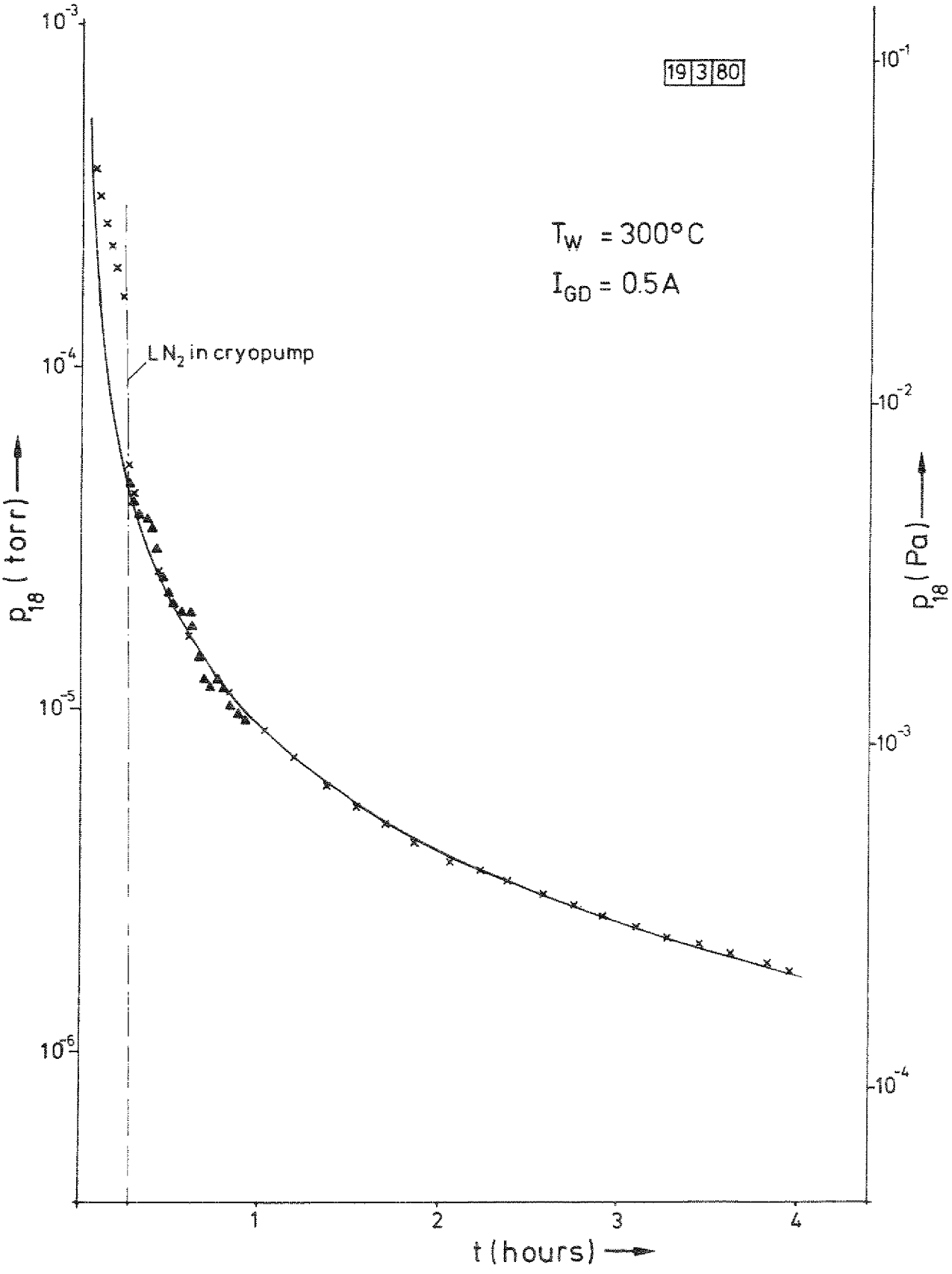

Fig 39.

The beginning of an optimized cleaning run

Our measurements indicate that a further source of plasma contamination, namely arc spots (§ V.2), is considerably reduced and possibly completely suppressed when our prehandling procedure is initiated with walls at moderate temperatures (e.g. 200 ^{o}C). This agrees with the earlier observations of Simonov /22/ on the tokamak T 2 and on his simulation experiment. It is encouraging to note that, when the prehandling had been applied once at elevated wall temperatures, repeated reoxidation of the wall by exposure to air did not lead to the reappearance of arc spots, even when the RG discharge was restarted with walls at room temperature.

It is likely that the arc spots which we have observed in our previous experiments and in this device whenever new unbaked cold inserts were exposed to the RG discharge resulted primarily from the presence of insulating films (probably oil) on the surface /23/ and not from preexisting sharp surfaces edges or needle-like structures /24/. The latter would presumably have remained effective when the wall temperature was raised. It is moreover difficult to imagine how they could smoothly disappear at T_W = 200 ^{o}C and no longer act as trigger when discharges were later initiated at room temperature.

Another mechanism suggested /4, 25/ for the initiation of arcs bases on the observation / 18b, 26/ that very large amounts of hydrogen become dissolved in SS or inconel walls when their surfaces are exposed to high fluxes of atomic H^{o} and H^{+} particles. Hydrogen (H_2) gas can then precipitate into lattice defects or at grain boundaries, building overpressurized gas pockets. Surface cracking, leading to a localized release of H_2 at high densities, could then trigger the arc. The effect should only occur when the wall is near room temperature and disappear when $T_W \gtrsim 150$ ^{o}C. Evidence for such surface cracking has been found earlier /27/ but only when cooled probes had been exposed to intense flux densities of atomic hydrogen during long times ($\gtrsim$ 10 hours): the diffusion constant of H in stainless steels is small ($\mathcal{D} \approx 1{,}4 \times 10^{-12}$ cm^{2}s^{-1} at T_W = 25 ^{o}C) and hydrogen does not have time to reach the pockets and to precipitate into them in the early phase of a first exposure to atomic hydrogen. Thus the observation of arc spots during the first minutes of the exposure of new parts of the apparatus to an RG discharge cannot be accounted for by this mechanism.

As mentioned in § 5.3, the amount of evidence gathered to date is still insufficient to draw definitive conclusions. It has however been observed that an initial bake-out of the surface at 200 ^{o}C (probably cracking or volatilizing the oil films before the exposure to the RG discharge) is sufficient to avoid the occurence of arc spots, even when the first plasma discharge is later initiated with walls at room temperature.

Our measurements (§ V,3) have confirmed the fact that the reduction /4/ of the carbon layer, down to a level where the expected rate of C contamination during hot plasma discharges is very low, does not present serious difficulties: large CH_4 and CO removal rates can already be achieved when the walls are at room temperature. Similar observations have been made concurrently during the glow discharge cleaning of PDX /12/ and of ASDEX /11/. We have therefore not concentrated our effort on this aspect of the problem. Our measurements have simply confirmed the facts that:

- the clean-down time to a point where further release of hydro-carbons and of carbon oxides becomes negligible can be short,
- the removal rates increase with increasing wall temperature (see e.g. fig. 24, and /4/) indicating that the reations proceeds probably via a surface-near solid state chemical reaction, and that
- after the first clean-down of the inner wall and reexposures to air, the amount of hydrocarbons and of carbon oxides released when discharges are re-initiated is very small (see e.g. fig. 26).

The small amounts of CO observed at the start of a new RG discharge after an oxidation procedure could either be due to a slight recontamination of the surface from the gas phase (e.g. by oil vapour) or result from the migration to the surface of some lattice carbon from the stainless steel. The ratio P_{28}/P_{18} of the partial pressures of CO and of H_2O is somewhat larger when more time elapses between the reoxidation procedure and the RG discharge. However, even then, the CO release rate has never been found to be larger than 3 % of that of H_2O, (except when methane was deliberately added to the filling gas).

Large amounts of CO are released from walls which are first exposed to RG or glow discharges in hydrogen /5a, 11, 12/. A similar release was observed earlier /4/ during exposures to low energy hydrogen atoms and was tentatively ascribed to the possible reduction of a compound, for instance a carbonate, in the surface-near layer. The experiments described here, using the admixture of methane (§ VI.b), suggest another "simple" explanation which however applies only to the case of the glow discharge in hydrogen: the ionisation of CH_4, produced by the reduction of the carbon layer, followed by the acceleration of the resulting ions in the cathode voltage drop, could lead to CO formation via a surface reaction. The existence of the effect is evidenced on fig. 37 and 38. The enhanced release of CO by an RG discharge in pure neon shows however that an additional ion-induced mechanism probably also exists. The CO formation mechanism appears this to be quite complex!

VII.2. Water release

VII. 2.a General remarks

In discussing the deoxidisation of SS surfaces, it should be kept in mind that
- the alloy contains different elements, mainly iron, nickel and chromium (Table 2).
- both bi- and trivalent oxides result from the oxidation procedures and that
- the oxygen concentration decreases rapidly as one goes from the surface into the bulk material /2,3/.

Table II: Composition of SS 1.4301 (type AISI 304) in percents:

Fe :	68 - 73	Si	$\leq$ 1
Cr :	17 - 20	C	$\leq$ 0.07
Ni :	8.5 - 10	P	$\leq$ 0.045
Mn :	$\leq$ 2	S	$\leq$ 0.03

The first point has been discussed recently by H.F. Dylla /7/. It is difficult to deoxidize completely a surface since chromium oxide, even more so manganese titanium and aluminium oxides if traces of these metals are present in the alloy, are strongly bonded; their reduction should be slow even at elevated wall temperatures. This implies on the other hand that such residual "irreducible" oxides are not strong contaminating factors: little water release should result from their reduction during hot plasma discharges.

For this reason, the emphasis has not been laid here on the achievement of completely oxygen-free surfaces, (as could have been verified by Auger analysis techniques) but rather on the development of a surface prehandling technique which ensures that even at elevated temperatures and in the presence of a plasma discharge in hydrogen, the release rate of water should be as small as possible. Thus residual gas analysis has been used as main diagnostics technique to follow the evolution of the cleaning procedure. After all, the results of the Petula tokamak /29/ with a chamber of aluminium oxide indicate that strongly bonded oxides behave rather well as first wall material.

During hot plasma discharges, some "irreducible" oxides remaining on the stainless steel surface are sputtered off. Resulting oxygen ions, recondensing on the wall, may form bonds with for instance iron or nickel atoms; easily reducible oxides result which build up a new source of O-contamination unless they are eliminated by renewed discharge cleaning. This may be why the most efficient discharge cleaning procedure in TFR has turned out to be /30/ to produce a succession of low T_e toroidal discharges with a limited number of high power tokamak discharges in between. In glow discharges, the plasma potential with respect to the wall is $\approx$ + 400 V; some (in this respect beneficial) sputtering results, which would not occur if a prehandling by a radio frequency plasma or by low energy hydrogen atoms had been used: in any case an increase of this sputtering through the admixture of neon to the hydrogen at the end of an RG cleaning procedure was not found to reincrease the H_2O release rate up to a measurable level.

The combination of the three factors indicated above leads to a complex evolution of the H_2O release: trivalent Fe oxides, closest to the surface /31/, should be reduced during the fast initial phase, leaving behind essentially divalent Fe oxides; nickel, iron and chrominum oxides are reduced at different rates[+)]; finally effects associated with diffusion of deeper lying oxygen to the surface are also expected. It is therefore not surprising that the observed release rates do not follow a simple exponential time variation especially during the early clean-down phase (see fig. 29, 39).

VII. 2.b A simplified model for the deoxidation reaction in the RG discharge

During the first minutes of the RG discharge, transient phenomena occur which are associated with the rapid build-up of the hydrogen concentration c in the surface-near layers of the wall material and with the two-stage kinetics of the chemical reduction reaction; these have been discussed previously /4, 5b/. In addition, the concentration of the tri- and bivalent oxides closest to the surface evolves rapidly. Finally, as shown in § III.2, inherent problems arise in the interpretation of the signals of the residual gas analyser whenever the H_2O concentration n_{18} (cm^{-3}) in the gas phase varies rapidly, (time scales $<$ 2 minutes).

The model presented here aims therefore at the description of the water release as it occurs some time after the cleaning procedure has started, namely at the times when the parametric variations discussed in § VI have been examined. It seems reasonable to assume that the reducible oxides are then mainly bivalent

[+)] Quantitative evaluations are however made more difficult by the fact that the bonding energies in the SS lattice differ probably from values in the pure metals.

and to assume that the fractional coverage θ_o of the surface with oxides is no longer close to one.

Apart from this, the following assumptions are made:

- c is proportional to $(\alpha\varphi_i)^{1/2}$ where $\alpha\varphi_i$ is the flux density of atomic hydrogen penetrating per unit time through the surface. The validity of this assumption has been demonstrated elsewhere /18, 26/. The results presented in § IV.1 show that $\alpha\varphi_i$ is a linear function of I_{GD}, whence:

$$c^2 = A_1 \alpha\varphi_i = A_1 \left[(\alpha\varphi_i)_{rf} + A\, j_{GD} \right]. \qquad \text{(VII.1)}$$

$A_1 = (2\sigma k_r)^{-1}$, where σ is the surface roughness factor and k_r the (phenomenological) rate constant for the recombination of dissolved H into gaseous H_2 on the SS surface /4/.

- The rate $v_{18}^{(j)}$ at which water is released from the surface as a consequence of the reduction of the metal oxide $MO^{(j)}$ is proportional to the exposed area S, to the concentration $c_{MO}^{(j)}(cm^{-2})^{+)}$ of the residual oxide $MO^{(j)}$ present under the surface and to c^2. I.e. we have $v_{18}^{(j)} = S\, k_{18}^{(j)}\, c_{MO}^{(j)}\, c^2$.

The total <u>rate</u> v_{18} <u>of water release</u> is then:

$$v_{18} = S\, k_{18}\, c_{MO}\, c^2 = S\, k_{18}\, c_{MO}\, A_1 \alpha\varphi_i \quad (\text{molecules}^{-1}) \qquad \text{(VII.2)}$$

where we have used the abbreviation $k_{18}\, c_{MO} = \sum_j k_{18}^{(j)}\, c_{MO}^{(j)++)}$. The linear variation of v_{18} with $\alpha\varphi_i$ has been previously verified /4/.

H_2O, once released, leaves the vessel in three diffent ways:

- Water vapour is pumped away at the rate:

$$v_p = S_p\, n_{18} \ (\text{molecules}\ s^{-1}); \qquad \text{(VII,3)}$$

+) If $\kappa_{MO}^{(j)}(cm^{-3})$ is the volume concentration of $MO^{(j)}$, than $c_{MO}^{(j)} = \int \kappa_{MO}^{(j)}\, dx$ where the integral is made over the depth of the oxide layer.

++) The relative amounts of the oxides vary with time, due to the different rate constant $k_{18}^{(j)}$. Thus $k_{18}\, c_{MO}$ does not vary with time in a simple way. But in the short time interval δt during which a parametric variation is examined, $k_{18}\, c_{MO}$ can be assumed to be a constant, provided that $\delta t \ll (\partial \ln c_{MO}^{(j)}/\partial t)^{-1}$ for every $MO^{(j)}$ species.

- Water vapour reoxidizes the surface at the rate (§ IV.3):

$$v_{ox} = S(1 - \theta_o)\, k_{ox}\, n_{18} \; ; \qquad \text{(VII.4)}$$

the phenomenological rate constant k_{ox} is again an average over the different metal atoms covering the surface,

- Water vapour can finally be ionized in the RG plasma (§ IV.2); the resulting (mainly) H_2O^+ and HO^+ ions are accelerated by the cathode drop potential of about 400 V. Impact dissociation results, leading to an ion induced reoxidation rate v_I. In analogy with the measurements made in methane (fig. 20) and in ammonium (fig. 21), we write (cf eq. IV.5)for v_I at $P_2 \approx 2.8 \times 10^{-3}$ torr:

$$v_I = S(\alpha_I + k_I\, j_{GD})\, n_{18} \approx Sp(0{,}2 + 4\, I_{GD})\, n_{18} \qquad \text{(VII.5)}$$

when j_{GD} is the current density in the RG discharge. It seems likely that α_I and k_I increase (because the electron density increases) when P_2 is raised.

Writing now the water particle balance and noting that the variation of n_{18} in the GDV is slow, we obtain:

$$V \frac{dn_{18}}{dt} = v_{18} - v_p - v_{ox} - v_I \approx 0 \qquad \text{(VII.6)}$$

Substituting equations (VII.1 - VII.5) into equ. (VII.6), solving for n_{18} and multiplying by Sp yields:

$$v_p = Sp\, n_{18} = Sp\, A_1\, k_{18}\, c_{MO}\, \frac{(\alpha \varphi_i)_{rf} + A\, j_{GD}}{Sp/S + (1 - \theta_o)\, k_{ox} + \alpha_I + k_I\, j_{GD}} \; ; \qquad \text{(VII.7)}$$

v_p is the rate at which water leaves the vessel, i.e. the cleaning rate.

For pure rf discharges ($j_{GD} = 0$) we have:

$$(v_p)_{rf} = Sp\, A_1\, k_{18}\, c_{MO}\, \frac{(\alpha \varphi_i)_{rf}}{Sp/S + (1 - \theta_o)\, k_{ox} + \alpha_I} \; . \qquad \text{(VII.8)}$$

VII.3 Discussion of the parametric variation of the cleaning rate v_p

a) Variation as a function of the filling pressure P_2 of hydrogen

The decrease of P_{18} which occurs when P_2 increases (fig. 30) is the only parametric dependance which cannot be explicitly read from equ (VII.7). As mentioned in /31/ and in § VII.2.b, an increase of P_2 in the RG discharge (at constant j_{GD}) is expected to increase the electron density in the plasma. This should increase the rate of ionisation of the H_2O molecules and consequently the value of k_I. To explain the measurements shown on fig. 30 and those discussed in the following paragraph, one needs to assume that k_I increases by a factor of three to four when P_2 is raised from 2.8 to 12 x 10^{-3} torr. We write therefore tentatively:

$$\alpha_I + k_I\, j_{GD} = (\alpha'_I + k'_I\, j_{GD})\, P_2 \qquad \text{(VII.9)}$$

wherin α'_I and k'_I are supposed to be independant of P_2.

b) Variation as a function of the current denstiy j_{GD}

The model predicts that v_p should vary hyperbolically with j_{GD}, as has been experimentally observed (fig. 29 and fig. 40, below). Combining equ (VII,7 and 8), we obtain indeed:

$$v_p = (v_p)_{rf}\ \frac{1 + B\, j_{GD}}{1 + C\, j_{GD}} \qquad \text{(VII.10)}$$

where

$$B = A/(\alpha\varphi_i)_{rf} \qquad \text{and} \qquad C = k_I/\left[Sp/S + (1 - \theta_o)k_{ox} + \alpha_I\right] \qquad \text{(VII.11)}$$

When the current density is increased, the cleaning rate should vary from $(v_p)_{rf}$ towards an asymptotic value $(v_p)_\infty$ which can be higher or lower than $(v_p)_{rf}$:

$$(v_p)_\infty = (B/C)\ (v_p)_{rf} \qquad \text{(VII.12)}$$

The difference between the B values deduced from the two measurements at P_2 = 2.8 x 10^{-3} torr (fig. 29) results mainly from the reduction of the rf power, from 72 W in nov. 1979 down to 32 W later. This lowers the $(\alpha\varphi_i)_{rf}$ values (fig. 5.b) and increases the value of B (equ. VII.16). The different C values might result from the different surface coverage ratios θ_o during the two runs.

Whether the cleaning rate increases or decreases when the RG discharge is started depends, for a given rf power level, on the values of Sp/S, of $(1 - \theta_o)k_{ox}$ and (through k_I) on P_2.

When P_2 is raised, k_I is expected to increase; Sp decreases. This leads to a rapid increase of C (equ. VII.11). Already at a pressure of $1{,}2 \times 10^{-2}$ torr (fig. 29), we reach the state where C = B; the cleaning rate is independant of the glow discharge current. As mentioned in § VI.5, at higher pressure and/or when the pump speed is deliberately reduced, the cleaning rate decreases when the glow discharge current is applied and when its intensity is increased.

c) Variation as a function of the pump speed (using the throttle valve TV 1)

The measurements (§ VI.6) during which the pump speed was changed using TV 1 can also be understood from equ. (VII.7): at high wall temperatures ($T_W \geq 300\ ^oC$) and large discharge currents ($I_{GD} \geq 0.5$ A), both k_{ox} and $k_I\ j_{GD}$ are larger than Sp/S. The ratio of the cleaning rates achieved with TV 1 opened (2) and throttled down (1) is:

$$\frac{v_p^{(2)}}{v_p^{(1)}} = \frac{Sp^{(2)}}{Sp^{(1)}} \cdot \frac{Sp^{(1)} + K_{cond}}{Sp^{(2)} + K_{cond}} \qquad \text{(VII.13)}$$

with

$$K_{cond} = S(1 - \theta_o)k_{ox} + S\ \alpha_I + S\ k_I\ j_{GD} \qquad \text{(VII.13a)}$$

Equations (VII.13) and (VI.3) are equivalent and we have seen that they represent well the experimental measurements (fig. 34).

d) Variation produced by the cryopump CF

To visualize the influence of a strongly enhanced pump speed, equ. (VII.7) is rewritten in the form:

$$v_p = S\ A_1\ k_{18}\ c_{MO}\ \frac{(\alpha\varphi_i)_{rf} + A\ j_{GD}}{1 + \frac{S\ k'_{ox}}{Sp} + \frac{S\ \alpha_I}{Sp} + \frac{S\ k_I\ j_{GD}}{Sp}} \qquad \text{(VII.14)}$$

where $k'_{ox} = (1 - \theta_o)\ k_{ox}$,
i.e. we obtain when Sp is very large:

$$v_p = S\ A_1\ k_{18}\ c_{MO}\ \left[(\alpha\varphi_i)_{rf} + A\ j_{GD}\right] = v_{18}.$$

The cleaning rate cannot (obviously) become larger than v_{18}, the rate at which water molecules leave the surface. At low wall temperatures ($T_W \leq 200\ ^oC$), small current densities ($j_{GD} \leq 5\ \mu A\ cm^{-2}$) and in a well evacuated vessel (Sp/S large), a cryopump, even of enormous size, cannot significantly improve the cleaning rate. But at high wall temperatures, larger current densities, and in particular in devices wherein adequate pump speeds cannot be achieved otherwise, a significant gain should result from the incorporation of a retractable cryopump.

The increase of Sp should (equ. VII, 14) broaden the domain wherein the cleaning rate varies linearly with j_{GD}. This has been verified experimentally:fig. 40 compares the variation of n_{18} as a function of I_{GD} which are measured at $T_W = 200\ ^oC$ without and with liquid nitrogen in the cryopump. In the latter case, the variation is practically linear, i.e. $v_p \approx v_{18}$ up to 1.5 A.

e) Variation as a function of the wall temperature T_W

The existence of an optimum wall temperature (above which the cleaning rate decreases) is a straightforward consequence of the model. This and our other measurements indicates that it is probably mainly iron oxide which is reduced during the main phase of the clean-down:

In equ (VII.7), we have written in thick faced letters those coefficient which are strongly (exponentially) temperature dependent. These are:

- k_{18} (activation energy Q_{18}), the rate constant of the reaction
  $MO + 2\,[H] \rightarrow M + H_2O$

where $[H]$ stands for hydrogen dissolved in the lattice,

- $A_1 = (2\,\sigma\,k_r)^{-1}$, where k_r (activation energy Q_r) is the rate constant for the surface recombination of $[H]$ into H_2 molecules and

- k_{ox} (activation energy Q_{ox}), the rate constant of the reaction[+)]
  $(M + H_2O \rightarrow MO + 2\,[H]$

[+)] Permeation measurements, during which the upstream sides of iron or steel membranes were exposed to water vapour, have shown that the main oxidation channel produces dissolved $[H]$ atoms (and not directly H_2 molecules).

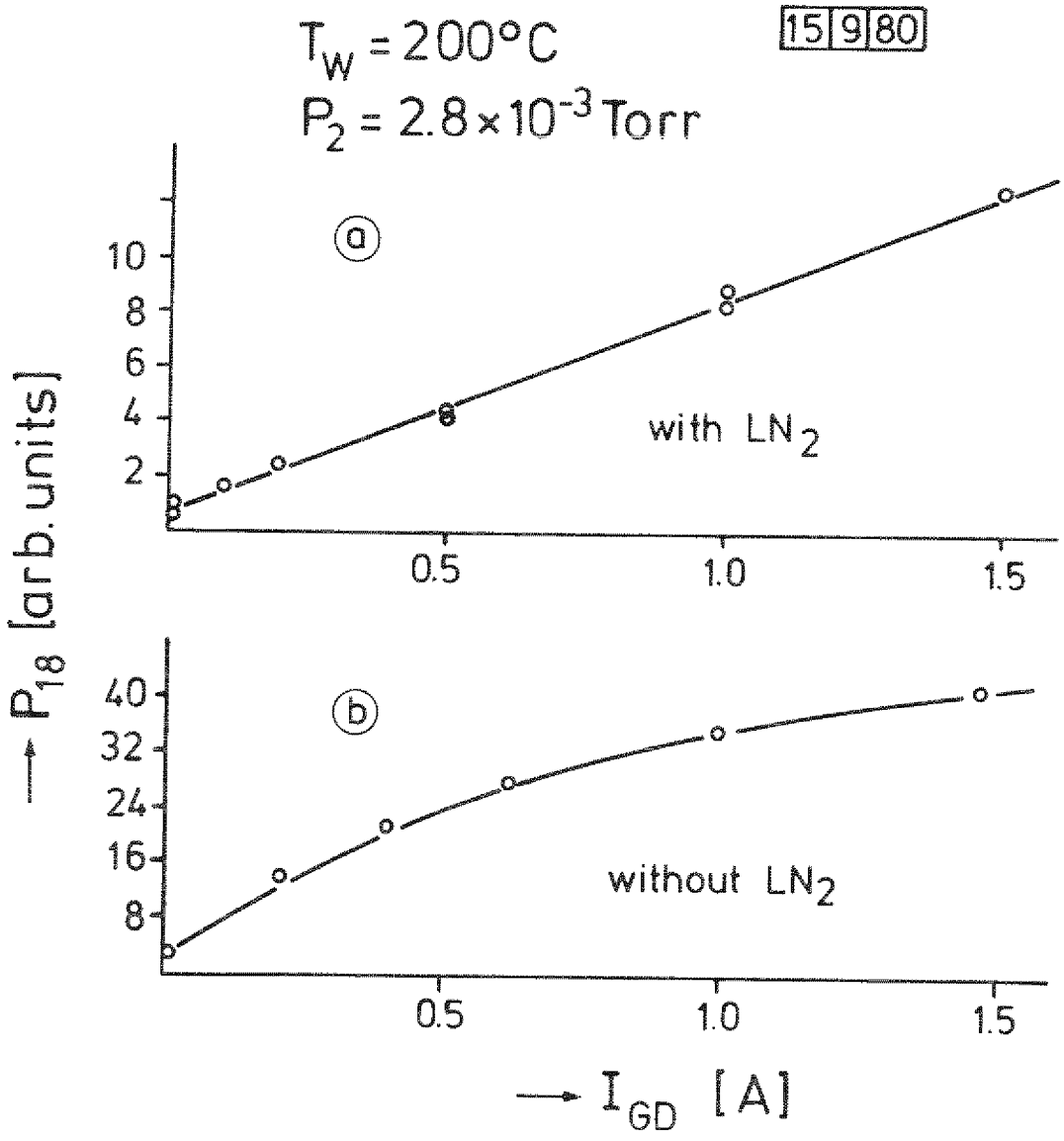

Fig 40.

Variation of n_{18} as a function of I_{GD}: a) without LN_2 in the cryopump,
b) with LN_2 in the cryopump CF

At low wall temperatures, $k_{ox} \ll Sp/S + \alpha_I + k_I j_{GD}$; the apparent activation energy of the cleaning rate should be[+]:

$$Q_{cl}^{(1)} = Q_{18} - Q_r.$$

At high wall temperatures, $k_{ox} \gg Sp/S + \alpha_I + k_I j_{GD}$. Q_{cl} should decrease down to

$$Q_{cl}^{(2)} = Q_{18} - Q_r - Q_{ox} = - \Delta H_{ox} - Q_r.$$

ΔH_{ox} is the enthalpy change involved in the reaction $MO + 2[H] = M + H_2O + \Delta H_{ox}$.

A reduction of Q_{cl} by 10 to 20 kcal should thus occur when T_W is raised up to 400 °C, where (§ IV.3) k_{ox} becomes the largest term in the denominator of equ (VII.7).

The results plotted on fig. 28 lead (at low T_W) to the value

$$Q_{cl}^{(1)} = 5{,}8 \text{ kcal/mole}$$

which agrees well with that of 6.8 kcal which had previously been measured for the deoxidation rate constant of SS surfaces exposed to quasi-thermal H^o atoms /5,b/. Recent experiments in this laboratory (to be published) have given, for the same SS, the value

$$Q_r = 16 \text{ kcal/mole}$$

Thus a value

$$Q_{18} = 21{,}8 \text{ kcal/mole}$$

results from the present measurements, in fair agreement with the value of 20.3 kcal/mole given in the literature /32/ for the water "desorption" rate from stainless steel.

Combining the value of $Q_{cl}^{(1)}$ with the preliminary one of Q_{ox} = 10 to 20 kcal/mole (§ IV.3) we deduce that

<u>the value of $Q_{18}^{(2)}$ should lie whithin the range of - 5 to - 15 kcal/mole</u>

I.e. the observed change of sign of Q_{cl} agrees with the model.

[+] If the hydrogen concentration c in the lattice were independent of T_W, the activation energy of the cleaning rate would be Q_{18}. But, in the case of RG discharge, c decreases rapidly when T_W increases: the penetration rate v_i of H depends mainly on I_{GD}: it has no activation energy. But the release rate v_r depends on the mobility of H on or to the surface; it increases, for a given c, rapidly as T_W is raised. When quasi-equilibrium is reached, i.e. when the rate of H diffusion into the lattice has become much smaller than the rate of surface recombination, we have $v_r \approx v_i$, i.e. $c^2 \approx \alpha \varphi / 2 \sigma k_r$. This leads to the appearance of the term $- Q_r$ in the following equation. "Quasi-equilibrium" establishes itself in this respect in one to four minutes in the GDV (to be published).

Similarly, from the observed value of Q_{18} and Q_{ox}, we deduce that the enthalpy of the reaction should lie in the range:

$$\Delta H_{ox} = Q_{ox} - Q_{18} = 1{,}8 \text{ to } -11{,}8 \text{ kcal/mole} .$$

From the reaction enthalpies at 200 °C:

$$Fe + \tfrac{1}{2} O_2 = FeO + 63{,}5 \text{ kcal/mole} \qquad H_2 + \tfrac{1}{2} O_2 = H_2O + 58 \text{ kcal/mole},$$

$$Ni + \tfrac{1}{2} O_2 = NiO + 57 \text{ kcal/mole}, \qquad H_2 = 2[H] - 4 \text{ kcal/mole } H_2,$$

$$2\,Cr + \tfrac{3}{2} O_2 = Cr_2O_3 + 272 \text{ kcal/mole},$$

we deduce the following ΔH_{ox} values:

$$NiO + 2[H] = Ni + H_2O + 5 \text{ kcal/mole } H_2O \text{ released},$$

$$FeO + 2[H] = Fe + H_2O - 1{,}5 \text{ kcal/mole } H_2O \text{ released},$$

$$\tfrac{1}{3} Cr_2O_3 + 2[H] = \tfrac{2}{3} Cr + H_2O - 29 \text{ kcal/mole } H_2O \text{ released}.$$

Thus the experimental value, even if preliminary, of ΔH_{ox} given above indicates that it is probably iron oxide which is reduced during the main clean down phase. This is note surprising in view of Table II (p. 76).

This discussion supports the conclusions of Dylla /7/ and Staib /32/ according to which, at room temperature, the main deoxidation results from the reduction of iron and nickel oxides whilst chromium oxide is too strongly bonded to be appreciably reduced. Our measurements indicate that this conclusion remains valid at $T_W = 400$ °C.

The reduction of the oxide layers on SS and on inconels should moreover be similar , and indeed the observations made on TFR /33/ with inconel walls agree with our measurements and with the conclusions of the model presented above. If anything, nickel-rich alloys should be more readily deoxidized, and should therefore be prefered.

VII.4. Water release at lower wall temperatures and in the QBP

In § VII.2 and VII.3, we have neglected the effects which result from the fact /4,5/ that the production of H_2O in the surface-near layers occurs in two successive steps, namely:

$$MO + [H] \rightleftharpoons MOH$$

$$MOH + [H] \rightleftharpoons M + H_2O,$$

(the intermediate product MOH has the character of a free radical). This neglect is justifiable when T_W is high ($\geqslant 200$ °C); the time lags which result from the detailed reaction mechanism are then short ($\leqslant 10$ minutes). The effects become however evident at lower flux densities (e.g. in the QBP) and when $T_W \leqslant 200$ °C in the GDV (cf. fig. 24). The plain curves $p_{18} = f(18)$ drawn on figs. 12 and 13 have been calculated from the equations of /4/.

At $T_W \leqslant 100\ ^oC$, hydroxide ($M(OH)_2$) formation results from the reaction of H_2O with the residual oxides and impedes the release of H_2O - as it is formed - to the gas phase and to the pump system. That this effect plays an important role is shown among others by the measurements of the P_{18} increase in the QBP after a step increase of the water inlet rate (§ III.2.b) and by the large amounts of water which "condensed" in the portholes of the GDV (§ III.4) when these were left at room temperature during a cleaning procedure.

VIII. CONCLUSIONS

A parameter domain exists wherein glow discharges in hydrogen - when applied for the first time to the walls of a stainless steel vessel - release large amounts of water vapour in addition to hydrocarbons and carbon oxides. If the surface has been previously decarburized and then exposed to air, similar amounts of water can again be released; the partial pressures of methane and of carbon oxides are then almost undetectable. The volatile products can be eliminated via the pump ports. Thus glow discharges in hydrogen can provide an efficient tool for the deoxidation and decarburization of the wall surface: as the discharge proceeds, the amounts of releasable surface contaminants decrease with time; the partial pressures of the hydrogenated products in the discharge become, within twenty four hours, smaller by a factor of 10^4 than the initial values (cf. fig. 26 and 27).

Typical parameters to achieve a rapid cleaning rate in a device having a pump speed $Sp = 0{,}2\ m^3\ s^{-1}$ and an inner area $S = 2\ m^2$ exposed to the glow discharge (i.e. the same ratio $Sp/S \approx 0.1\ m\ s^{-1}$ as TEXTOR and JET) are:

- a base pressure of H_2: $P_2 = 3 \times 10^{-3}$ torr
- a current density: $j_{GD} = 10 - 25\ \mu A\ cm^{-2}$ in the glow discharge and
- a wall temperature: $T_W = 300 - 400\ ^oC$.

One must operate at low P_2 values: when P_2 is increased (this also spoils the pump speed) the cleaning rate deteriorates. It becomes independant of the glow discharge current at $\approx 10^{-2}$ torr (fig. 29). At higher pressures, the cleaning rate decreases when the glow discharge current is applied: the glow discharge reduces then the cleaning action which results from the spontaneous H_2O outgasing of the wall.

In order to sustain the glow disharge in the $P_2 \approx 1$ mtorr domain, it has proven to be adventageous to use a combined radiofrequency-glow (RG discharge) system

whereby a weak rf discharge serves as a plasma source (virtual anode) for the glow discharge.

When the walls are at low (for instance room) temperatures, a moderately rapid release of hydrocarbons and carbon oxides is produced by the RG discharge as long as a carbon (C) layer is present on the surface. The release of water remains negligible, whether a C layer is present or not. Thus, at those temperatures, glow discharges in pure hydrogen cannot deoxidize the surfaces of plasma devices which have been operated for some times, i.e. decarburized, and then exposed to air for maintenance or the adjustment of diagnostics. The admixture of noble gases (He, Ne, Ar) does not enhance the H_2O release.

Operation of RG discharges in a mixture of 99 % H_2 and 1 % methane can however deoxidize the surfaces at a moderately rapid rate even at room temperature, (§ VI.b and fig. 37): CO is produced at the expense of CH_4. With 2,5 % of CH_4 some C becomes deposited. This can, however, easily be removed by a further exposure to a RG discharge in pure H_2.

At 100 ^{o}C, water release becomes appreciable when the RG discharge in pure H_2 is applied. Its rate increases rapidly when T_W is raised up to 350 ^{o}C, but decreases above T_W = 400 ^{o}C (fig. 28). Thus the achievement of very high wall temperatures is not necessary for such cleaning purposes.

An increase of the current density is advantageous in the low j_{GD} domain, but the cleaning rate tends to saturate when $j_{GD} \approx 25\,\mu A\ cm^{-2}$ (fig. 29). Very high glow discharge currents are not useful.

If the pump system of the device is too weak, a great benefit can be (drawn) from the installation of a retractable cryopump operating at liquid nitrogen temperature. The useful T_W and j_{GD} domains could moreover be extended to higher values by the incorporation of this cryopump. The resulting advantages of such a system must however be weighted against the resulting loss of access for diagnostics, design and construction problems to achieve the higher wall temperatures and inherent difficulties associated with the stable operation of glow discharges at large total plasma currents.

The model presented in § VII describes well all the main features of the parametric dependance. Its application is certainly limited to systems having roughly the same ratio $Sp/S \approx 0.1\ m\ s^{-1}$ as investigated here. We feel however that equ. (VII.7 and 9) can be used with confidence to scale the phenomena as a function of the available parameters.

The fact that arc spots have never been observed in our system after new built-in elements had been baked out at $T_W \geqslant 200\ ^{o}C$ is probably due to the UHV baking procedure. Here again, wall heating to at least moderate temperatures is a useful provision.

Finally the procedure indicated in § III.3 to precondition our residual gas analysis system has turned out to be effective and allowed to make quantitative measurements in the difficult surrounding of H_2O and H_2 gases.

Acknowledgements

This work has been carried out in the framework of a JET Article 14 contract. The technical assistance of MM. Gervelmeyer, Grobusch, Korr and Peuser has been invaluable. Some of the later measurements have been made in collaboration with F.L. Waelbroeck, Jr., ULB Bruxelles and T. Banno, University of Tokyo. Discussions with R.E. Clausing and H.F. Dylla on various aspects of this work were very useful.

REFERENCES

/1/ G.M. McCracken, P.E. Stott, Nucl. Fusion 19 (1979), 889

/2/ G. Betz, G.K. Wehner, L. Toth, A. Jochi, J. Appl. Phys. 45 (1974), 5312

/3a/ K.J. Dietz, E. Geissler, F. Waelbroeck, J. Kirschner, E.A. Niekisch, K.G. Tschersich, G. Stöcklin, E. Vietzke, K. Vogelbruch, J. Nucl. Mat. 63(1976), 167

/3b/ J. Kirschner, K.J. Dietz, F. Waelbroeck, Proc. 9th. Symp. Fusion Techn., Garmisch Partenkirchen, Pergammon Press (1976) EUR 5602, 65

/4a/ K.J. Dietz, F. Waelbroeck, Int. Symp. on Plasma-Wall Interactions, Jülich, Pergammon Press 1977, EUR 5782, 445

/4b/ K.J. Dietz, F. Waelbroeck, P. Wienhold, JOL-PP-1448, August 1977

/5a/ K.J. Dietz, F. Waelbroeck, P. Wienhold, Third Int. Symp. Plasma Chemistry, (IUPAC), Limoges, 1977

/5b/ K.J. Dietz, I. Ali-Khan, F. Waelbroeck, P. Wienhold, 4th. Int. Symp. Plasma Chemistry, Zürich, CH, Aug. 1979, (IUPAC Communications)

/6/ F. Waelbroeck, I. Ali-Khan, K.J. Dietz, P. Wienhold, J. de Physique, 40 (1970), C7 - 313

/7/ H.F. Dylla, J. Nucl. Mat., 94-95 (1980), in press

/8/ P.E. Stott, C.C. Daughney, R.A. Ellis, Nucl. Fusion, 15 (1975) 431

/9/ G.M. McCracken and H.F. Dylla, private communications

/10/ L. Oren, R.J. Taylor, Nucl. Fusion, 17 (1977) 1143

/11/ W. Poschenrieder, J. Nucl. Mat. 94-95 (1980), in press

/12/ Ph. Staib, H.F. Dylla, S.M. Rossnagel, J. Vac. Sci Technol. 17 (1980)

/13/ TFR Group, J. Nucl. Mat. 76-77 (1978) 587

/14a/ J.v. Seggern, K.G. Tschersich, J. Nucl. Mat. 76&77 (1978), 600

/14b/ J. v. Seggern, K.G. Tschersich, J. Nucl. Mat. 94-95 (1980), in press

/15/ I. Langmuir, J. Am. Chem. Soc. 34 (1912), 1310; 38 (1916), 2270

/16/ T.W. Hickmott, J. Chem. Phys. 32.3 (1960) 810

/17/ R.K. Gould, Univ. of Wisconsin rep 70 - 3544 (1969)

/18a/ I. Ali-Khan, K.J. Dietz, F. Waelbroeck, P. Wienhold, J. Nucl. Mat. 76-77 (1978), 337

/18b/ F. Waelbroeck, I. Ali-Khan, K.J. Dietz, P. Wienhold, J. Nucl. Mat. 85-86 (1979), 345

/19a/ L. Langmuir, J. Am. Chem. 6a. 40 (1918), 1361

/19b/ C.N. Hinshelwood in "Kinetics of Chemical Changes in Gaseous Systems" 2nd. Ed. (1929), chapt. VII

/20a/ D.D. Eley in "Chemisorption" (W.E. Garner, Ed.) Academic Press New York, (1975), 97

/20b/ E.K. Rideal, Proc. Cambridge Phil. Soc. 35 (1939), 130

/21/ G.M. McCracken, S.Y. Fielding, S.K. Erents, A. Pospieszczyk, P.E. Stott, Nucl. Fusion 18 (1978),35

/22/ V.A. Simonov et al. Nucl. Fusion Suppl. 4 (1962), 225

/23/ P. Mioduszewski, R.E. Clausing, L. Heatherly, J. Nucl. Mat., 85-86 (1979), 963

/24/ G.N. Fursei, P.N. Vorontsov-Vel'yaminov, Sov. Phys. Techn. Phys. 12 (1968), 1370

/25a/ I. Ali-Khan, K.J. Dietz, F. Waelbroeck, P. Wienhold, J. Nucl. Mat. 74 (1978), 132

/25b/ I. Ali-Khan, K.J. Dietz, F. Waelbroeck, P. Wienhold, J. Nucl. Mat. 74 (1978), 138

/26/ F. Waelbroeck, K.J. Dietz, P. Wienhold, J. Winter, I. Ali-Khan, H. Merkens, E. Rota, J. Nucl. Mat. 94-95 (1980), in press

/27a/ I. Ali-Khan, K.J. Dietz, F. Waelbroeck, P. Wienhold, J. Nucl. Mat. 76-77 (1978), 263

/27b/ I. Ali-Khan, K.J. Dietz, F. Waelbroeck, P. Wienhold, J. Nucl. Mat., 85-86 (1979), 1151

/28/ R.E. Clausing, private communications on measurements in ISXB, Doublet III.

/29/ P. Briand et al. Proc. Seventh Int. Conf. on Plasma Physics and Controlled Nuclear Fusion Research, Innsbruck, 23 - 30. Aug. 1978, IAEA, Vienna (1979) Vol. I, p. 65

/30/ TFR Group, J. Nucl. Mat. 94-95 (1980) paper E3, EUR-CEA FC 1059 - July 1980

/31/ Korrosion und Korrosionsschutz, F. Tödt (Ed), De Gruyter, Berlin 1961

/32/ Y. Strausser, Varian Report VR 51

/33/ Ph. Staib, S.M. Rossnagel, H.F. Dylla, J. Nucl. Mat. 94-95 (1980), in press